THE [illegible]
[illegible]-GAIN DIFFERENTIAL AMPLIFIER
OF [illegible]

by

Scott C. Doubin

Library
U. S. Naval Postgraduate School
Monterey, California

A DISSERTATION

PRESENTED TO THE

FACULTY OF PRINCETON UNIVERSITY

IN CANDIDACY FOR THE DEGREE

OF DOCTOR OF PHILOSOPHY

RECOMMENDED FOR ACCEPTANCE BY THE

DEPARTMENT OF PHYSICS

JUNE 1954

THE PERTURBED GAMMA-GAMMA DIRECTIONAL CORRELATION OF Cd^{114}

By

Scott C. Daubin

Thesis
D163
c.1

Library
U. S. Naval Postgraduate School
Monterey, California

This work was supported by the Atomic Energy Commission and the Higgins Scientific Trust Fund. Scott C. Daubin is a lieutenant in the U. S. Navy, at present attending Princeton University under the sponsorship of the U. S. Naval Postgraduate School, Monterey, California and the Office of Naval Research.

25143

ABSTRACT

The directional correlation of the 722 - 556 KEV gamma-gamma cascade in Cd^{114} was observed as a function of the physical and chemical state of the source. In the case of $InCl_3$ in a dilute aqueous solution of HCl it was deduced that the undisturbed correlation was obtained, and the following values were found for the LeGendre expansion coefficients: $A_2 = .090 \pm .011$, $A_4 = .022 \pm .016$. It was found that spin assignments of 2-2-0 for the first three levels of Cd^{114} together with the assumption that the first transition is an M1, E2 mixture with the following percentages: M1 - 95.8, E2 - 4.2 (both $\pm$ .6), gave a good theoretical fit to the observed curve in general agreement with results of other workers. The lifetime of the first excited level in Cd^{114} was measured and found to be less than or equal to 2.3×10^{-10} seconds. To observe the disturbed correlation the state of the source was altered to include glycerin solutions of several viscosities, the dry salt of $InCl_3$, and frozen aqueous and glycerin solutions. Calculation of the magnitude of the correlation perturbing interaction was based on a theory due to Abragam and Pound. The liquid sources showed no spoilages within the range of viscosities to which the liquid theory applies; however, the dry salt showed an interaction of greater than or equal to 700 mcs on the assumption of an electric quadrupole interaction, and greater than or equal to 163 mcs on the assumption of a magnetic interaction in classically describable fields. On the basis of field strength estimates in the former case, a lower limit to the $|$quadrupole moment$|$ of the first excited state of Cd^{114} is set at $.21 \times 10^{-24}$ cm^2.

Table of Contents

	Page
Chapter 1 - Introduction	1
Chapter 2 - Theory of Undisturbed Angular Correlation	3
Chapter 3 - Theory of Disturbed Angular Correlation	12
Chapter 4 - Choosing an Isotope	29
Chapter 5 - The Experiment	32
Part 5.1 - Apparatus	32
Section 5.1.1 - Apparatus, General	32
Section 5.1.2 - Apparatus, Mechanical	32
Section 5.1.3 - Apparatus, Electronic	33
Part 5.2 - Experimental Procedures	41
Section 5.2.1 - Runs and Checks	41
Section 5.2.2 - Sources	45
Part 5.3 - Data Reduction	47
Section 5.3.1 - Errors in General	47
Section 5.3.2 - Data Normalization	48
Section 5.3.3 - Geometrical Corrections	51
Section 5.3.4 - Statistics	60
Section 5.3.5 - Decay Scheme Corrections	67
Section 5.3.6 - Curve Fitting	69
Section 5.3.7 - Data Analysis Procedures	70
Part 5.4 - Results	76
Section 5.4.1 - General	76
Section 5.4.2 - Corrections	76
Section 5.4.3 - Undisturbed Correlations	77
Section 5.4.4 - Disturbed Correlations	81
Chapter 6 - Interpretation and Discussion	84
Part 6.1 - Undisturbed Correlations	84
Part 6.2 - Disturbed Correlations	86

Section 6.2.1 - Polycrystalline Sources 86
Section 6.2.2 - Liquid Sources 93
Part 6.3 - Statistical Validity 94
Appendix I - Positron Annihilation Component of Coincidence Rate 96
Appendix II - Effective Solid Angle 102
Appendix III - Geometrical Corrections For A Finite Source 105
Acknowledgement 110
Bibliography 111

List of Figures

Figure No.	Caption	Page
4-1	Decay Scheme of In^{114}	31
5.1.1-1	The Apparatus	32
5.1.2-2	Angle Measuring Assembly, Assembly	33
5.1.2-3	Angle Measuring Assembly, Details	33
5.1.3-1	Illustrating Time Uncertainty of Energy Selection	34
5.1.3-2	Photomultiplier Voltage Divider Unit and Bootstrap	35
5.1.3-3	Partial Spectrum of In^{114}	36
5.1.3-4	Pulse Amplifier	36
5.1.3-5	Differential Discriminator	37
5.1.3-6	Fast Double Coincidence Circuit	38
5.1.3-7	Overall Coincidence Response To Annihilation Radiation of Na^{22} (Wide Channel)	38
5.1.3-8	Overall Coincidence Response To Annihilation Radiation of Na^{22} (Narrow Channel)	38
5.1.3-9	Slow Triple Coincidence Circuit	39
5.2.1-1	Inter-Connection Diagram (TC-A)	42
5.2.1-2	Inter-Connection Diagram (CC-A)	42
5.2.1-3	Inter-Connection Diagram (RT-A)	42
5.2.1-4	Inter-Connection Diagram (RT-B)	42
5.2.1-5	Inter-Connection Diagram (CE-A)	42
5.2.1-6	Inter-Connection Diagram (CC-B)	42
5.2.1-7	Inter-Connection Diagram (CC-C)	42

5.2.1-8	Compton Scattering of the Gamma Rays of In^{114}	44
5.2.2-1	Source Holders	45
5.2.2-2	Viscosity vs Temperature of Glycerin-Water Solutions	45
5.2.2-3	Extended Source Mounting Arrangement	46
5.2.2-4	Point Source Mounting Arrangement	46
5.3.4-1	Time-Rate Plot	63
5.3.4-2	Probability That Two Observations Taken on a Normal Distribution Lie Greater Than X_o Standard Deviations Apart	66
5.4.2-1	Angular Resolution Curves	77
5.4.3-1	Determination of Observed Correlation Coefficients A_2 and A_4	77
5.4.3-2	Directional Correlation Function of the In^{114} Cascade Gamma Rays (722-556 KEV), Corrected and Uncorrected	78
5.4.3-3	Gamma-Gamma Directional Correlation Coefficients In 2(M1,E2)2(E2)0 Cascade As Function of Quadrupole Intensity	80
5.4.3-4	Comparative Directional Correlation Functions of the In^{114} Cascade Gamma Rays (722-556 KEV)	80
5.4.4-1	Anisotropy As a Function of $\Omega_o\tau_N$ For Quadrupole Interaction in Axially Symmetric Fields, Polycrystalline Source	81

5.4.4-2 Observed Anisotropy As a Function of Interaction, $\Omega_e \tau_N$, Electric Quadrupole Interaction 82

5.4.4-3 Observed Anisotropy As a Function of Interaction, $\Omega_o \tau_N$, Magnetic Interaction 82

Chapter 1 - Introduction

The first paper on angular correlation of successive nuclear radiations in which the explicit theoretical correlation functions were derived was by Hamilton (1H40). It was apparent from the begining that here was a very powerful means of investigating the low-lying excited states of nucleii. But successful experiments had to wait many years for advances in electronics to provide coincidence circuits of sufficiently short resolving time and for the improvement of radiation detection techniques. The first successful attempt to observe an angular correlation was by Brady and Deutsch in 1947 (1B47), and to Co^{60}, Sc^{46}, Y^{86}, and Cs^{134} belong the distinction of being the first isotopes to have their gamma-gamma correlations measured conclusively. But really precise measurements of angular correlations still had to wait until means of detection more efficient and reliable than Geiger counters could be developed. For in this work one measures a statistical function and is therefore plagued by statistical errors; hence for precision a great number (hundreds of millions) of quanta must be counted. And under these conditions Geiger counters proved quite inadequate. But a new day dawned with the first development of the scintillation crystal-photomultiplier tube technique by Marshall and Coltman (1M47). It was now possible in a single day to measure a correlation to the accuracy it would have required many years to achieve using Geiger counters. And the experimental art was greatly enhanced by the work of Hofstadter (1H50) on scintillation crystals of sodium iodide activated by small amounts of thallium as an impurity; these crystals provided means of measuring gamma ray energies with

high precision and efficiency. Thus we find in the late 1940's and early 1950's a tremendous increase in the work, experimental as well as theoretical, in angular correlation, and the first paper of Hamilton's is now accompanied by over four hundred others.

Chapter 2 - Theory of Undisturbed Angular Correlation

The study of the properties of low-lying excited nuclear states is greatly facilitated by a nuclear spectroscopic "tool" known as "angular correlation", or more completely "angular correlation of successive nuclear radiations". The short lifetime of most excited nuclear states makes their investigation by direct means such as resonance methods next to impossible. Hence we must probe these states indirectly, and the method that comes immediately to mind in the case of low-lying states is to study the radiations which preceed and succeed them. When we investigate some property of these radiations as a function of the angle between their propagation vectors we do "angular correlation". As one can imagine, the field is very broad; however, it can be subdivided both as to the nature of the radiations involved and as to the particular property of the radiations under investigation. In the former case, the theory is broad enough to include any of the well known nuclear emissions, viz. beta rays, gamma rays, alpha particles, neutrinos, in any allowed combination, viz. β-γ, γ-γ, α-γ, β-β, β-ν. In the latter case, there are two general properties of the radiations which divide the field of angular correlation into (a) "directional correlation", wherein one is interested in the relative probability of emission of the second radiation as a function of angle relative to the first, and (b) "polarization correlation", wherein one is interested in the absolute or relative polarizations of either or both of the radiations as a function of included angle. The original theoretical investigation in this field was concerned with gamma-gamma directional correlation and as mentioned previously was done by Hamilton (1H40). Since this investigation is concerned with gamma-gamma directional correlation, we will

sketch Hamilton's arguments in some detail.

Hamilton starts by considering a nucleus in an excited state, A_ℓ, where ℓ refers to the magnetic quantum number and A refers to all other quantum numbers. This nucleus is to decay to a ground state, C, by way of an intermediate state, B. In so doing it must emit two gamma quanta, each characterized by a propagation vector, $\vec{k}$, and a polarization unit vector, $\hat{e}$. (The propagation vector, $\vec{k} = k\vec{k}_0$, where $\vec{k}_0$ is a unit vector in the direction of propagation and $k = \frac{2\pi}{\lambda}$ where λ is the wavelength of the gamma ray). Subscripts 1 and 2 on the propagation vectors hereafter will refer to the first and second transitions respectively.

There are two very general propositions concerning a radiating system of such nuclei which underly this theory. They are stated below without proof:

(1) Assuming the radiation is detected by direction insensitive counters, each of the three states involved is oriented completely at random. The expression "oriented completely at random" as used here has a very precise meaning, which is:

(a) equal populations among the magnetic substates, and

(b) random, i.e. unrelated, phases among the wave functions of the magnetic substates.

(Orientation at random is necessary in order that each substate be an independent radiating system).

(2) Each of the two readiations involved is completely isotropic.

At first it may seem nothing short of amazing that out of propositions (1) and (2), which apparently express the "acme of isotropy", we can derive a theory which predicts an anisotropy, i.e. a correlation.

But this is so, and this idea occupies a central place in the theory. The clue to resolving the apparent anomaly is that if we put a condition on the population we consider and count only that sub-population in B whose preceeding radiation went in a certain direction, θ_1 , with respect to the z axis, then the distribution of this sub-population is not necessarily equal nor are its phases necessarily random. This condition can be compared to that reported by the census taker, "The population of this state is uniformly distributed in area, however those whose parents came from Ireland live predominantly in the northeast". So much for similes.

This idea is important enough to belabor a little further with a quantitative approach. Let the relative transition probability per unit time from state A_ℓ to state B_m be $g_{\ell m}$. Then from (1) the total rate of radiation from each substate in A must be equal, hence:

(3) $\sum_m g_{\ell m}$ is independent of ℓ , and since the various substates of B must be equally populated:

(4) $\sum_\ell g_{\ell m}$ is independent of m . And since the radiation is isotropic by (2), each mode of a given multipole order of radiation must be equally excited:

(5) $\sum_\ell g_{\ell,\ell+m}$ is independent of m , where $-L \leq m \leq +L$ if L is the multipole order of the radiation.

Let $\phi_{L,m}(\theta_1)$ be the angular distribution of a multipole of order L carrying an angular momentum whose z axis projection is given by m . The relative number of quanta in the $A_\ell \rightarrow B_m$ transition for example that proceed into a solid angle $d\omega$ at an angle of θ_1 with the z axis is given by $g_{\ell m}\phi_{L,\ell-m}(\theta_1)d\omega$. It can further be shown that the following is a property of the distribution functions:

(6) $\sum_{m=-L}^{L} \phi_{L,m}(\theta_1)$ is independent of θ_1 .

We will now proceed to show that these relations imply mathematically that the first transition is isotropic - - - which they must, for they were based on that hypothesis (2).

From the conservation of angular momenta:

(7) $\ell = m + m$

Let the angular distribution of the first transition be given by $W(\theta_1)$. Then:

(8) $W(\theta_1) = \sum_{\ell} \sum_{m=-L}^{L} g_{\ell,\ell-m}\, \phi_{L,m}(\theta_1)$

Applying (5), (8) becomes:

(9) $W(\theta_1) = \sum_{\ell} g_{\ell,\ell} \sum_{m=-L}^{L} \phi_{L,m}(\theta_1)$

which by (6) is independent of θ_1 , hence isotropic.

We will now show mathematically that the total population of the states B_m is independent of m , which again is directly from hypothesis, but that the sub-population, arising from radiations in the direction θ_1 is not necessarily independent of m , hence the second radiation from these particular substates is not necessarily isotropic:

Let P_m be the relative probability that a state B_m is occupied.

Let $P_m(\theta_1)$ be the relative probability that a state B_m is occupied through a radiative transition proceeding in the direction θ_1 with respect to the z axis.

Then we can write immediately:

(10) $P_m = \sum_{\ell} g_{\ell m}$ which by (4) is independent of m , and:

(11) $P_m(\theta_1) = \sum_{\ell} g_{\ell,m} \phi_{L,\ell-m}(\theta_1)$ which by (10) is not necessarily independent of m . This was to be shown.

After going through a derivation based upon a system of quantized radiators and field oscillators, Hamilton obtains the following expression for the complete correlation function:

$$(12)\quad W(\vec{\kappa}_{o1},\vec{\kappa}_{o2}) = \sum_1 \sum_2 \sum_{\ell,p} \left| \sum_m (A_\ell | H(\vec{\kappa}_{o1},\vec{e}_1) | B_m)(B_m | H(\vec{\kappa}_{o2},\vec{e}_2) | C_p)^* \right|^2$$

where $\sum_1$ and $\sum_2$ represent averaging over all non-observed properties of the radiations 1 and 2 such as polarization, and where $H(\vec{\kappa}_o,\vec{e})$ is the perturbing Hamiltonian, given by:

$$(12a)\quad H(\vec{\kappa}_o,\vec{e}) = -\int \vec{\imath}\cdot\vec{A}\,dv = -q_\beta c^{-1}\vec{e}\cdot\int \rho\vec{r}\, e^{i(\kappa\vec{\kappa}_o\cdot\vec{r})}\,dv$$

where $\vec{A} \equiv$ vector potential of the radiation field taken in the gauge where scalar potential is zero,

$\vec{\imath} \equiv$ current density of the radiating system,

$\rho \equiv$ charge density of the radiating system,

$q_\beta \equiv$ time dependent amplitude of radiation field oscillator and is independent of position,

$\vec{r} \equiv$ position vector, and

$\vec{e}, \vec{\kappa}_o, \kappa$ as before.

The cross terms in (12) resulting from the summation over m before squaring make it very unwieldy. Hamilton goes on to show that these cross terms arise because the phases in state B are no longer random, that if the phases were random the cross terms would vanish, and hence the summation over m could take place after squaring. He further shows that the phases are random if one takes the z axis as the direction of the first emission. Several authors have proved this theorem also, but an especially simple proof is due to Lippmann (1L52) and is included here because of its physical insight. Lippmann's proof is based on a fundamental quantum mechanical theorem: " - the probability of a transition from an initial to a final state, via a set of intermediate states contains interference terms only when it is not possible to measure (- without disturbance -) the intermediate state; if the experiment is inherently capable of specifying the particular intermediate state the system passes

through, the classical law of compounding independent probabilities holds and no interference terms occur -[11]. Since we are measuring precise angles, a plane wave description of the emitted particles is appropriate (- $\vec{k}_{01}$ and $\vec{k}_{02}$ well defined -). Now if the z axis is chosen parallel to $\vec{k}_{01}$, then the description of the emission of the first particle is invariant under a rotation of the coordinate system about $\vec{k}_{01}$ (assuming we average over polarizations); hence the total magnetic quantum number as well as the quantum numbers of the emitted particles (L_1, m_1) are constants of the motion. (It can be shown by other means that under these conditions $m_1 = \pm 1$). If we consider our radiating system to be a single nucleus, the substate, A_ℓ , before the first emission is in principle measurable, and since our measurement of the first quanta did not disturb the system, the specification of substate B_m follows on the basis of the conservation of angular momentum. Then the theorem (about the absence of cross terms) follows.

Thus when we define $\vec{k}$ as a unit vector parallel to the z axis, we lose our cross terms and (12) reduces to:

$$(13)\quad W(\vec{k}, \vec{k}_{02}) = \sum_1 \sum_2 \sum_{\ell,p,m} \left| (A_\ell | H(\vec{k}, \vec{e}_1) | B_m)(B_m | H(\vec{k}_{02}, \vec{e}_2) | C_p) \right|^2$$

If we let the relative probability for a transition from state B_m to state C_p at a direction θ relative to the z axis be $P_{mp}(\theta)$, then:

$$(14)\quad P_{mp}(\theta) = \sum_2 \left| (C_p | H(\vec{k}_{02}, \vec{e}_2) | B_m) \right|^2$$

And with a similar definition for the first transition (13) becomes:

$$(15)\quad W(\theta) = \sum_{\ell,m,p} P_{\ell m}(0)\, P_{mp}(\theta)$$

(15) is presented here because of the interesting manner in which the individual transition probabilities decompose:

(16) $P_{mp}(\theta) = \left[(I_b\ L_2\ m\ m_2 | I_b\ L_2\ I_c\ p) \right]^2 F_{L_2}^{m_2}(\theta)$

with $\vec{I}_b = \vec{L}_2 + \vec{I}_c$

and $m = m_2 + p$

where $I_b \equiv$ the spin of state B_m,

$I_c \equiv$ the spin of state C_p,

$L_2 \equiv$ the multipole order of the second radiation,

$m \equiv$ the magnetic quantum number of state B_m,

$p \equiv$ the magnetic quantum number of state C_p, and

$m_2 \equiv$ the magnetic quantum number of the second radiation.

The first factor in (16) is the well known Clebsch-Gordon coefficient in the notation of Condon and Shortley (1C35). It depends only upon the quantum numbers of the radiation and the states involved, and gives the intensity for the particular transition. The second factor gives the angular distribution for the particular transition and depends only upon the quantum numbers of the radiation. Falkoff and Uhlenbeck (1F50) give the general expression for the angular distribution functions and the particular examples given are for diple and quadrupole radiation.

Hamilton expressed (13) finally as a cosine power series in which due to the properties of the $F_L^m(\theta)$ only even powers appear:

(17) $$W(\theta) = \sum_{K=0}^{K'} a_{2K} \cos^{2K}\theta$$

The series terminates and Yang (1Y48) showed that the highest K is given by:

(18) $K' \leq L_1$, $K' \leq L_2$, $K' \leq I_b$

whichever is least.

Hamilton calculated a_2/a_0 and a_4/a_0 for all combinations of multipolarities up to and including quadrupole.

It was later found that if one expresses the correlation function as a series in LeGendre polynomials,

(19) $$W(\theta) = \sum_{K=0}^{K'} A_{2K} P_{2K}(\cos\theta)$$

the coefficients, A_{2K}, can be expressed quite generally and explicitly, and that (18) still applies. This was first shown by Gardner (1G49) for the case of conversion electrons, and was later extended by others to arbitrary radiations. It turns out that the A_{2K} can be decomposed into two factors:

(20) $$A_{2K} = (AB)_{2K}(BC)_{2K}$$

where the first factor contains parameters relevent only to the first ($A \rightarrow B$) transition and the second factor, those parameters relevent only to the second ($B \rightarrow C$) transition. The expression for the first factor is given below, the second being similar in all respects:

(21) $$(AB)_{2K} = \sum_{m_1} [(L_1 L_1 m_1 - m_1 | L_1 L_1 2K 0)] (-1)^{m_1} F_{L_1}^{m_1}(0) \times W(I_b I_a 2K L_1; L_1 I_b)$$

where the W is the "Racah coefficient", Racah (1R42), and all other factors are as given before (16).

Using (21) we can now calculate gamma-gamma directional correlations explicitly, with a few reservations as indicated below. For example, one can find the Clebsh-Gordon coefficients in Condon and Shortley (1C35), the Racah coefficients can be found in (2B52), and the $F_{L_1}^{m_1}(0)$ can be found in (1F50).

However, these correlation coefficients, A_{2K} , have been calculated explicitly and presented in convenient form by Lloyd (1L51).

Now, it seems, it would be appropriate to point out two

limitations on the theory as developed so far and as applied to gamma-gamma directional correlations:

Limitation 1 - The above theory refers only to pure multipole transitions. It cannot handle, for example, parity forbidden transitions which proceed partly by magnetic 2^n-pole and partly by electric $2^{n\neq1}$-pole radiations.

Limitation 2 - The above theory assumes that the intermediate state is unperturbed. As was pointed out previously, the existence of a directional correlation depends upon unequal populations among the various sub-states B_m. A perturbation applied to the intermediate state would tend to cause a mixing of these states and hence a relaxation towards a uniform population. Any such equalization would then by propositions (1) and (2) above cause a reduction in the correlation.

Limitation 2 has been removed by Ling and Falkoff (1L49). They calculated the effects of various mixing ratios in the magnetic n-pole and electric n≠1-pole mixed transitions. Their results however are complicated by the presence of an undetermined relative phase factor in the ratio of these matrix elements. Lloyd (2L51) showed however that only a relative phase of 0^o or 180^o had physical significance.

Limitation 2 is still very much with us. However it has turned out to take on more the qualities of an asset than a limitation. For by studying the reduction in the correlation caused by the perturbation of the intermediate state we can learn something about the electric and magnetic moments of this state. This study becomes the field of "disturbed angular correlations" and is the subject of the next chapter.

Chapter 3 - Theory of Disturbed Angular Correlation

General interest in the subject of disturbed angular correlation arose when several correlations were observed which did not fit any consistent theoretical predictions. The situation was further confused in that the observed correlations seemed to depend on the physical and chemical state of the source. The most famous of these "anomalous correlations" is the gamma-gamma cascade in Cd^{111}, the daughter by K capture of In^{111}; see for example Boehm and Walter (1B49)), Roberts and Steffen (1R51), and Frauenfelder (2F51).

It became apparent that these "spoilages" of the correlation might be the result of a perturbation of the intermediate state during its period of existence between the emissions of the first and second quanta. For, as we have seen one of the basic assumptions of the "undisturbed" theory is that the intermediate state remain unperturbed during its lifetime. Several authors, including Goertzel (1G46) and Alder (1A52) have developed successful theories based on the interaction of various nuclear moments of the intermediate state with perturbing fields. We shall confine ourselves to tracing a theory due to Abragam and Pound (1A53) which is recommended by its generality.

Abragam and Pound show that the effects of such a perturbation can always be represented in the form:

$$(1)\quad W(\theta) = \sum_{k} G_{2k} A_{2k} P_{2k}(\cos\theta)$$

where the A_{2k} are the "unperturbed" coefficients and the G_{2k} which contain all of the perturbing effects act as damping factors on the unperturbed coefficients.

They point out several interesting points in connection with the G_{2k} relative to the type of source; namely:

(a) If the source is in the form of a polycrystalline powder the G_{2K} approach a minimum or "hard core" value as the magnitude of the perturbing interaction increases without limit; hence the correlation is never completely destroyed.

(b) If the source is in the form of a single crystal, $0 \leqslant G_{2K} \leqslant 1$, depending on the orientation of the crystal axis and the strength of the interaction.

(c) If the source is in the liquid state the G_{2K} can approach zero as the magnitude of the perturbing interaction increases without limit.

Abragam and Pound start with Hamilton's basic directional correlation equation (2-13), slightly modified to conform to the former's notation:

(2) $$W(\theta) = \sum_{1,2} \sum_{\alpha,c,\beta,\beta'} (\alpha|H_1|\beta)(\beta|H_2|c)(c|H_2|\beta')(\beta'|H_1|\alpha)$$

where α, c represent quantum numbers of the first and third states respectively, and β, β' represent quantum numbers of any complete set in the intermediate state, B. H_1 and H_2 are the interaction Hamiltonians for the emission of the first and second particles respectively (See 1-12).

Let us suppose that the first emission takes place at time $t = 0$, and that during time t the intermediate state is perturbed by some Hamiltonian $\vec{K}$. The effects of this interaction can be represented by an evolution operator, $\vec{U}(t)$, acting on the intermediate state:

(3) $$\gamma(t) = \vec{U}(t)\beta$$

where $\gamma(t)$ represents the intermediate state vector after transormation by the interaction.

$\vec{U}(t)$ can be represented as follows:

(4a) $\vec{U}(t) = e^{-i\frac{\vec{K}t}{\hbar}}$

for static $\vec{K}$, or:

(4b) $\vec{U}(t) = e^{-i\frac{\int_0^t K(t')dt'}{\hbar}}$

for time dependent $\vec{K}$.

If now we substitute (3) into (2) we have the time dependent correlation function:

(5) $\omega(\theta,t) = \sum_{1,2} \sum_{\alpha,c,\beta,\beta'} (\alpha|H_1|\beta)(\beta|\vec{U}^{\dagger}(t)H_2|c)(c|H_2\vec{U}(t)|\beta')(\beta'|H_1|\alpha)$

where $\vec{U}^{\dagger}$ is the Hermetian conjugate of $\vec{U}$.

We must now consider the probability of emission of the second particle between time t and $t+dt$. This was ignored in the undisturbed theory because it yielded only a constant multiplicative factor. However, in our case we must consider the fact that the relative probability for emission of the second radiation between time t and $t+dt$ is given by:

$$\frac{1}{\tau_N} e^{-t/\tau_N} dt$$

where we consider the source as a whole. If we record all events taking place until time t_2 , our function becomes:

(6) $W(t_2,\tau_N,\theta) = \sum_{1,2} \sum_{\substack{\alpha,c,\\ \beta,\beta'}} \int_0^{t_2} e^{-\frac{t}{\tau_N}} (\alpha|H_1|\beta)(\beta|\vec{U}^{\dagger}H_2|c)(c|H_2\vec{U}|\beta')(\beta'|H_1|\alpha)\frac{dt}{\tau_N}$

If $\vec{K}$ is static we can choose for β , the eigen vectors of $\vec{K}$, which we define as b ; then (6) becomes:

(7) $W(t_2,\tau_N,\theta) = \sum_{1,2} \sum_{\substack{\alpha,c,\\ b,b'}} \int_0^{t_2} e^{-\frac{t}{\tau_N}+i\frac{(E_b-E_{b'})t}{\hbar}} \frac{dt}{\tau_N} (\alpha|H_1|b)(b|H_2|c)(c|H_2|b')(b'|H_1|\alpha)$

and if we let $t_2 \to \infty$, we have finally the result obtained also by Goertzel (1946):

(8) $W(\tau_N,\theta) = \sum_{1\,2} \sum_{\alpha,c,b,b'} \frac{(\alpha|H_1|b)(b|H_2|c)(c|H_2|b')(b'|H_1|\alpha)}{1 - i\frac{(E_b-E_{b'})}{\hbar}\tau_N}$

Abragam and Pound's next step is to reformulate the correlation function in a form convenient for the isolation of the perturbing terms. They use an expression similar to one derived originally by Alder (1A52):

$$(9)\quad \omega(t,\vec{\Omega}_1,\vec{\Omega}_2) = \sum_{i,2} \sum_{\substack{K_1,K_2,\\ \mu_1,\mu_2}} \mathrm{I}(K_1)\mathrm{II}(K_2)\,\mathrm{III}(K_1K_2\mu_1\mu_2 t)\, Y_{K_1}^{\mu_1}(\vec{\Omega}_1) Y_{K_2}^{\mu_2}(\vec{\Omega}_2)$$

where the $Y_K^{\mu}(\vec{\Omega})$ are ordinary spherical harmonics in which $\vec{\Omega}_1$ and $\vec{\Omega}_2$ specify the direction of emission of the first and second quanta respectively, I and II are coefficients which are independent of the perturbing Hamiltonian; and all of the effects of the perturbation are contained in III.

If the perturbing field can be described classically, $\mathrm{III}(K_1K_2\mu_1\mu_2 t)$ is expressed by:

$$(10)\quad \mathrm{III}(K_1K_2\mu_1\mu_2 t) = \sum_{\substack{m\,m'\\ m''\,m'''}} (\mathrm{I}K_1m'\mu_1|\mathrm{I}K_1\mathrm{I}m)(\mathrm{I}K_2m'''\mu_2|\mathrm{I}K_2\mathrm{I}m'') \times (m|\vec{U}^{+}|m'')(m'''|\vec{U}|m')$$

where the first two factors are Clebsch-Gordon coefficients in the notation of Condon and Shortley (1C35), the $\vec{U}$ is an evolution operator, and the m's are the eigen values of the intermediate states $\mathcal{B}_m$ which are chosen to be eigen functions of I_z.

If the perturbing Hamiltonian, $\vec{K}$, is static and if we define b as an eigen state of this Hamiltonian, then the $\vec{U}$ can be represented as:

$$(11)\quad \vec{U} = \sum_b |b)(b|\, e^{-i\frac{E_b t}{\hbar}}$$

With this substitution (10) becomes:

$$(12)\quad \mathrm{III}(K_1K_2\mu_1\mu_2 t) = \sum_{\substack{m\,m'\\ m''\,m'''\\ b\;b'}} (\mathrm{I}K_1m'\mu_1|\mathrm{I}K_1\mathrm{I}m)(\mathrm{I}K_2m'''\mu_2|\mathrm{I}K_2\mathrm{I}m'') \times (m|b)(b|m'')(m'''|b')(b'|m') \times e^{i\frac{(E_b-E_{b'})t}{\hbar}}$$

Now, considering the source as a whole just as in (6) if all coincidences are registered we must integrate $\omega(t)$ with a decay weighting factor:

$$(12a)\quad W = \int_0^\infty \omega(t) e^{-\frac{t}{\tau_N}} \frac{dt}{\tau_N} = \sum_{1,2} \sum_{K_1 K_2 \mu_1 \mu_2} I_{(K_1)} II_{(K_2)} III_{(K_1 K_2 \mu_1 \mu_2)} Y_{K_1}^{\mu_1}(\vec{\Omega}_1) Y_{K_2}^{\mu_2}(\vec{\Omega}_2)$$

Then the integrated coefficient, $III_{(K_1 K_2 \mu_1 \mu_2)}$, becomes:

$$(13)\quad III_{(K_1 K_2 \mu_1 \mu_2)} = \sum_{\substack{m\ m' \\ m''\ m''' \\ b\ b'}} (I K_1 m' \mu_1 | I K_1 I m)(I K_2 m''' \mu_2 | I K_2 I m'') \times (m|b)(b|m'')(m'''|b')(b'|m') \times \left[1 - i\frac{(E_b - E_{b'})\tau_N}{\hbar}\right]^{-1}$$

From (9) and (13) we can see why if the interaction Hamiltonian for the perturbation is invariant under a rotation about the z axis and if the first particle goes in the direction of the z axis then the correlation is undiminished. In the first place, if the particle goes in the z direction, the only term of the $Y_{K_1}^{\mu_1}(0)$ which does not vanish will be where $\mu_1 = 0$. Since the Hamiltonian is invariant under a rotation about the z axis, it commutes with I_z, hence $E_b = E_m$ and from the first Clebsch-Gordon coefficient in (13) we see that since $m = m' + \mu_1$ that $m = m'$. Thus $E_b = E_{b'}$ in (13) and the denominator reduces to unity. Now due to the various summations over b and b', we have the multiplicative factors of $\delta_{m,m''}$ and $\delta_{m''',m'}$ which when we remember that $m = m'$, imply that $m'' = m'''$ hence $\mu_2 = 0$. Then $III_{(K_1 K_2 0 0)} = \frac{2I+1}{2K+1}\delta_{K_1,K_2}$ which is the normalized form. We have thus shown that under these conditions the theory predicts the well known experimental result that the correlation is unperturbed.

We are now ready to consider the problem of the crystalline powder, or polycrystalline source, as it is called. The observed correlation, $\overline{W(\Psi)}$, is obtained by averaging (9) or (13) over

all possible orientations of the various micro-crystalline frames of reference which is equivalent to integrating the spherical harmonics, $Y_{K_1}^{\mu_1}(\vec{\Omega}_1) Y_{K_2}^{\mu_2}(\vec{\Omega}_2)$, over the unit sphere, keeping always the angle between $\vec{n}_1$ and $\vec{n}_2$ fixed; this angle we call Ψ . If we do this we find from the orthogonality of the spherical harmonics that the only non-vanishing products are where $K_1 = K_2 = K$ and $\mu_1 = \mu_2 = \mu$. It also turns out that the integral so defined is independent of μ . The observed correlation can then be written, if we average (9) to obtain the time dependent correlation:

$$(14)\quad \overline{W}(t) = \sum_K G_K(t) A_K P_K(\cos\Psi)$$

where:

$$(15)\quad G_K(t) = \frac{1}{2I+1} \sum_\mu III(KK\mu\mu t)$$

If we average the integrated correlations we obtain:

$$(16)\quad \overline{W}(\tau_N) = \sum_K G_K(\tau_N) A_K P_K(\cos\Psi)$$

where

$$(17)\quad G_K(\tau_N) = \int_0^\infty G_K(t) e^{-\frac{t}{\tau_N}} \frac{dt}{\tau_N}$$

Notice that the G_K factors which contain all of the effect of the perturbing Hamiltonian are simple reduction factors which cause no mixing of the unperturbed coefficients. Also, the G_K factors depend only upon the intermediate state and not upon the preceeding or succeeding radiative transitions.

We give below an explicit expression for the time dependent as well as integrated G_K's where the perturbing field can be <u>described classically</u> and has <u>axial symmetry</u> with respect to the micro-crystalline axes:

$$(18)\quad G_K(t) = \frac{1}{2I+1} \sum_{m,m',\mu} (IKm'\mu | IKIm)^2 e^{i\frac{(E_m - E_{m'})t}{\hbar}}$$

(19) $$G_K(\tau_N) = \frac{1}{2I+1} \sum_{\substack{m,m' \\ \mu}} \frac{(I K m' \mu | I K I m)^2}{1 - i\frac{(E_m - E_{m'})}{\hbar}\tau_N}$$

So far we have said nothing of the nature of the perturbing interaction, i.e. whether magnetic or electric in nature. If we assume for a moment that we are concerned with the interaction of the nuclear electric quadrupole moment with the average electric field gradient, classically describable and axially symmetric, at the nucleus, then the perturbing Hamiltonian is already diagonalized and its eigen values are:

(20) $$E_m = \frac{eQ\left(\frac{\partial^2 V}{\partial z^2}\right)\left[3m^2 - I(I+1)\right]}{4I(2I-1)}$$

where eQ is the nuclear quadrupole moment, defined:

$$eQ \equiv \sum_{j=1}^{Z} \int e(3\cos^2\theta_j - 1) r_j^2 \left|\Psi(\vec{r}_1 \cdots \vec{r}_A)\right|^2 d\tau$$

the summation going over all protons where θ_j is the angle between $\vec{r}_j$ and the nuclear symmetry axis.

If we now substitute (20) into (18) we obtain an explicit expression for the effects of the electric quadrupole interaction which for $I = 2$ we write:

(21) $$G_{2e}(t) = \frac{1}{5}\left[\frac{13}{7} + \frac{2}{7}\cos\omega_{oe}t + \frac{12}{7}\cos 3\omega_{oe}t + \frac{8}{7}\cos 4\omega_{oe}t\right]$$

$$G_{4e}(t) = \frac{1}{9}\left[\frac{29}{7} + \frac{12}{7}\cos\omega_{oe}t + \frac{16}{7}\cos 3\omega_{oe}t + \frac{6}{7}\cos 4\omega_{oe}t\right]$$

where ω_{oe} is the energy difference divided by $\hbar$ between the levels which are split the least by the interaction; for $I = 2$ this yields, $\omega_{oe} = \frac{eQ\left(\frac{\partial^2 V}{\partial z^2}\right)}{8}$

If on the other hand we consider a perturbation due to a classically describable, axially symmetric with the various micro-crystalline axes, magnetic field which interacts with the magnetic moment of the nucleus, we have:

(22) $$E_m = -\vec{\mu}\cdot\vec{H} = -\frac{\mu H m}{I} = -\hbar\omega_{o_m} H m$$

where μ is the nuclear magnetic moment in nuclear mag-

netic moment in nuclear magnetons, H is the magnetic field, m the magnetic quantum number, and ω_{0m} is the angular velocity of Larmour precession given by $\frac{\mu H}{\hbar I}$.

As before, by introducing (22) into (18) we obtain for $I = 2$:

(23) $$G_{2m}(t) = \frac{1}{5}\left[1 + 2\cos\omega_{0m}t + 2\cos 2\omega_{0m}t\right]$$

$$G_{4m}(t) = \frac{1}{9}\left[1 + 2\cos\omega_{0m}t + 2\cos 2\omega_{0m}t + 2\cos 3\omega_{0m}t + 2\cos 4\omega_{0m}t\right]$$

There are two important features of (21) and (23) which bear noting:

(a) The $G_k(t)$'s are periodic functions of time with a maximum value of unity and a period of $\frac{2\pi}{\omega_0}$. This periodicity arises from the axially symmetric nature of the fields which split the energy levels in rational multiples of the minimum splitting. Fields of lower than axial symmetry remove the necessarily periodic nature of the $G_k(t)$'s.

(b) The integrated $G_k(2\tau_N)$'s , given by (17), which are observed by a coincidence circuit whose resolving time is long compared to the nuclear lifetime, have a lower limit (given by the leading terms in (21) and (23)) known as the "hard core". This implies that the anisotropy will also have a "hard core" no matter how strong the interaction, $\omega_0\tau_N$. As will be seen, this is not necessarily so in liquid sources, where a sufficiently strong interaction can reduce the anisotropy to zero.

The theory of spoilage by axially symmetric, classically describable perturbing fields in polycrystalline sources as described above has been tested experimentally and in some cases (1K53) gives correct results. However, the results of Aeppli et. al. (1A51) and Steffen (2S53) (1S53) on various compounds of Cd^{111}, the daughter by K capture of In^{111}, show reductions in anisotropies to values lower than predicted by the theory of

axially symmetric perturbing fields as put forth above. The undisturbed anisotropy of the Cd^{111} cascade is about -0.2; the axially symmetric theory predicts a "hard core" anisotropy of about -0.05. For example Steffen (2S53) reported among others the following anisotropies:

Source::	Anisotropy:
$InCl_3$ dry @ 20°C	-.012 ± .005
@ 540°C	-.022 ± .006
InI_3 dry @ 20°C	-.020 ± .006
@ 200°C	-.021 ± .006
Average of above	-.019 ± .003

It is not surprising that the spoilage theory based on the assumption of simple axially symmetric fields does not give precise results. We shall present below a discussion of two of the possible mechanisms for the spoilage of polycrystalline sources below the predicted hard core values.

The first explanation has to do with the symmetry of the fields experienced by the nucleus. The fields in polycrystalline sources are extremely complex, and even if the indium atom in a single isolated crystal were in a field of axial symmetry, when there are many millions of microcrystals close together, oriented at random, and pressing on one another from all sides, there is good reason to believe that the aforementioned axially symmetric fields could be distorted to a lower degree of symmetry. Also, following a process such as K capture in In^{111}, the daughter cadmium atom may have sufficient recoil energy to displace it from its former axially symmetric lattice site. Abragam and Pound (1A53) calculate the effects of fields of lower than axial symmetry. They give the hard

core values for G_K's in rhombic fields for various values of the spin of the intermediate state. They find that there is indeed a reduction of the G_K's over and above that obtained with axially symmetric fields; however, the resulting reduction in the anisotropy is still not sufficient to explain the results of 1S53 and 1A51. For information we list here the results of their calculations for the hard cores for I = 2:

	Rhombic Fields	Axially Symmetric Fields
$G_2(\text{lim})$	10/35	13/35
$G_4(\text{lim})$	18/63	29/63

It may be of interest to note here that if the perturbations remove all degeneracies, the hard core value of G_k should be $G_k(\text{lim}) = \frac{1}{2k+1}$. Comparing this with the above results we see that the rhombic fields apparently remove some but not all of the degeneracies present in the axially symmetric case.

The second possible mechanism for spoilage below the predicted hard core value, and it seems the most fruitful to date, has to do with the excited state of the electronic configuration of the daughter atom. Immediately following K capture the daughter atom is in a very highly excited atomic state with a hole in the innermost shell. The electronic configuration returns to the ground state by the emission of X-radiation and the production of Auger elections as the "hole" moves outward. As more and more Auger electrons are produced the atom tends to assume a considerable charge, and each Auger electron itself adds another "hole" to the configuration. After a short while the atom begins to "look" like a "Swiss cheese" as Frauenfelder puts it. Under such conditions the nucleus experiences extremely

large and rapidly fluctuating magnetic fields and electric field gradients due to its own electron cloud. It seems possible that this could cause a time dependent perturbation very similar to that which would be experienced by the nucleus of an ion in a liquid under the influence of the random motion of its neighbors; let us call this the "confused configuration effect". And in a liquid, as will be seen, there is no lower limit or hard core to the anisotropy for a sufficiently strong interaction. On the other hand if the nucleus were to "see" during its lifetime fields due to its own electrons which were constant for a while and which would then vary stepwise, it is possible that it could get down to one hard core value in this time and then with the stepwise variation in the electronic configuration, start down toward a new and still lower hard core. Let us call this the "quasi-static configuration effect".

To test the validity of the K capture excitation hypothesis Kraushaar and Pound (1K53) performed a directional correlation experiment using the 396 KEV isomeric level of Cd^{111} as the parent of the decay. Here, the electron shells of the cadmium atom are unperturbed during the decay, except possibly by internal conversion. Kraushaar and Pound used several sources differing in chemical and physical state. It was found that the maximum spoilage of the anisotropy occured in a polycrystalline source of hexagonal $CdCl_2$, and significantly this reduction was down to, but not below, the hard core as predicted by the theory of axially symmetric fields.

We will now introduce what is called the "shell relaxation time", τ_s, which we can think of as the mean time required for the electronic configuration to return to the ground state

following a strong excitation such as K capture. We list below two typical values of τ_s for different materials from (1H52):

Material:		:
Impurity Centers in Ionic Crystals	>>	10^{-8} seconds
Metals	$\approx$	10^{-12} seconds

We can fit three experiments into the pattern of explanation of the "excited configuration" hypothesis. In the experiment of Albers-Schonberg et. al. (2A53), using a source consisting of a single axially symmetric crystal of indium metal, the effect is noteworthy because of its absence. For certain orientations of the crystal axis the observed anisotropy was essentially unperturbed which hardly seems possible on the basis of the "excited configuration" hypothesis. This can be explained, however, as the result of an extremely short shell relaxation time in metals ($\approx 10^{-12}$ seconds, above). In Cd^{111} the lifetime of the intermediate state is 8.5×10^{-8} seconds, and when the shell relaxation time is very much shorter than the nuclear lifetime the effect has too little time to take place and shows but little disturbance to the anisotropy. This is similar to the case in liquids wherein the correlation time is very much shorter than the nuclear lifetime; the liquid theory will be presented later.

On the other hand, the experiment of Steffen (2S53) cannot be explained on the basis of the "confused configuration" effect, if we believe the figure above of $\tau_s >> 10^{-8}$ s. for impurities in ionic crystals. For here $\tau_s > \tau_N$, and under such conditions the nucleus sees practically constant fields due to its own electronic configuration, as will be seen. This requires the application of a modified polycrystalline theory considering the quantum mechanical coupling between the nucleus and electron cloud, taking

into consideration the fact that the angular momentum of the shell, J, is changing during the nuclear lifetime. This, it would seem, is an example of the "quasi-static configuration effect" mentioned earlier. It may be that the reductions in anisotropy below the hard core values observed by Steffen (2S53) could be due to a combination of two independent effects of comparable magnitude, viz. (a) the "quasi-static configuration effect", and (b) the crystalline field effect treated by Abragam and Pound (1A53). In a situation like this we could have an electric quadrupole interaction with the crystalline electric field gradients and simultaneously the superimposed magnetic and electric interactions with the "own-electron" configuration which have not yet "cooled" down to the ground state. The theory has not yet been worked out for such a situation; but this seems a reasonable explanation for the occurence of G_k hard cores lower by a factor of two than those predicted on the basis of "axially symmetric fields" alone.

Futher justification of the "quasi-static" view follows from a simple estimate of the times involved for the outward progression of the K-capture produced hole in the atom. For a first approximation, if we consider the atom alone independent of its neighbors and neglect the additional holes produced by Auger electrons, then we can calculate the time required for the radiation process on the basis of a model in which an electron jumps from the n shell to the n-1 shell with a speed given by shielded hydrogen wave-functions. The first transitions between highly excited atomic states of large energy differences are very fast, being of the order of 10^{-15} seconds; while the later transitions are relatively slow, lying in the range for optical

transitions, or about 10^{-8} seconds. But the important point is that the times for the various transitions are related roughly as a geometric progression, the second requiring about 10 times the time required for the first, etc. This means that on the average during the lifetime of a particular nucleus it has experienced essentially a constant field resulting from the last electron configuration in existence before the nucleus decayed to the final state. In addition, the sum of the times required for the early transitions , if less than 10^{-11} seconds would cause no perturbation just on the basis of its short duration. All of the above seems to lend support to the "quasi-static hypothesis as the additional spoilage mechanism.

On the other hand, because of the possible similarity of the processes experienced by the nucleus after K capture to those in a liquid, we will sketch the results of Abragam and Pound's (1A53) theory of correlation spoilage in liquid sources.

The time dependent correlation in liquids is analyzed using (9). Taking the z axis as the direction to the first counter, μ_1 vanishes as discussed under (13), and since there is no preferred direction in the source μ_2 also vanishes. Then we have:

$$(24)\quad \omega(\theta,t) = \sum_{K_1 K_2} I(K_1)\, II(K_2)\, III(K_1,K_2,0,0,t)\, Y^0_{K_1}(0)\, Y^0_{K_2}(\theta)$$

where the terms are thos of (13) and:

$$(25)\quad III(K_1 K_2 0 0 t) = \sum_{m,m'} (I K_1 m 0 \mid I K_1 I m)(I K_2 m' 0 \mid I K_2 I m') \left|(m' \mid \vec{U}(t) \mid m)\right|^2$$

where $\left|(m' \mid \vec{U}(t) \mid m)\right|^2$ is the probability that a nucleus in an initial state m at t = 0 will find itself in state m' at time t. This relaxation process is what spoils the correlation, for as pointed out in Chapter 2, an unequal population among

the various magnetic substates of the intermediate level is necessary to produce a correlation. Furthermore it can be shown that the rate at which this relaxation process takes place is related linearly to the rate at which the correlation coefficients, A_{2k}, (1) diminish.

In the development of the theory the concept of "correlation time", τ_c , enters. Qualitatively, one can think of the correlation time as the mean time required for a nucleus to interchange its neighbors.

It turns out in the development of the expression for the time dependent transition probability above that when $t \gg \tau_c$, but with the condition that the transition probability is very much less than unity, we can use the theory of polycrystalline sources to describe liquid phenomena. We apply this result by expanding (21) in a power series in t^2 and replacing t^2 by $2t\tau_c$. It is interesting to note that although the G_k's thus obtained fall off as the first power in t, they are still larger than the G_k's from polycrystalline sources because $\tau_c \ll t$. Similarly the not unexpected result that where $\tau_c \gg t$ we may apply polycrystalline solid results to liquid sources evolves from the theory. This is reasonable in that the fields of an infinitely viscous liquid would approach roughly those of a solid except perhaps as related to spatial regularities. It is also interesting to note that in this latter region the "fall-off" of the G_k's as a function of time is parabolic as $t \longrightarrow 0$, just as we find in (21).

In the region in between where the correlation time is neither large nor small with respect to t, explicit results are developed applying only to liquid sources. These results

apply also where $\tau_c \ll t$, but not where $\tau_c \gg t$. The integrated G_k's for $I = 2$ are given as follows:

Electric Quadrupole Interaction:

$$(26)\quad G_2(\omega_{oe}\tau_N) = \frac{1}{1 + \frac{17}{160}\omega_{oe}^2\tau_N\tau_c}\,,\quad G_4(\omega_{oe}\tau_N) = \frac{1}{1 + \frac{1}{16}\omega_{oe}^2\tau_N\tau_c}$$

where

$$\omega_{oe} = \left| \frac{e\,Q\left\langle \frac{\partial^2 V}{\partial z^2} \right\rangle_{AV}}{\hbar} \right|$$

Magnetic Dipole Interaction:

$$(27)\quad G_2(\omega_{om}\tau_N) = \frac{1}{1 + \frac{7}{160}\omega_{om}^2\tau_N\tau_c}\,,\quad G_4(\omega_{om}\tau_N) = \frac{1}{1 + \frac{7}{48}\omega_{om}^2\tau_N\tau_c}$$

where

$$\omega_{om} = \left| \frac{\mu \langle H \rangle_{AV}}{I\,\hbar} \right|$$

It may be of interest to compare the shape of the spoiled anisotropy curve based on G_k's which come from no particular physical model with that resulting from (21) and (23). The purpose is to show the similarity in shape for small values of $\omega_o\tau_N$ of the anisotropy curves arising from $G_k(t)$'s quite different in nature. This is done in Section 5.4.4 based on the following remarks:

Let us construct a $G_k(t)$ in the form of a periodic square wave of half width δ_K , as shown in the diagram at right. Then the integrated $G_k(\omega_o\tau_N)$'s which we will label $G_k'(\omega_o\tau_N)$ are given by:

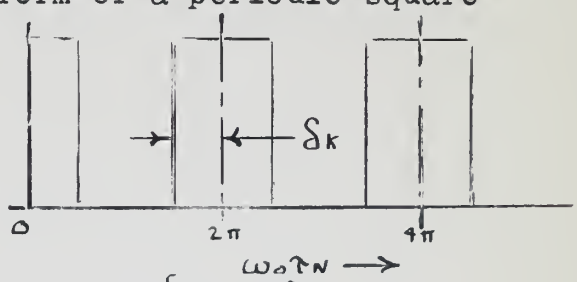

$$(28)\quad G_K'(\omega_o\tau_N) = 1 - e^{-\frac{\delta_K}{\omega_o\tau_N}} + \frac{2\sinh\left(\delta_K/\omega_o\tau_N\right)}{e^{\frac{2\pi}{\omega_o\tau_N}} - 1}$$

Note that the hard core values are given by $\frac{\delta_K}{\pi}$.

The G_k' can be related by applying a modified form of Abragam and Pound's Eq. 41 (1A53), for integral I:

$$(29) \qquad \sum_{K=0} (4K+1)\, \delta_{2K} = (2I+1)\,\pi$$

Chapter 4 - Choosing an Isotope

Out of all the hundreds of isotopes, how does one pick one on which to perform an angular correlation experiment? We sketch below the procedure we used in the hope that it will be of some future assistance. The procedure consists in giving each "candidate" a series of tests and using the comparative overall results as a basis for selection.

These tests can be classified as follows:

1. Decay Scheme
2. Availability
3. History

Decay Scheme

The first thing that must be done is to establish the existence of a cascade. Then the disturbing influence of radiations within the energy resolving power of the apparatus must be considered, and whether these radiations are also in cascade. It will be found in connection with "History" that most of the simple cases have already been studied, hence the necessity for good energy resolution will become more and more important. If we consider gamma-gamma cascades it will be found that in connection with the energies of the radiations there are two very important considerations, viz. (a) that if the lower energy is above a certain minimum then one can use "energy selection shielding" as discussed in Section 5.2.1, and (b) if both energies of the cascade are close enough to one another so that each channel can be sensitive to both radiations, then the coincidence counting rate will be up by a factor of four over the case in which each channel is sensitive to only one of the radiations. (1H53) is a good reference for decay schemes and various other information concerning isotopes. Interpretation

of results becomes easier when we know that at least one of the transitions involved is a pure multipole as we saw in Chapter 2; this is insured if we choose an even-even nucleus where in all known cases except one (Ge^{72}) the first excited state has a spin-parity assignment of 2-plus and a ground state of zero-plus; this insures that the transition between these states will be pure electric quadrupole. See (3S53) for information on excited states of even-even nucleii. The total internal conversion coefficient is also a limiting constraint in the choice if one wishes to do gamma-gamma angular correlation. We chose an arbitrary upper limit to the K-plus-L coefficients of 10; anything above this number we would reject. In general it turns out that for a Z greater than 60 and energy less than 175 KEV the transition will be too highly converted for E2 transitions. (3B52) page 618 and (1G51) give formulae and experimental results relating to internal conversion. As was seen in Chapter 3, in an investigation of "spoiled" correlations the lifetime of the intermediate state is important, and in general should be greater than 10^{-10} seconds, although this lower limit is somewhat flexible. (1G51) contains formulae and experimental results relating to lifetime.

Availability

The availability of an isotope is determined by the availability and lifetime of the parent. If local facilities are unable to produce the isotope then we are limited in general to parent lifetimes of at least several days. (1H53) has information relating to the production of isotopes.

History

Unfortunately there is as yet no comprehensive survey of

experimental results in angular correlations under one cover. So after passing "Decay Scheme" and "Availability" tests and isotope's angular correlation history must be looked up. Of particular interest in disturbed angular correlation work are those cases where previous work has shown anomalies, such as in Pd^{106}.

Our choice of Cd^{114} was based on considerations similar to the above and also due to the history of spoilage in its sister isotope Cd^{111}. See Fig. 4-1 for the decay scheme. Our interest lay in the first excited state in Cd^{114} via the 722-556 KEV gamma-gamma cascade.

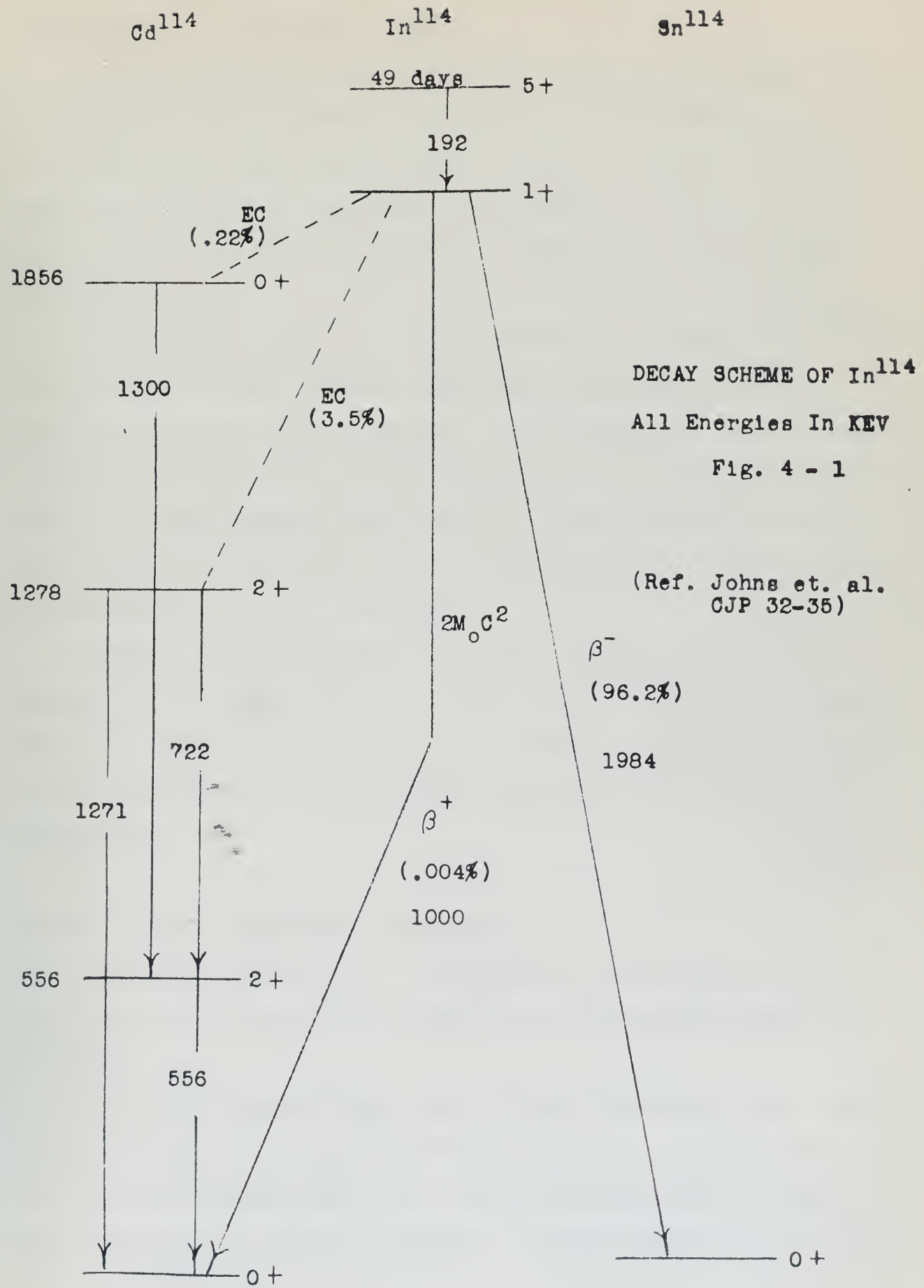

DECAY SCHEME OF In^{114}

All Energies In KEV

Fig. 4 - 1

(Ref. Johns et. al. CJP 32-35)

Section 5.1.1 - Apparatus, General

A directional correlation apparatus must provide means for the detection and exclusion of radiation and for the recording of events. The term "directional" brings to mind the question, "Relative to what?" The answer necessitates the use of two channels, one to fix a direction in space, the other to measure a relative angle.

The exclusion function of the apparatus is very broad. First of all it must exclude radiations proceeding at other than the selected angle. Second, it must exclude in each channel pulses arising from unwanted radiations of various energies. Third, it must compare the pulses in the two channels in time and exclude all those which do not occur simultaneously or within a small time, τ, of one another.

Finally, the apparatus must record certain unexcluded, or selected if you will, events occuring during a given time interval and present them in a convenient manner. To accomplish these ends the apparatus is divided into mechanical and electronic components.

Section 5.1.2 - Apparatus, Mechanical

The mechanical parts of the apparatus are extremely simple and consist of the source box and its included angle measuring assembly.

The source box provides means to mount the source and angle measuring assembly, absorb unwanted radiation, as well as shield the immediate neighborhood from the soft components. It also provides means to change or maintain the temperature of the source and to inhibit frost formation on the source holder, which is accomplished by keeping the box airtight and drying the entrained

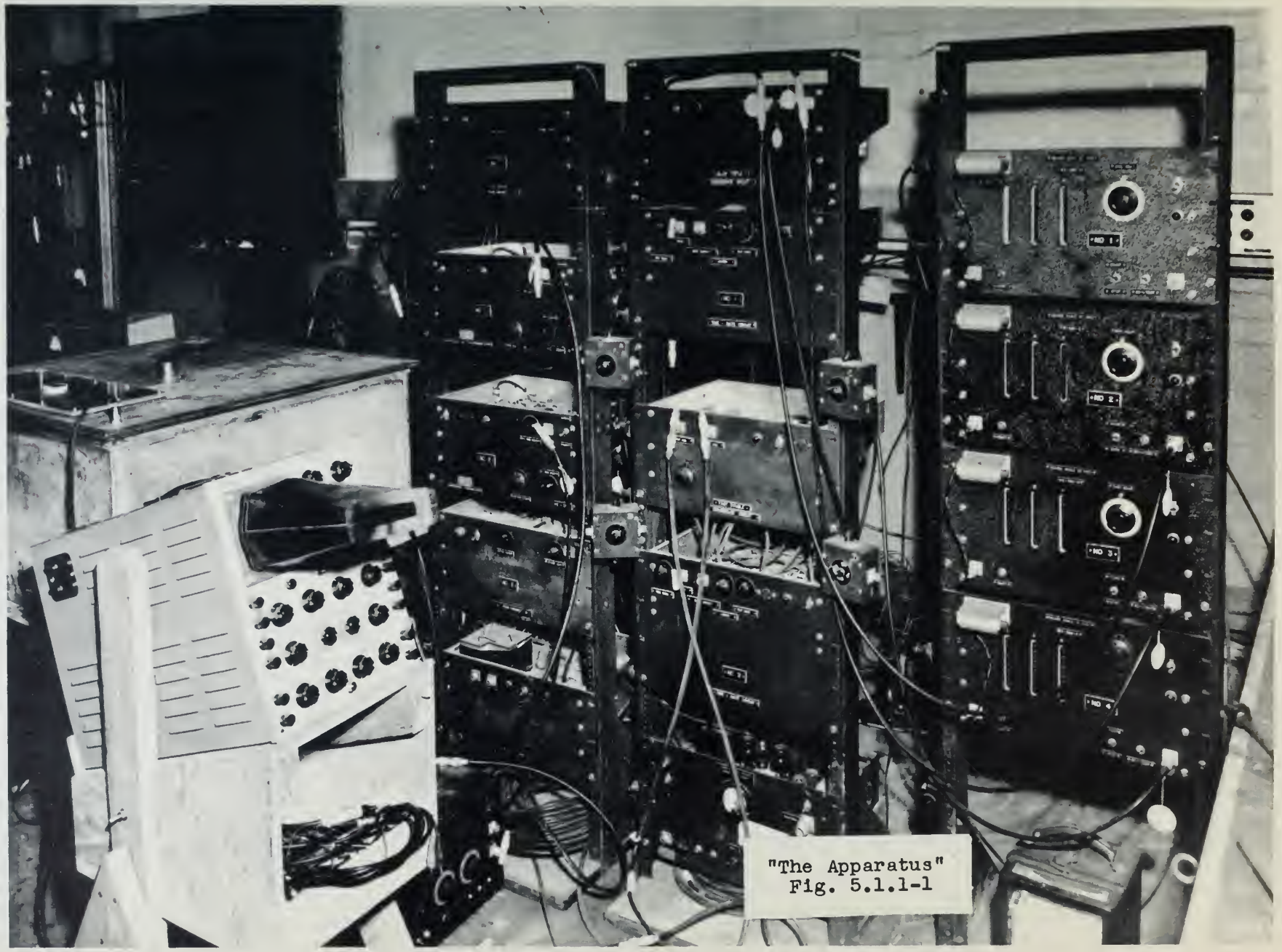

"The Apparatus"
Fig. 5.1.1-1

air. (Activated Alumina 8-14 mesh was used as a descicant and performed satisfactorily). The source box measured 33x33x16 inches; it was designed with a removable top with an additional opening for easy access, normally closed with a lucite window. A small hole was provided in the center of the top to serve as a liquid air filling connection and another hole was provided in the lucite window for dry ice filling.

The angle measuring assembly (Fig. 5.1.2-2,3) consists of a fixed detector and a movable one. The movable detector can be rotated through an angle of 180 degrees from 90 to 270 degrees relative to the fixed detector. Danger of damaging the lead shield of the scintillation crystals precludes more acute angles. Provision is also made for varying the detector solid angle subtended at the source in thirteen integral steps. This varies the geometrical half angle of the subtended cone from about 19½ degrees to about 5 degrees. Due to scattering effects and the finite size of the source the effective half angles are somewhat broader than the figures quoted (See Section 5.3.3).

The detectors themselves are on mounts which hold the axis 6"7/16 off the base plate. Lead shields are provided which interpose a minimum of 1½ centimeters of lead between the crystals when the detectors are at right angles. The crystals are discussed in connection with the photomultiplier tubes in Section 5.1.3.

Section 5.1.3 - Apparatus, Electronic

General

The electronics have four primary tasks, viz., detection of the radiation, energy selection in each channel,

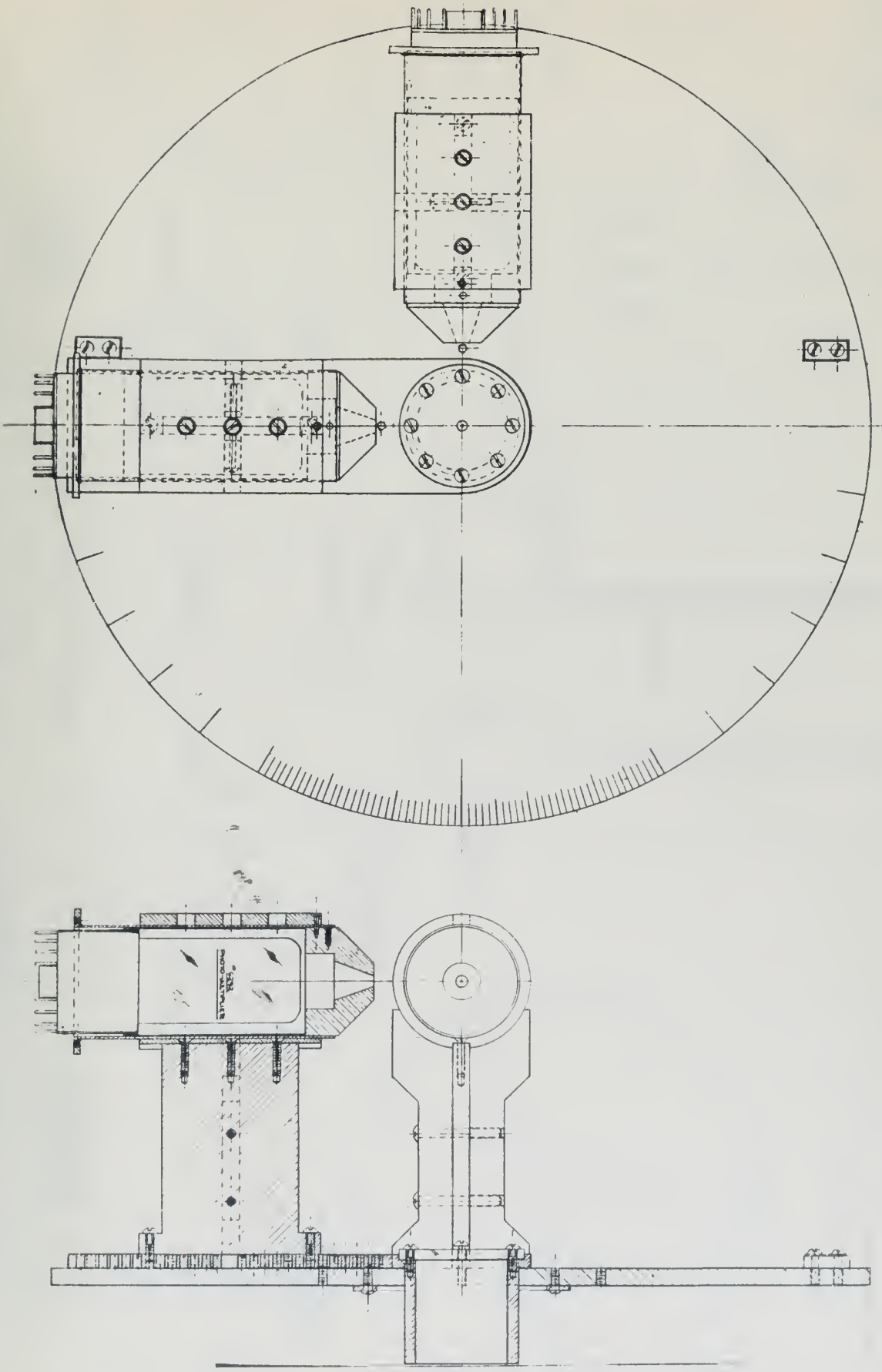

Angle Measuring Assembly, Assembly
Fig. 5.1.2-2

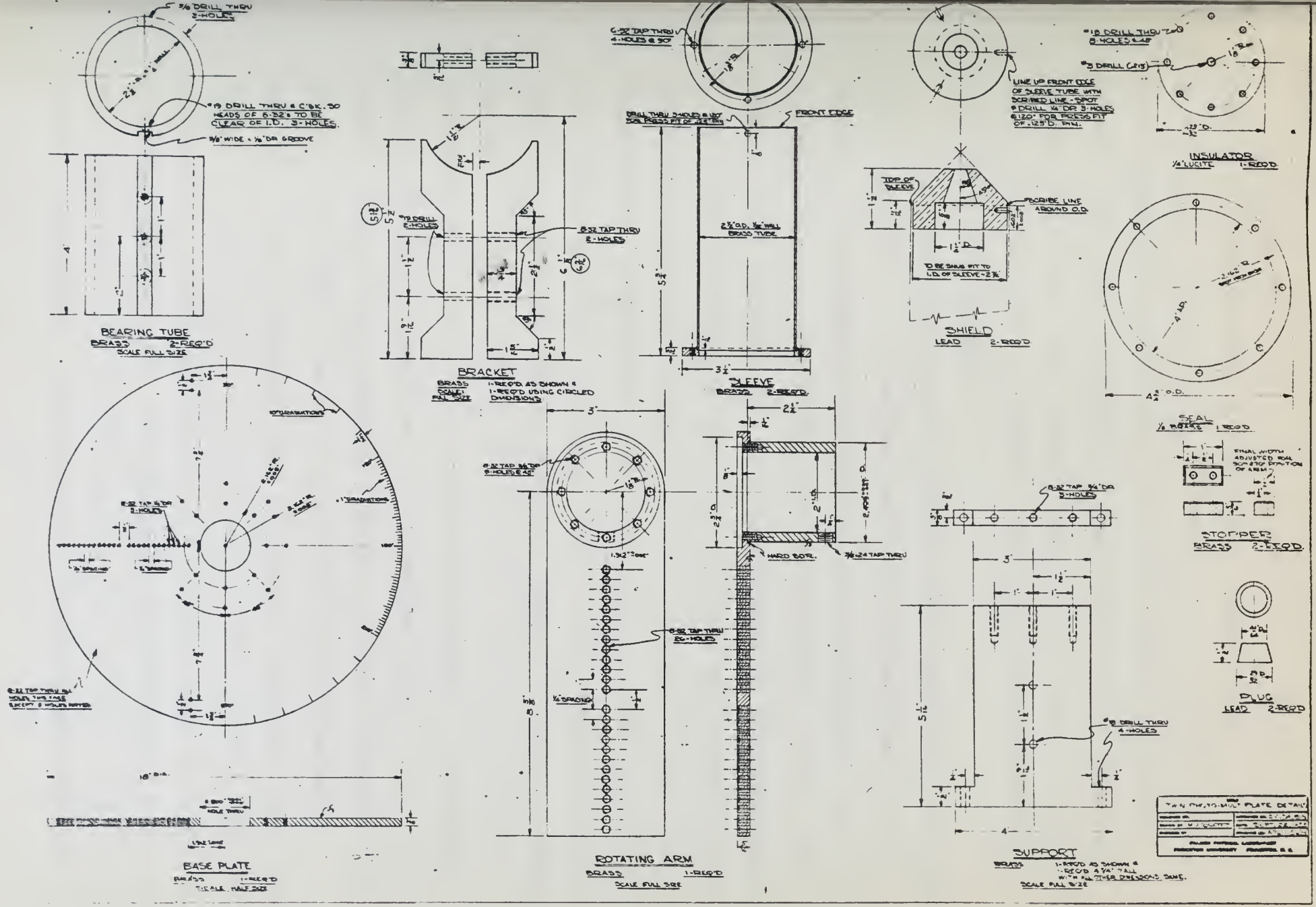

Angle Measuring Assembly, Details
Fig. 5.1.2-3

time comparison between channels, and counting.

Detection is performed by the crystal-photomultiplier combination and associated components and amplifiers. Energy selection is performed by the differential discriminators, time comparison is performed in the fast double coincidence circuit. The final selection of those pulses which have passed both the "time" and "energy" tests is performed in the slow triple coincidence circuit. Counting and presentation are done by the scalers.

It is found necessary to separate the functions of time and energy selection. The reason for this is illustrated in Fig. 5.1.3-1. It is based on the principle of operation of the differential discriminators which will be discussed in more detail later in this section. But for the purposes of this explanation it is merely necessary to know that one must use a finite channel width ΔE, i.e., the only pulses which will "operate" the differential discriminator are those from the linear amplifier in a range, E_1 to E_2 (See Fig. 5.1.3-1). Now assume that photopeak pulses arising from simultaneous gammas of identical energy may give rise to a pulse from the linear amplifier anywhere within ΔE; this is due to the statistical spread in the photopeak pulse height introduced by the photomultiplier tube. The time of firing of the "baseline" Schmitt circuit determines the time of the output pulse of the differential discriminator, and this circuit fires when the voltage of the input pulse rises to E_1. It can be seen directly from the figure that a time uncertainty Δt is thus introduced in the output pulse of the differential discriminator. (We normally operated with $\Delta E \approx 45$ v which gave rise to $\Delta t \approx 4 \times 10^{-7}$ sec.). One is thus constrained to use a coincidence circuit operated by pulses generated when

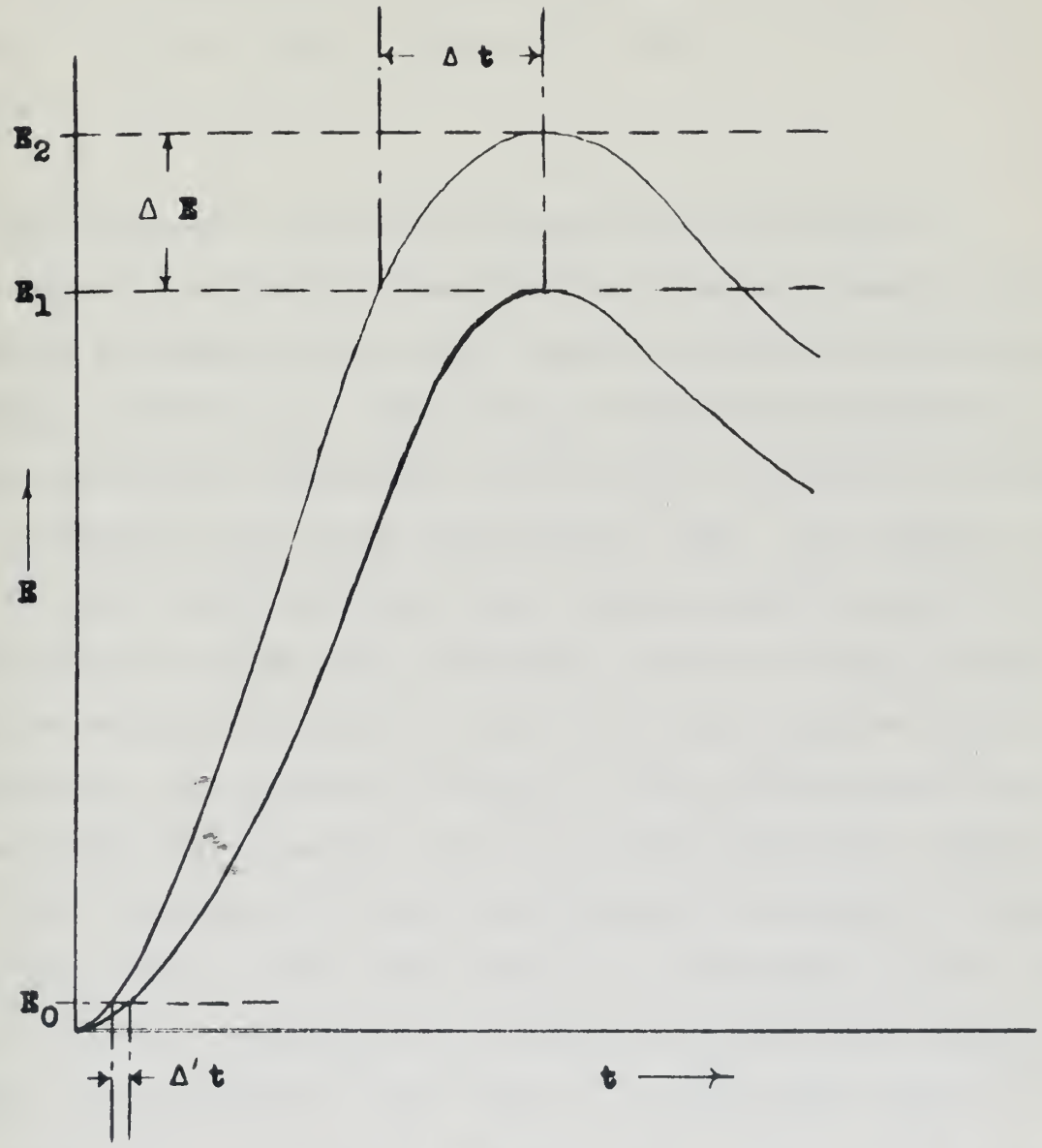

Illustrating Time Uncertainty of Energy Selection

Fig. 5.1.3c1

the pulse height reaches some lower value such as E_o. It is clear that $\Delta' t$ is much smaller than Δt. For this reason we use the pulses from a fast amplifier, which saturates on the first few volts of the photomultiplier pulse, to operate the fast double coincidence circuit.

Block diagrams of the entire apparatus with the interconnections for various types of runs and checks are shown in Section 5.2.1.

Photomultipliers, Crystals, and Associated Components

DuMont Type 6292 photomultiplier tubes were used. They were operated at about 127 volts per stage, adding up to a total high voltage of 1800 volts. Under these conditions exceptionally large output pulses were obtained (40 volts for the 722 KEV photopeak) with extremely good energy resolution (~6%). An ordinary cathode follower would not pass such a large negative pulse with a short rise time down even a moderate length of coaxial cable. This is because one needs a relatively large cathode resistor to maintain the quiescent voltage at the cathode greater than the pulse height to be passed, and this large resistance together with the capacitance of the cable prevent the passage of short rise time pulses. For these reasons a "bootstrap" circuit was used, in which the cathode resistance is effectively replaced by a variable resistance in the form of a vacuum tube (Fig. 5.1.3-2). The pulses had a rise time of about 4×10^{-7} seconds and a decay time of about 4.5×10^{-6} seconds. The decay time constant was set by the 68K resistor at the collector of the photomultiplier together with the total capacitance to ground at this point (about 30 uuf).

Relatively small scintillation crystals were used. They were 1 inch in diameter by ½ inch thick Harshaw Type X4L2; they

Photomultiplier Voltage Divider Unit and Bootstrap

Fig. 5.1.3-2

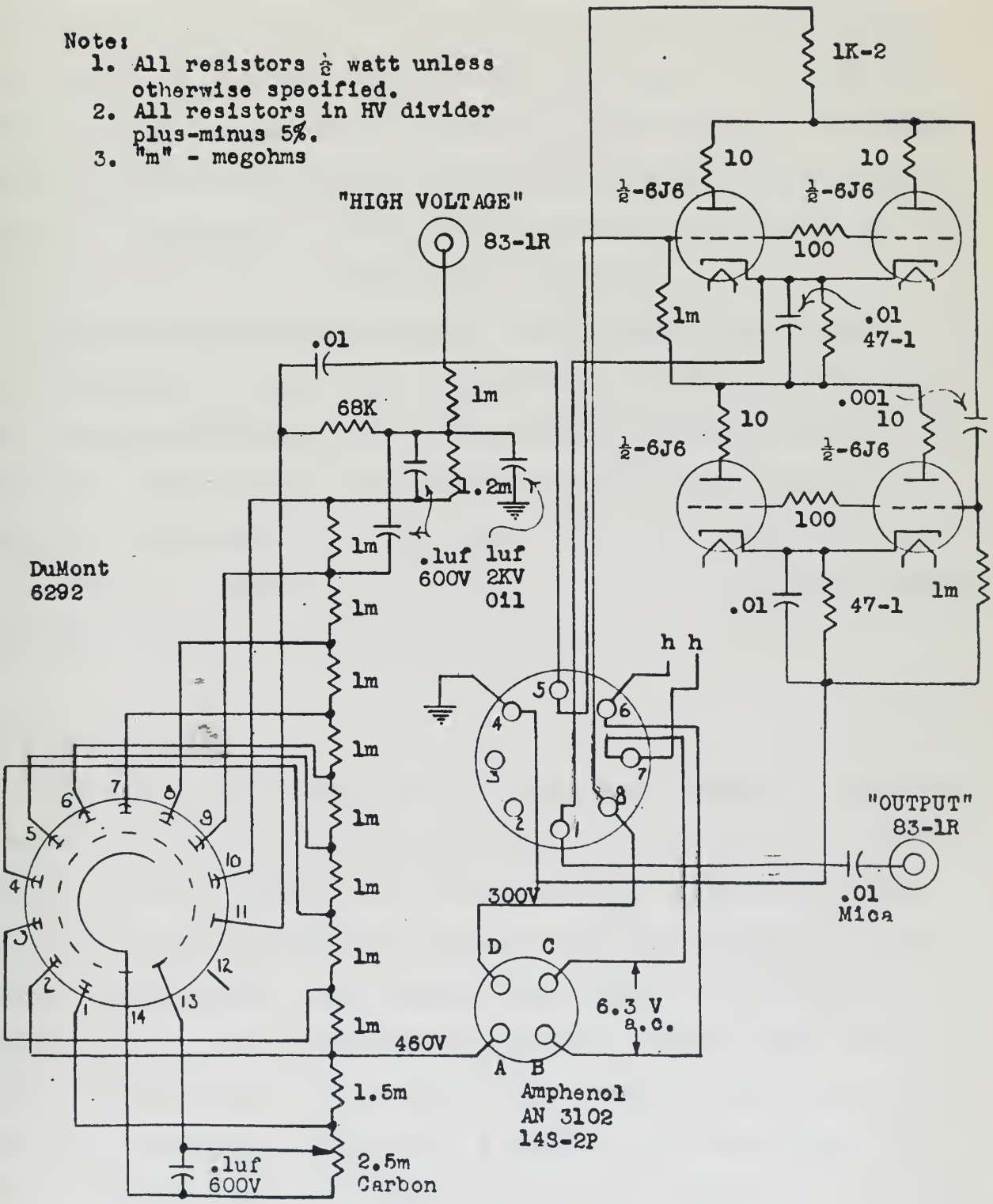

were mounted in a hermetically sealed can made of .032" 2-S aluminum which was internally coated with MgO. Ordinary white vaseline was used to provide optical contact between the window of the crystal can and the photocathode. Crystals were NaI(Tl).

The 460 volt battery applied to the second dynode (Fig. 5.1.3-2) had the purpose of maintaining the early stage electron gain both large and constant. This tends to increase the energy resolution as well as reduce the effects of high voltage fluctuations. The good energy resolution of this crystal-photomultiplier combination is illustrated in the observed partial spectrum of the gamma rays in the decay of In^{114} (Fig. 5.1.3-3).

There is apparently a transit time uncertainty of about 2×10^{-8} seconds in these tubes under these conditions, which makes this set-up undesirable for lifetime measurements by delayed coincidences. This point is discussed more fully later on in this section in the paragraph on the fast double coincidence circuit.

Atomic Instrument Company high voltage power supplies (Model 316) were used and performed satisfactorily.

Pulse Amplifiers

The pulse amplifiers (Fig. 5.1.3-4) were designed to provide a moderately fast pulse output together with a linear pulse output in the same chassis. In the case of the linear output the term "amplifier" is rather a misnomer; the term "inverter" would be more appropriate. The already large negative pulses from the photomultiplier are inverted and amplified slightly and then fed to the differential discriminator which requires positive pulses. The linear amplifier consists of a heavily fed back single 6AG7 stage whose grid operates about 50 volts above ground. Gain from -1.6 to -80 is adjusted by varying the amount of unbypassed cathode resistance. The pulses from the sodium iodide - photomultiplier

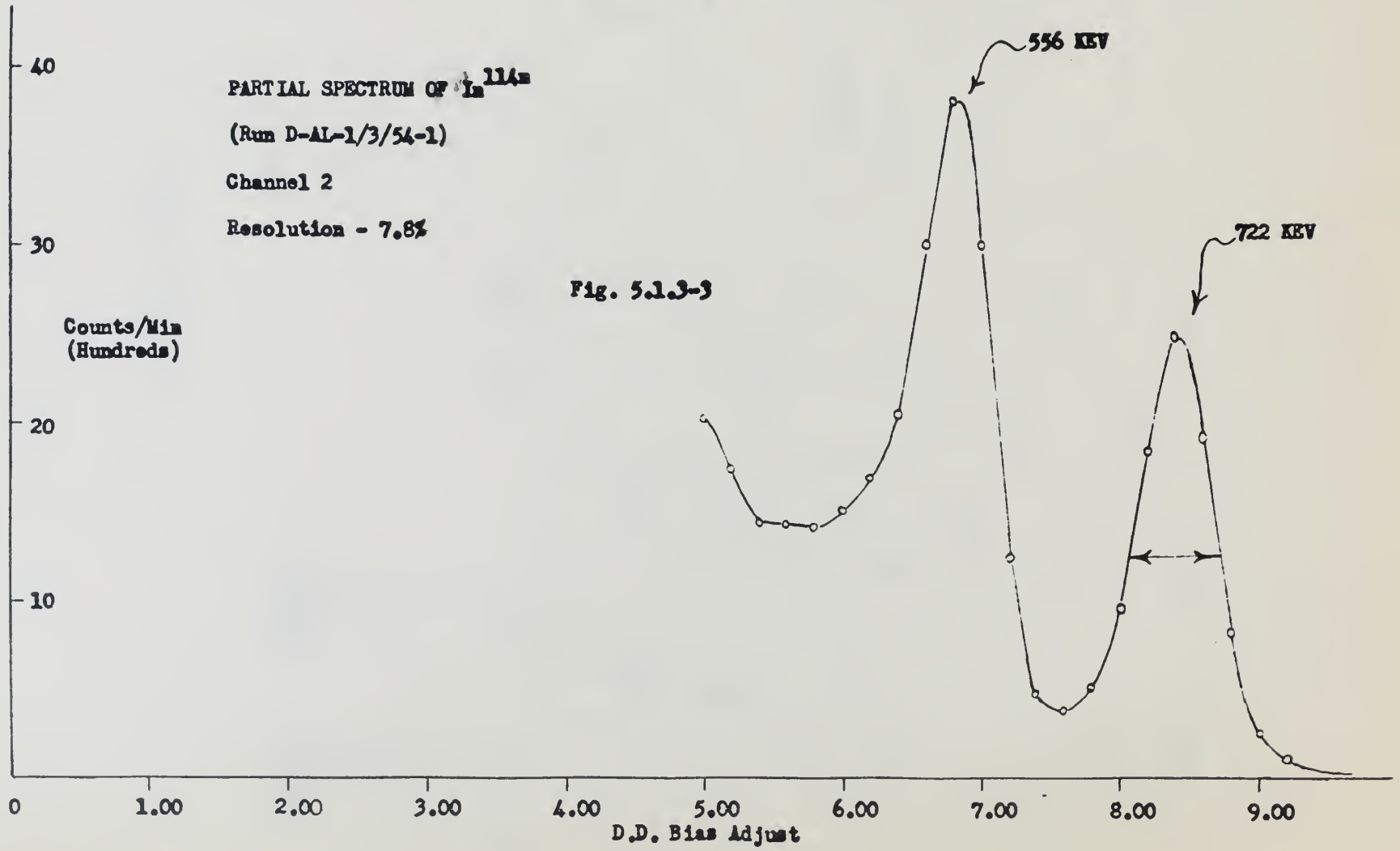
PARTIAL SPECTRUM OF In114m
(Run D-AL-1/3/54-1)
Channel 2
Resolution - 7.8%
556 KEV
722 KEV
Counts/Min
(Hundreds)
40
30
20
10
0
1.00
2.00
3.00
4.00
5.00
6.00
7.00
8.00
9.00
D.D. Bias Adjust

Fig. 5.1.3-3

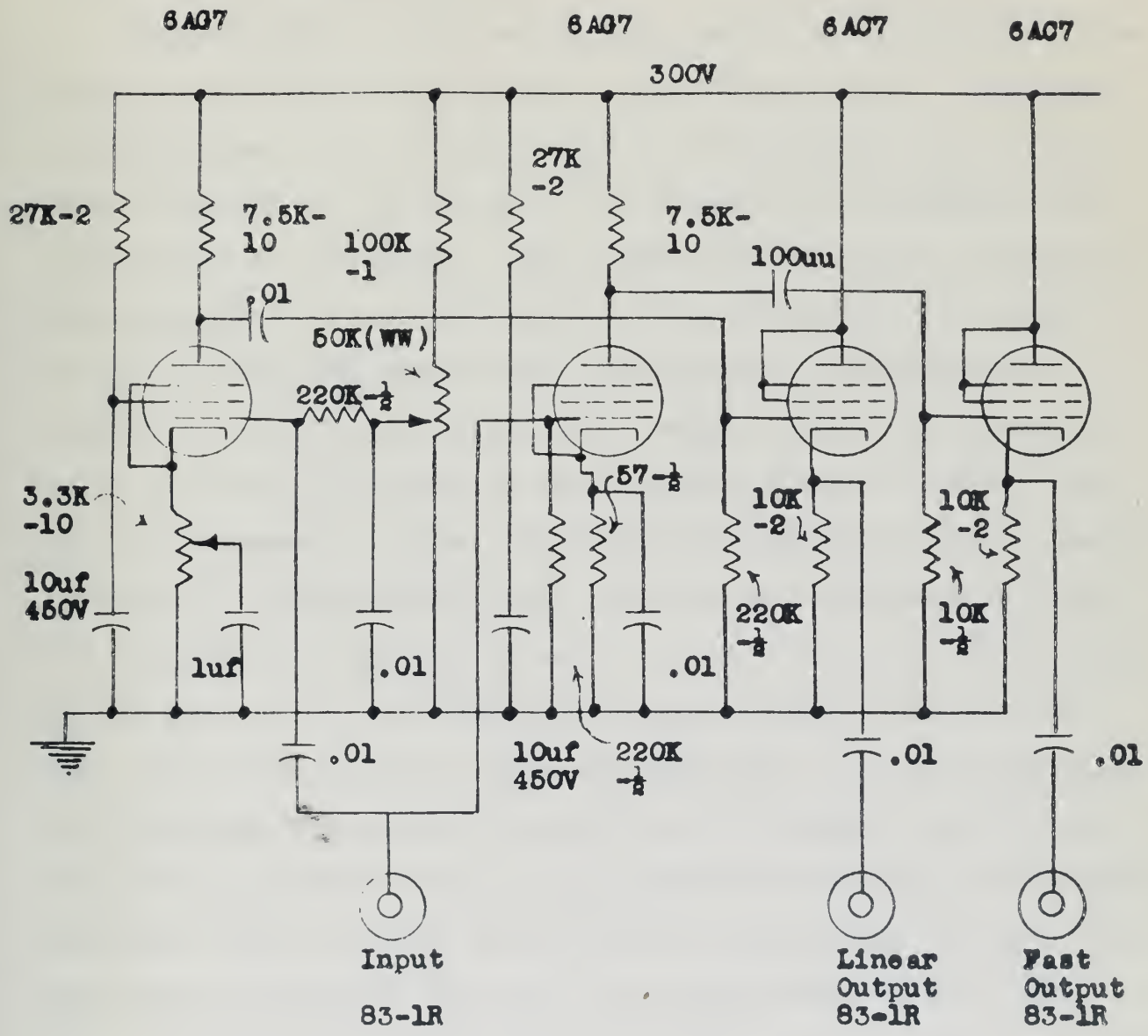

Pulse Amplifier
Fig. 5.1.3-4

combination (~40 volts, 4×10^{-7} seconds rise time) when amplified in the fast amplifier have a rise time of about 5×10^{-8} seconds and a height of about 8 volts when clipped with 4 meters of RG-7/U.

Differential Discriminators

These operate on the well known circuit of two integral discriminators feeding into an anti-coincidence circuit. Modifications were made to a standard type of differential discriminator which resulted in the saving of six tubes and in ruggedness and reliability of operation. These modifications center around the anti-coincidence circuit (Fig. 5.1.3-5). Briefly, the operation is as follows. The square wave generated by the "Base Line" Schmitt circuit is differentiated strongly and is fed through a delay line into one input of the anti-coincidence circuit. The delay is necessary to give the "Delta E" Schmitt circuit a chance to fire IF IT IS GOING TO FIRE. Here we have two possibilities: (1) the "Delta E" Schmitt IS going to fire, i.e., the input pulse is too big, or (2) the "Delta E" Schmitt IS NOT going to fire, i.e., the input pulse is within the "window". In the first case the square wave generated by the "Delta E" Schmitt is fed into the anti-coincidence circuit and prevents the delayed, differentiated pulse from the "Base Line" Schmitt from passing through, i.e., the "Delta E" Schmitt gates the anti-coincidence circuit off. Thus, in case (1) we get no output pulse. In the second case there is no gating pulse from the "Delta E" Schmitt and our delayed, differentiated pulse from the "Base Line" Schmitt is passed through the anti-coincidence circuit, then amplified, and then fed as a trigger pulse to a blocking oscillator whose output is the output of the differential discriminator.

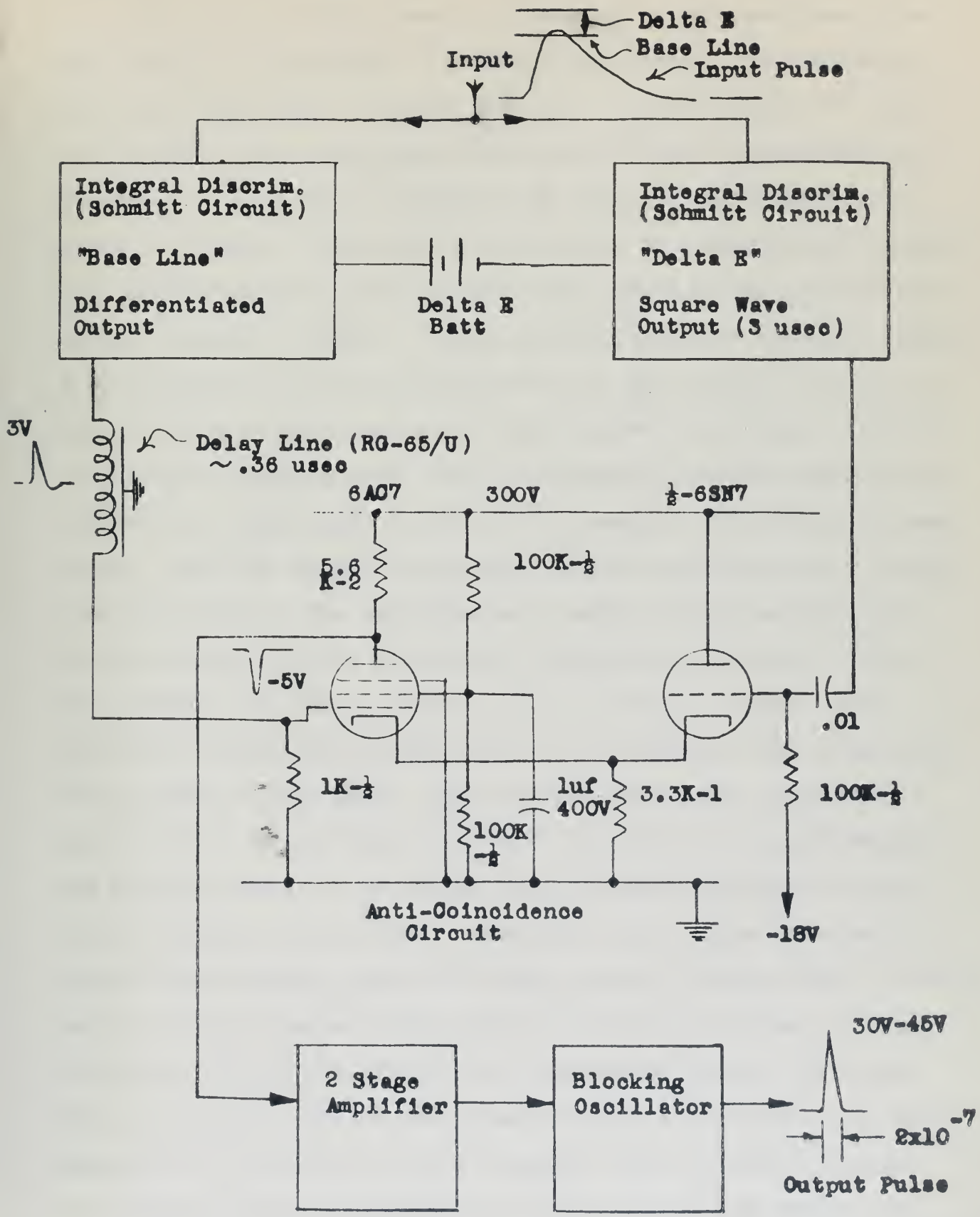

Differential Discriminator
Fig. 5.1.3-5

Fast Double Coincidence Circuit

The heart of this piece of apparatus is the non-linear element, which in this case is a 6BN6 vacuum tube. The virtues of this particular tube are that the plate characteristics of two of its grids, the quadrature and limiter grids, are practically identical. A negative voltage of 3½ volts on either grid with a plate voltage of 60 volts is sufficient to prevent plate current. The tube is operated normally with both grids in the cut-off condition (about -5 volts). Semi-standard positive pulses of about 8 volts from the fast pulse amplifier in each channel are fed in, one to the quadrature and one to the limiter grid (Fig. 5.1.3-6). If they are "simultaneous" the tube conducts and the pulse is amplified in a 6AH6 stage and fed out through a 6J6 cathode follower stage. The fast double coincidence circuit determines the overall resolving time of the apparatus as a whole. The resolving time of this circuit can be adjusted in two ways as follows: (1) by "shortening" the input pulses, i.e., by using a faster, more strongly clipped input pulse, and (2) by adjusting the bias level on the grids of the 6BN6. Both methods were used; method (2) turned out to be extremely sensitive to the grid bias adjustment and made the use of a precision potentiometer necessary in the cathode circuit of the 6BN6. Resolving time curves obtained by delayed coincidences using the single channel method (Fig. 5.2.1-3) and the double channel method (Fig. 5.2.1-4) are shown in Figs. 5.1.3-7,8. Since the annihilation radiation has zero lifetime, the broadening of the double detector curve is introduced by the apparatus. That this is not a "channel width" effect is shown by comparing Figs. 5.1.3-7 and 5.1.3-8 in which two widely different channel widths were used and which resulted in approximately

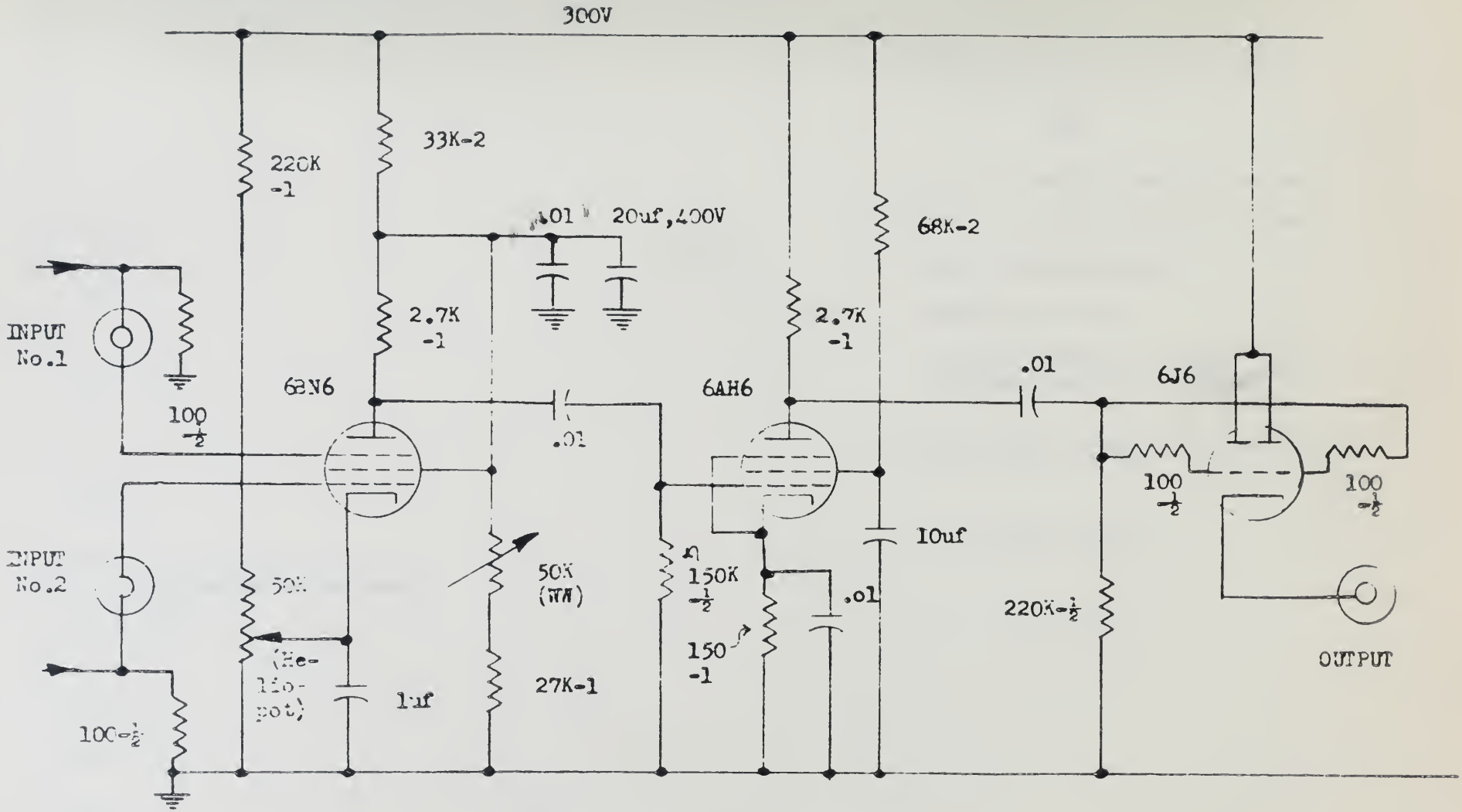

FAST DOUBLE COINCIDENCE CIRCUIT
Fig. 5.1.3-6

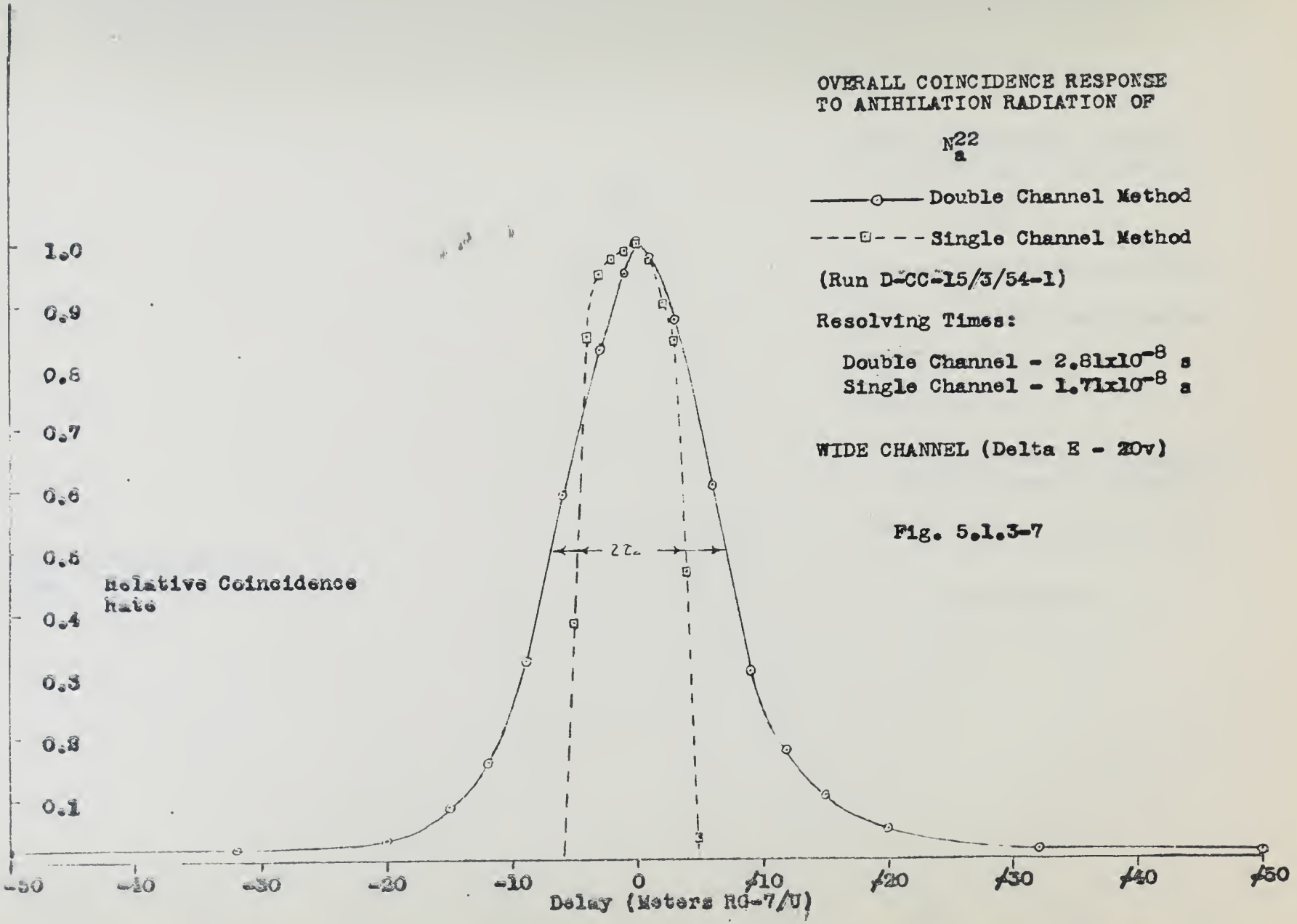
OVERALL COINCIDENCE RESPONSE
TO ANIHILATION RADIATION OF
N_a^{22}
Double Channel Method
Single Channel Method
(Run D-CC-15/3/54-1)
Resolving Times:
Double Channel - 2.81x10⁻⁸ s
Single Channel - 1.71x10⁻⁸ s
WIDE CHANNEL (Delta E - 20v)
Fig. 5.1.3-7
Relative Coincidence Rate
1.0
0.9
0.8
0.7
0.6
0.5
0.4
0.3
0.2
0.1
2τ
-50
-40
-30
-20
-10
0
+10
+20
+30
+40
+50
Delay (Meters RG-7/U)

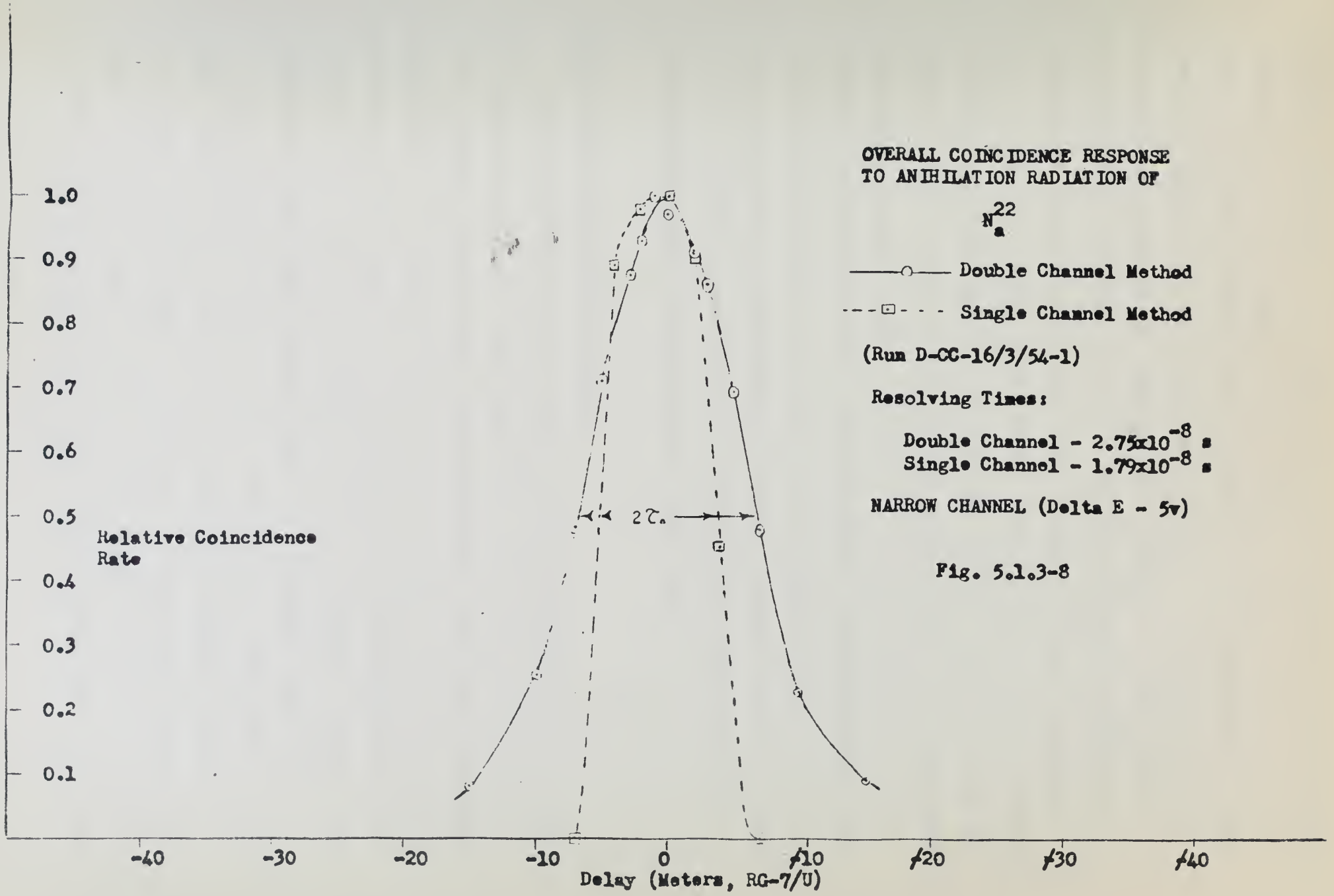
OVERALL COINCIDENCE RESPONSE
TO ANIHILATION RADIATION OF
N_a^{22}
Double Channel Method
Single Channel Method
(Run D-CC-16/3/54-1)
Resolving Times:
Double Channel - 2.75×10^{-8} s
Single Channel - 1.79×10^{-8} s
NARROW CHANNEL (Delta E - 5v)
Fig. 5.1.3-8
Relative Coincidence Rate
1.0
0.9
0.8
0.7
0.6
0.5
0.4
0.3
0.2
0.1
$2\tau_o$
-40
-30
-20
-10
0
+10
+20
+30
+40
Delay (Meters, RG-7/U)

the same broadening. We thus look to the photomultiplier-crystal combination as the source of the "jitter" which causes the broadening. That this jitter is not caused by the uncertainty in the time of creation of the first photoelectron at the photocathode can be shown by applying formulae due to Bell, et. al. (1B52). That this time uncertainty is not caused by varying trajectory lengths for the avalanche electrons has been shown by measurements by Alford (unpublished) using a pulsed light source. However, as Alford has shown again, the average transit time is a very definite function of which part of the photocathode is illuminated; the average transit time is about 10^{-8} seconds longer for photoelectrons emitted from the circumference of the photocathode than for those emitted from the center in the DuMont 6292's. If our photocathode were illuminated by several intense bursts of light randomly spaced in area over the photocathode, then our effect of broadening might be explained on this basis.

Slow Triple Coincidence Circuit

This circuit acts as a sort of recombining point in the flow of pulses through the whole apparatus, where the two functions, viz., energy selection and time comparison, which were previously separated, are rejoined (Fig. 5.2.1-1). Each of the three input pulses, one from each of the differential discriminators and one from the fast double coincidence circuit, triggers a square wave generator whose output pulse length is adjustable from 0.2 to 1.5 micro-seconds (Fig. 5.1.3-9). The pulses from each of these three circuits are then fed to a non-linear element consisting of crystal diodes (1N56) in parallel. If the three pulses overlap in time, the common plates of the crystal diodes rise sharply, and this pulse is then fed through a class C amplifier. The out-

SLOW TRIPLE COINCIDENCE CIRCUIT

FIG. 513-9

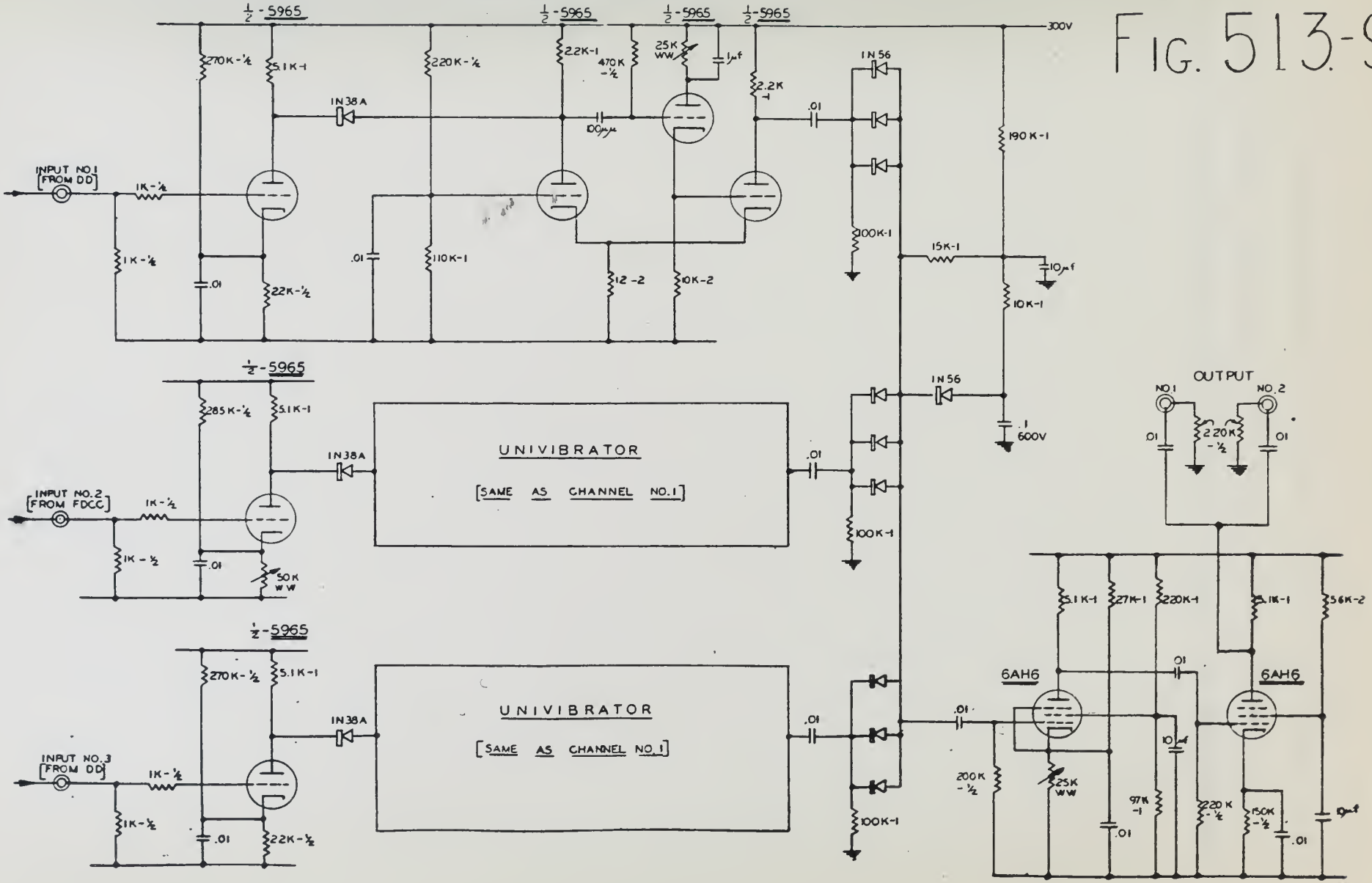

put of this circuit, which is "energy selected coincidences", then goes to a scaler where the pulses are counted and recorded. The square wave generator is a plate triggered univibrator; the cathode follower coupling of the two halves of the univibrator results in a rise time of about 5×10^{-8} seconds for these square pulses.

Part 5.2 - Experimental Procedures

Section 5.2.1 - Runs and Checks

The various types of runs and checks to gather information of the source or the equipment are best understood by referring to the inter-connection diagrams which follow.

Type Run:	Designation	Channel Width	Variable	Fig. 5.2.1-
Total Coincidence Counting Rate	TC	Wide	θ	1
Chance Coincidence Counting Rate	CC	Wide	θ	2
Resolving Time, Single Channel Method	RT-A	Wide	Delay	3
Resolving Time, Double Channel Method	RT-B	Wide	Delay	4

The checks include operational and characteristic checks. Operational checks, or "alignment checks", merely serve to tell if the apparatus is properly tuned. These were performed daily before each run and occaisonally at the end of a run when there was reason to believe that something had "gone wrong". Characteristic checks are tests to ascertain that we are actually measuring what we think we are measuring.

Operational Checks

Window Set - This involved setting the photopeak pulse heights of the 722 KEV or the 556 KEV gamma rays in each channel to a predetermined height, then by means of the pulser to set the lower window edge at a pulse height corresponding to 430 KEV. This figure was arrived at from the Compton scattering chart of the gamma rays present in the decay of In^{114}, Fig. 5.2.1-8; see also Section 5.3.3. Then, using the pulser again, delta-E was adjusted to a predetermined value to include both lines (722-556 KEV) in each channel.

Explanation of Abbreviations Used In Figs. 5.2.1-1,2,3,4,5,6,7

PM	Photomultiplier Tube
CF	Cathode Follower ("Bootstrap")
PMHV (AIC)	Photomultiplier High Voltage Power Supply (Atomic Instrument Company, Model 316)
LO	Linear Output of Pulse Amplifier
FO	Fast Output of Pulse Amplifier
DIFF. DISC.	Differential Discriminator
FDCC	Fast Double Coincidence Circuit
STCC	Slow Triple Coincidence Circuit
S	Scaler
SCOPE	Cathode Ray Oscilloscope, Tektronix Model 511A

All interconnection lines represent coaxial cable RG-7/U unless otherwise stated.

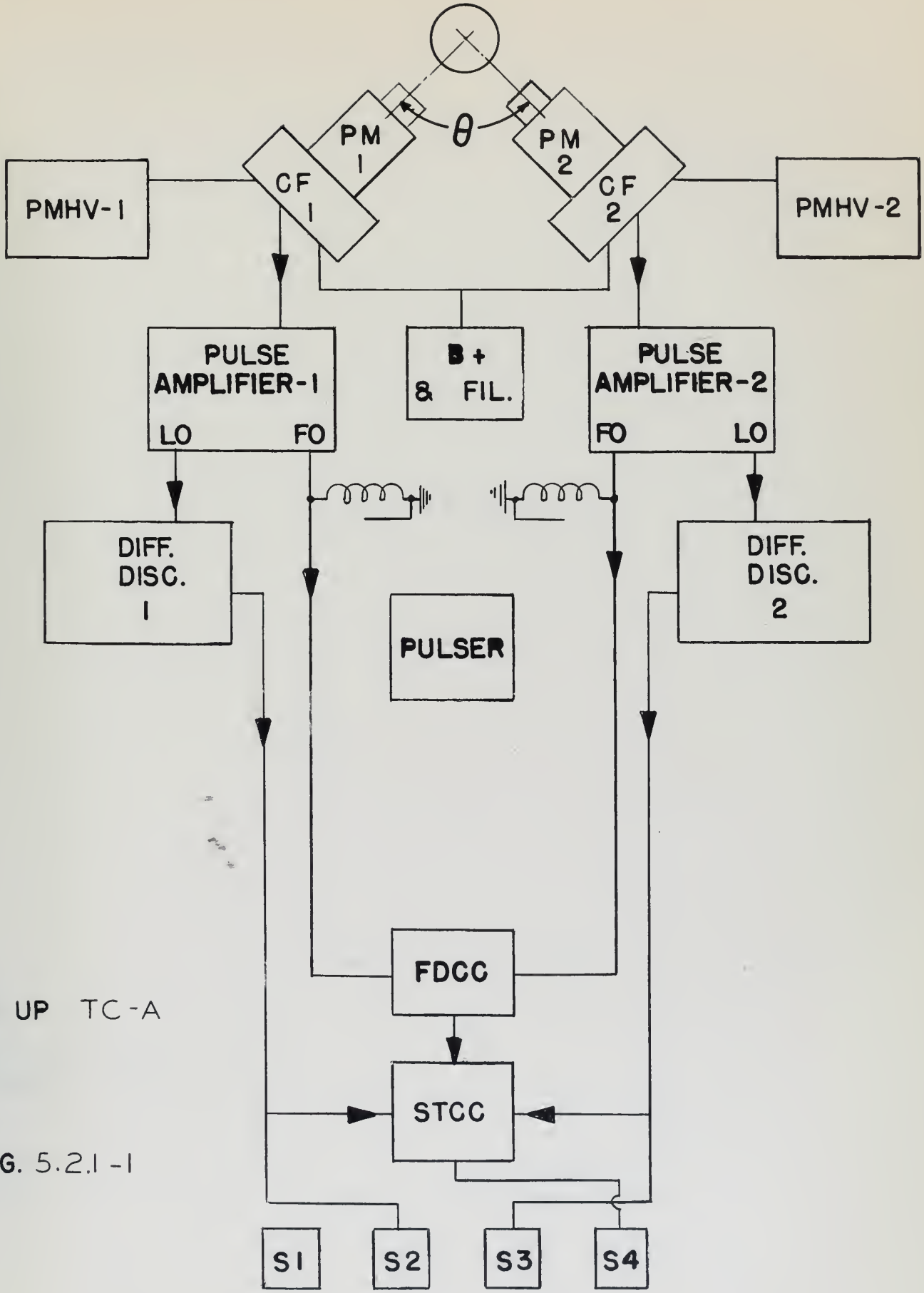

SET UP TC-A

FIG. 5.2.1-1

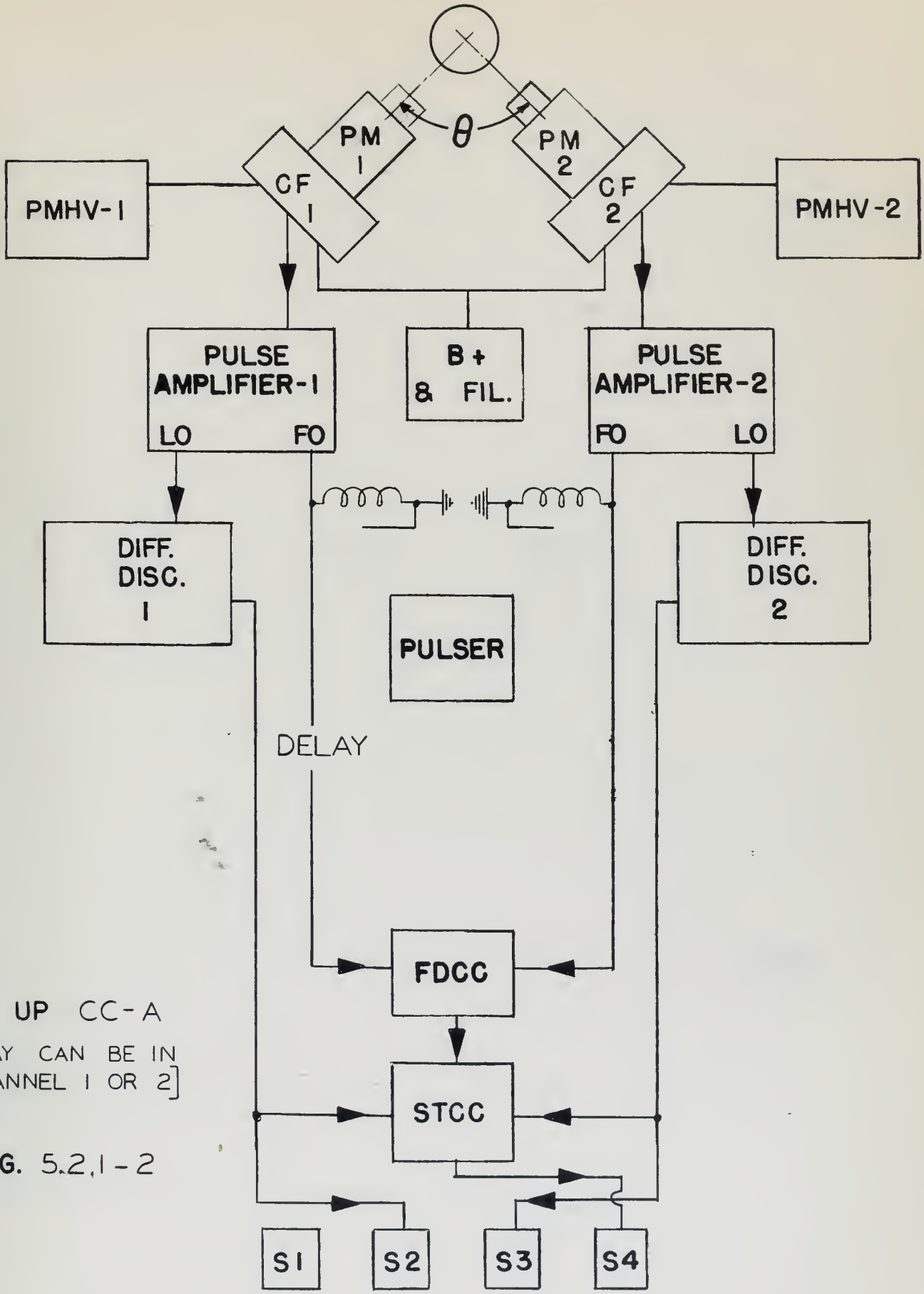

SET UP CC-A

[DELAY CAN BE IN CHANNEL 1 OR 2]

FIG. 5.2.1-2

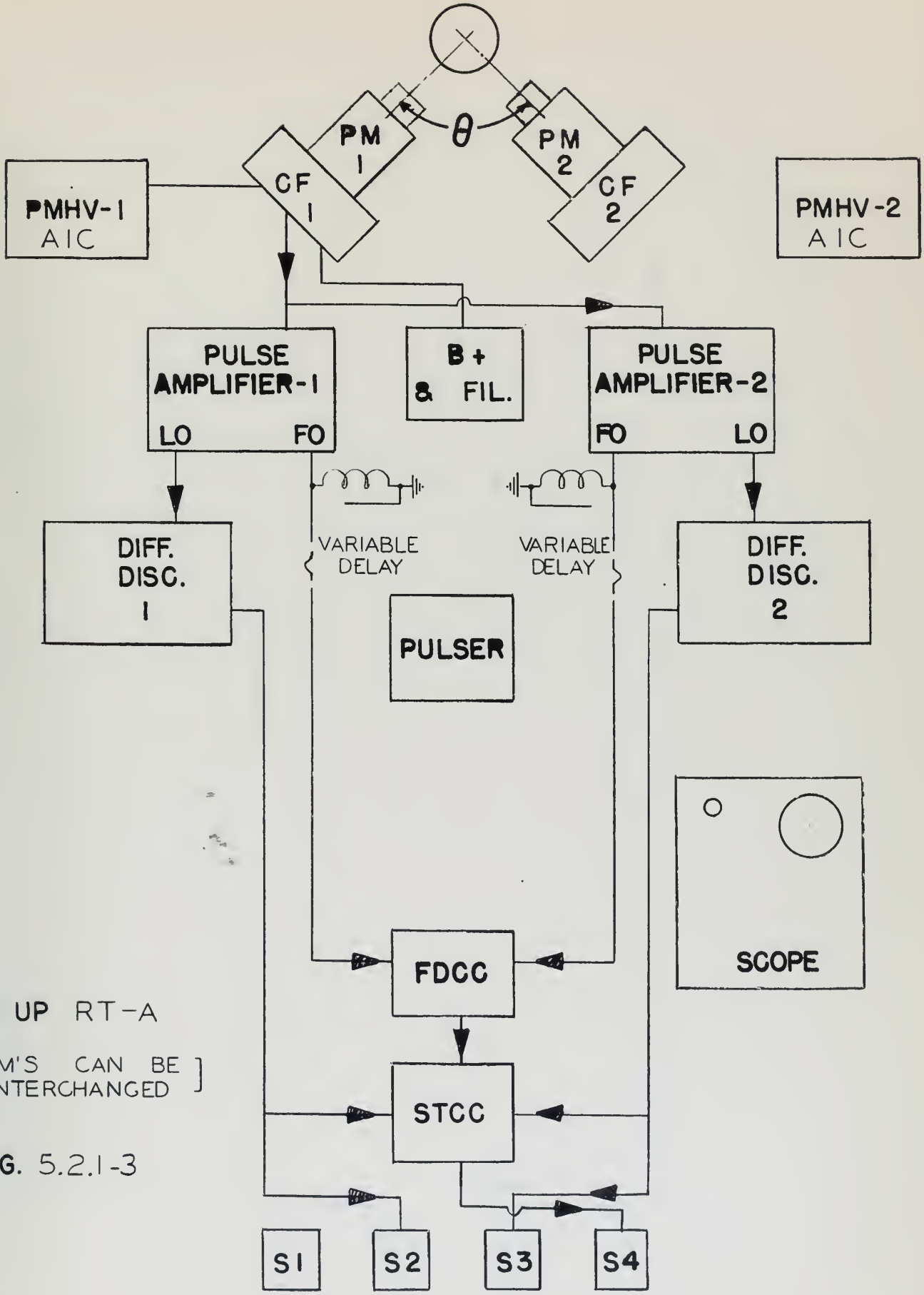

SET UP RT-A

[PM'S CAN BE INTERCHANGED]

FIG. 5.2.1-3

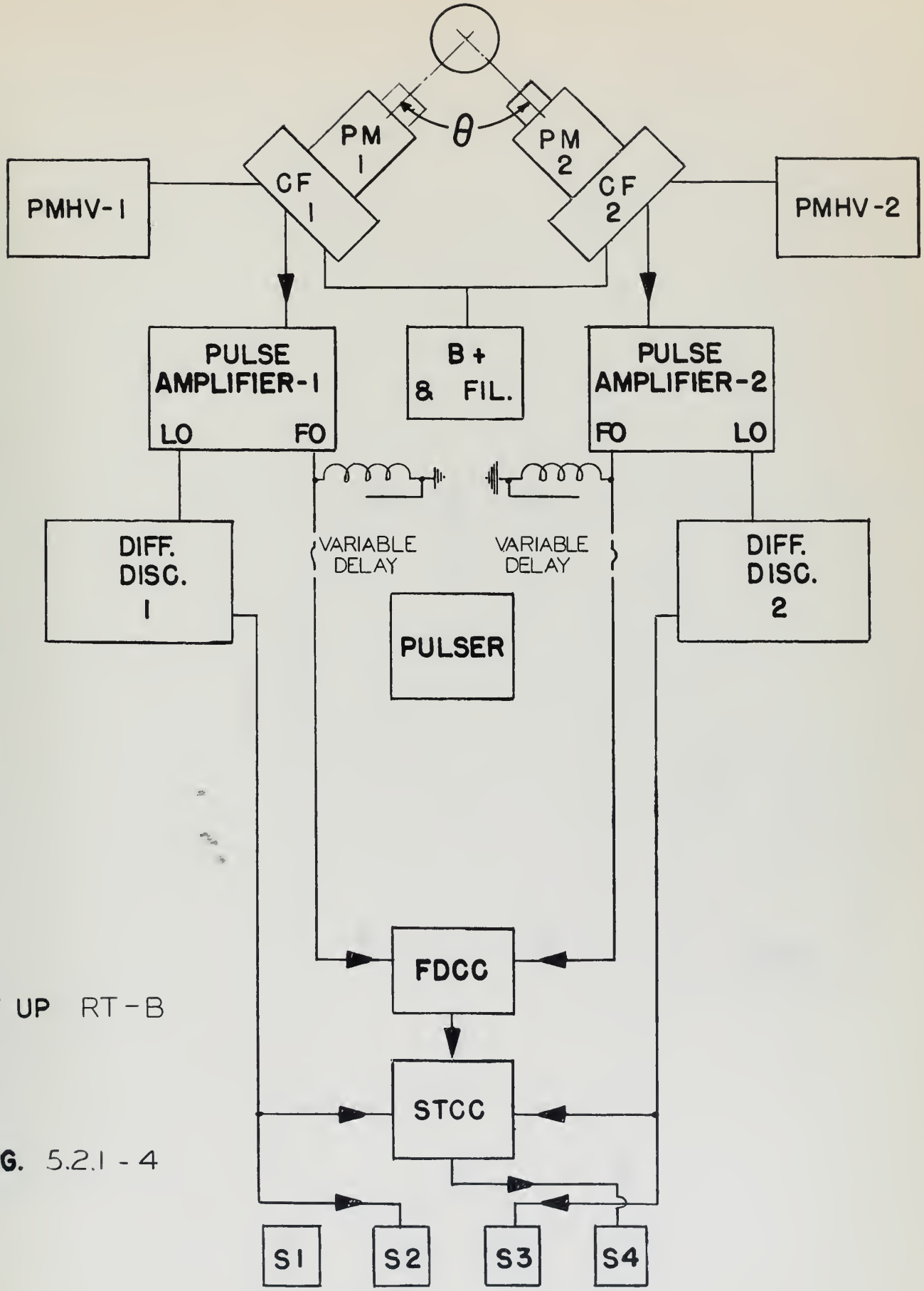

SET UP RT-B

FIG. 5.2.1 - 4

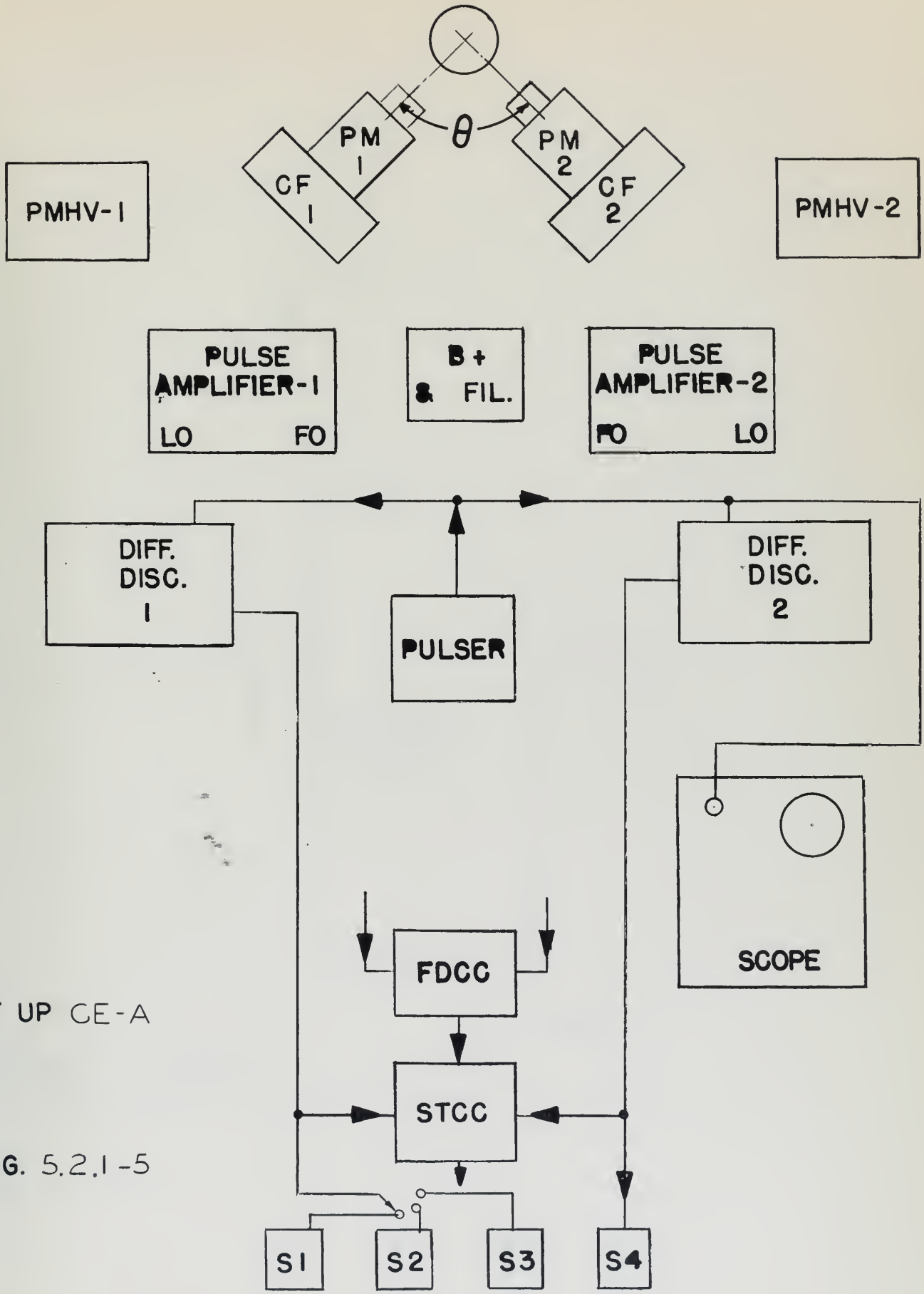

SET UP CE-A

FIG. 5.2.1-5

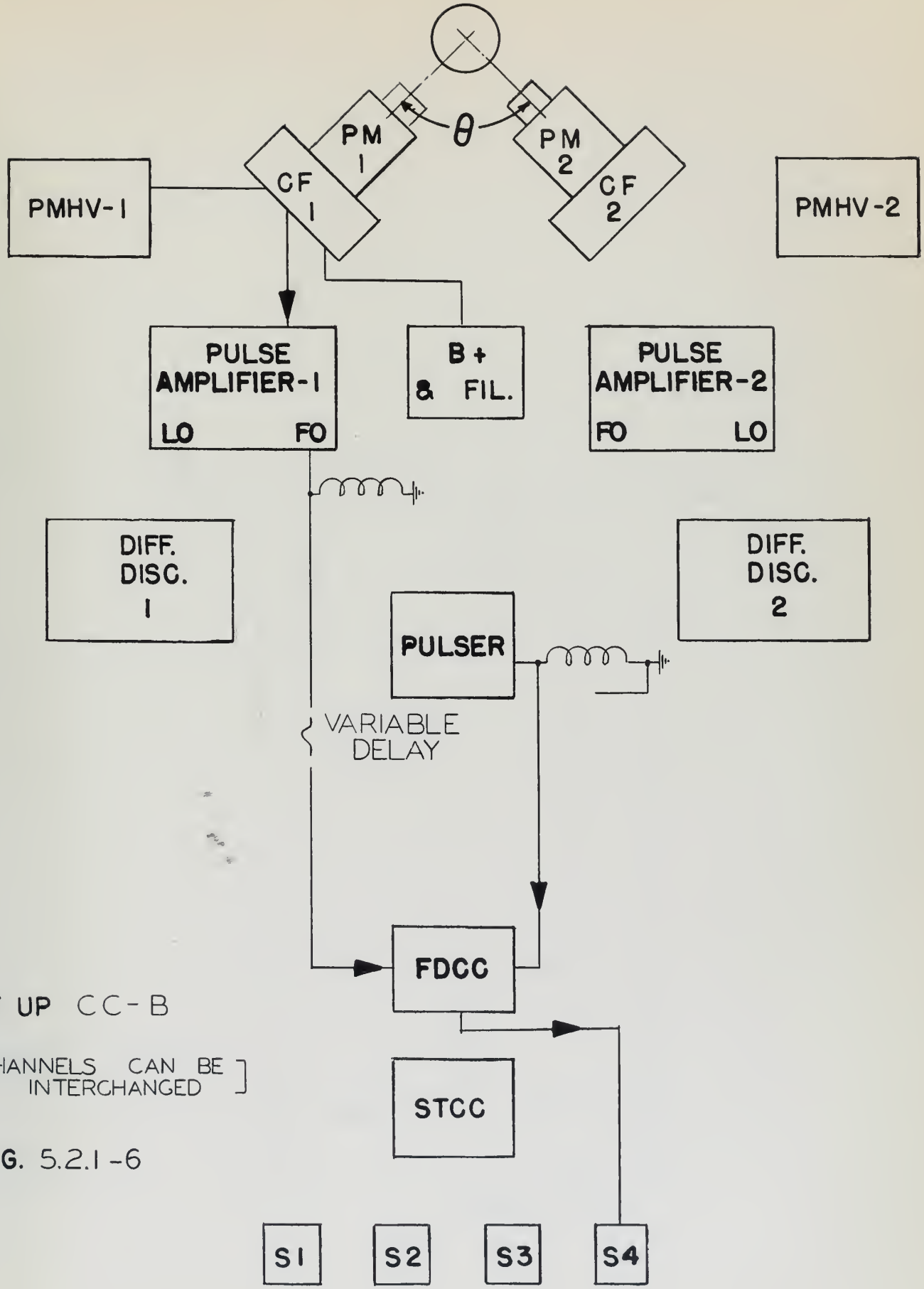

SET UP CC-B

[CHANNELS CAN BE INTERCHANGED]

FIG. 5.2.1-6

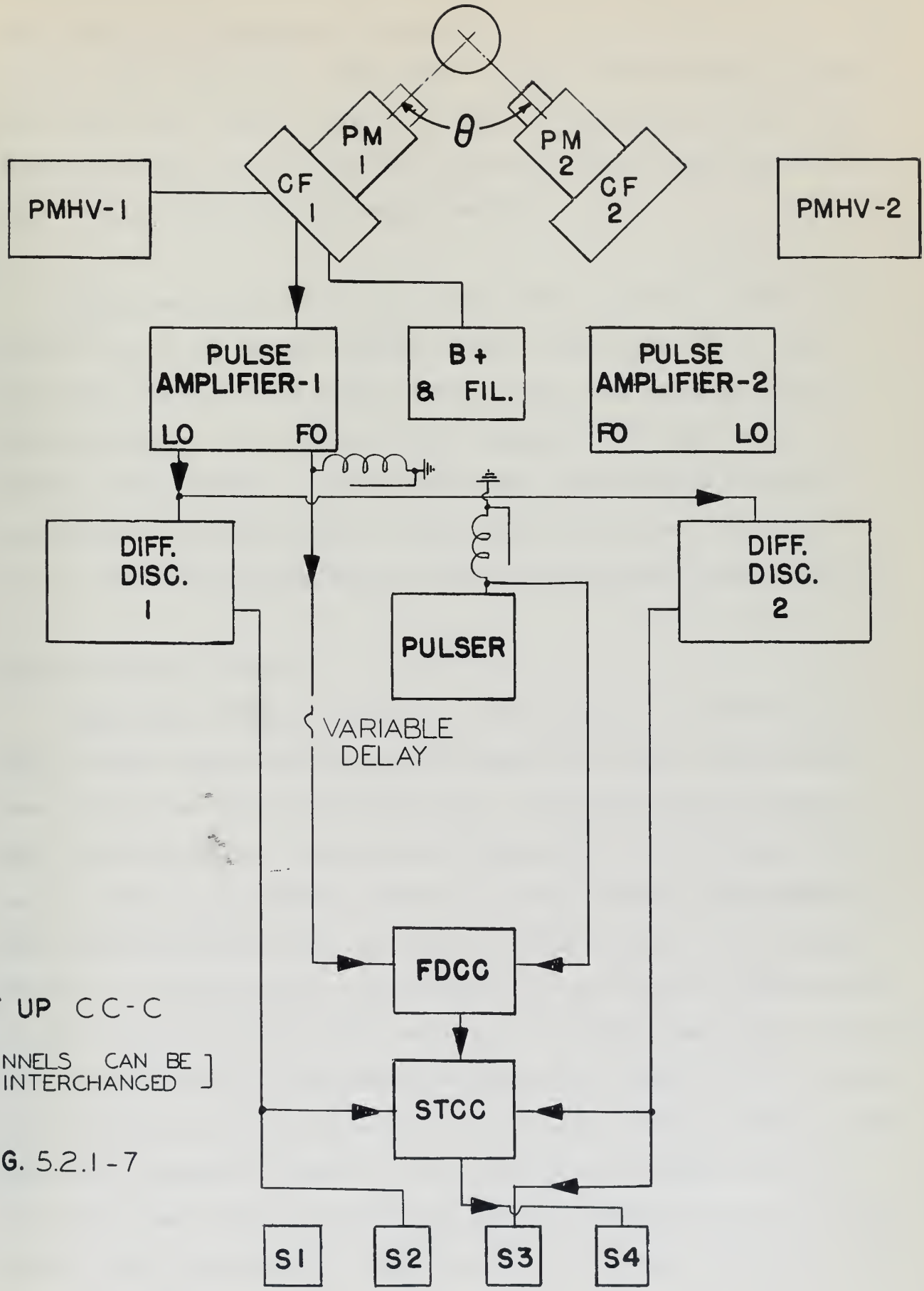

SET UP CC-C

[CHANNELS CAN BE INTERCHANGED]

FIG. 5.2.1-7

Slow Triple Coincidence Circuit Cout-Out Test - This tests the overall performance of the energy and time discrimination functions of the apparatus. The input to each differential discriminator and each input to the fast double coincidence circuit are removed in turn. The output of the slow triple coincidence circuit should disappear with each removal.

Scaler Counting Efficiency Test (Fig. 5.2.1-5) - With the pulser set at the normal single channel frequency and so that the pulse height falls within each window, the scalers should count together. Two scalers were compared at a time, viz., S2:S3, S2:S4, S3:S4. It was found that they counted together accurately to within plus or minus .01%. This test also partially checks the performance of the differential discriminators.

Characteristic Checks

Cable Loss (Figs. 5.2.1-6,7) - Attenuation in the 50 meter RG-7/U delay cable could cause the measured chance coincidence rate to be less than it actually is. Using the set-up shown in Fig. 5.2.1-6, there is an observed dimunition of counting rate as the delay is increased, whereas no such droop is observed in the energy sensitive case as shown in Fig. 5.2.1-7. The former effect is evidently due to attenuation of the lower energy pulses in the fast amplifier output which are normally just above threshold for the fast double coincidence circuit, and which do not trigger the differential discriminators in any case; whereas those pulses which are energetic enough to fall within the window are still above the fast double coincidence circuit threshold in the latter effect. We conclude that cable loss in the energy sensitive case is negligible.

Scattering - Two ways in which the scattering of gamma rays could adversely affect us are (1) by scattering from crystal to crystal which would cause a spurious coincidence to be registered under certain conditions, and (2) by a change in the scattering conditions in or near the source which would then be unaccounted for by the geometrical corrections. (1) is accounted for in two ways: (a) by the detector lead shields (Section 5.1.2), and (b) by the location of the window base line. (a) is useful at 90^{o} but of no use at all at 180^{o}, whereas (b) is most effective at 180^{o}. Fig. 5.2.1-8 shows the enrgy of the scattered quantum versus scattering angle for the gamma rays present in the decay of In^{114}. For a crystal to crystal scattered coincidence, the gamma ray must scatter at least through 90^{o}. The window base line of 430 KEV is chosen so that in the worst possible case (the weak 1300 KEV component), the window excludes all rays scattered through more than 78^{o}.

The effective broadening of the solid angle of the detectors due to scattering from the shields, in the source, etc., is another matter and is discussed under "Geometrical Corrections", Section 5.3.3. However, these corrections would not correct for (2) above, i.e., VARIATIONS in the scattering conditions due to frost on the source holder, variation in the phase of the source, and the presence of a thermo-couple in the source, etc. In order to check for these variations in scattering conditions, two angular resolution runs were made using Na^{22}, one under conditions of maximum scattering, i.e., using a thermo-couple in a heavily frosted source holder, and one under minimum scattering conditions, i.e., at room temperature with no thermo-couple. Effective increase in scattering conditions would show up as a broadening of the angular resolution curve. Results, however, showed no detectible

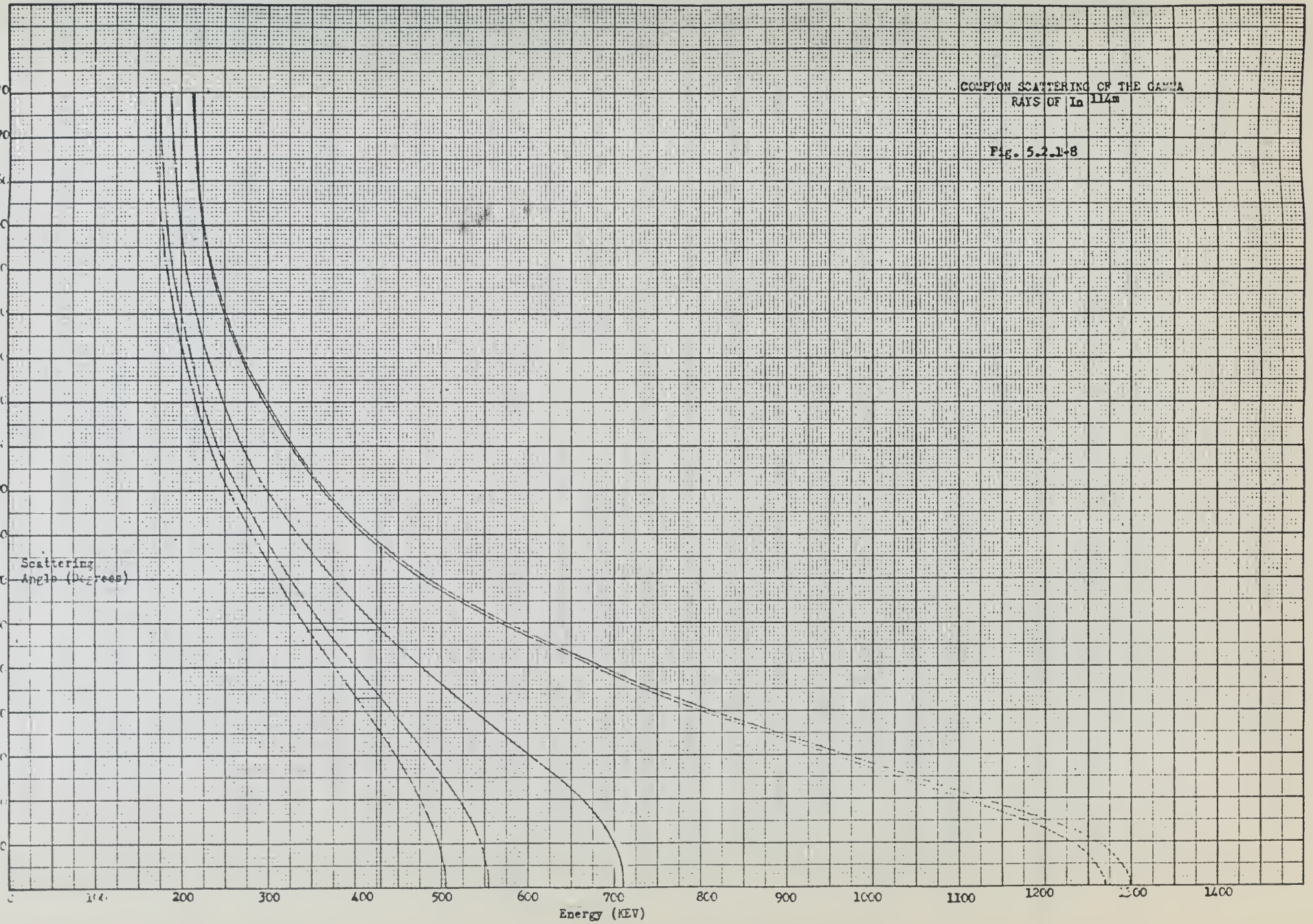
COMPTON SCATTERING OF THE GAMMA RAYS OF In 114m
Fig. 5.2.1-8
Scattering Angle (Degrees)
180
170
160
150
140
130
120
110
100
90
80
70
60
50
40
30
20
10
200
300
400
500
600
700
800
900
1000
1100
1200
1300
1400
Energy (KEV)

difference in the curves. We conclude, therefore, that the effective scattering conditions remained constant throughout the experiment.

Section 5.2.2 - Sources

Sources were prepared of In^{114} and Na^{22}. Both of these isotopes came from Oak Ridge in the form of chlorides in dilute aqueous solutions of hydrochloric acid.

In^{114} came as $InCl_3$ in a .38N solution of HCl. Two separate shipments of 10 mc each were received, (1) having a specific activity of 171 mc/gm and a concentration of 1.90 mc/ml and (2) having a concentration of 87 mc/gm and a concentration of .96 mc/ml.

Four separate In^{114} sources were prepared, three of them of the extended source geometry shown in Fig. 5.2.2-1 and one (200 uc) merely evaporated to dryness then sandwiched between to "1/8 aluminum plates for lifetime measurements using another apparatus. Of the three sources using the "extended geometry", two were in liquid form and one was in solid form. The solid was obtained by evaporating 1 mc of shipment (1) to dryness in the "solid" type extended geometry lucite vial (Fig. 5.2.2-1). Of the liquid sources, one was of "1 centipoise" viscosity, i.e., used just the way it arrived from Oak Ridge (shipment (1)), and the other was of temperature-variable viscosity, prepared from shipment (2) as follows. Two cc of the stock solution were evaporated to .05cc, then GP pure glycerin (greater than 99% pure) was added to make 1.95 cc. The remaining volume of .05 cc was filled by the thermo-couple. This solution was duplicated using non-radioactive indium for experimental determination of viscosity versus temperature. Relative viscosities were measured using a simple "rate-of-fall" viscosimeter. The results are shown in Fig. 5.2.2-2.

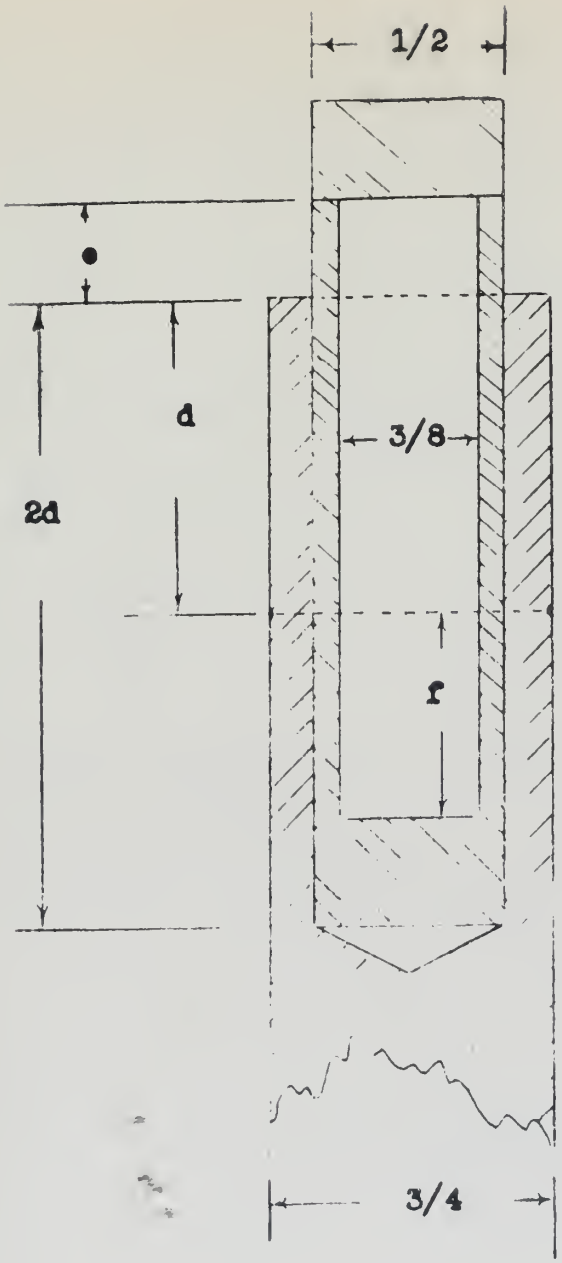

EXTENDED SOURCE HOLDER

d= "13/16

e= "1/4

f= ".276 (Solid Source)

= ".551 (Liquid Source)

Volume of Source:
Solid - 1 cm^3
Liquid - 2 cm^3

Depth of Hole in Lucite
= d + e + f

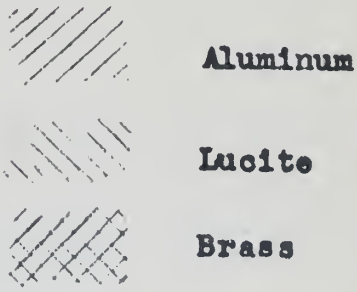

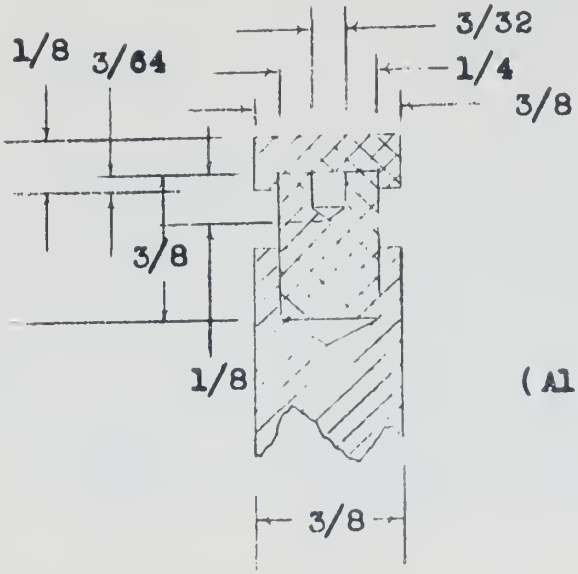

POINT SOURCE HOLDER

SOURCE HOLDERS

Fig. 5.2.2-1

(All Dimensions In Inches)

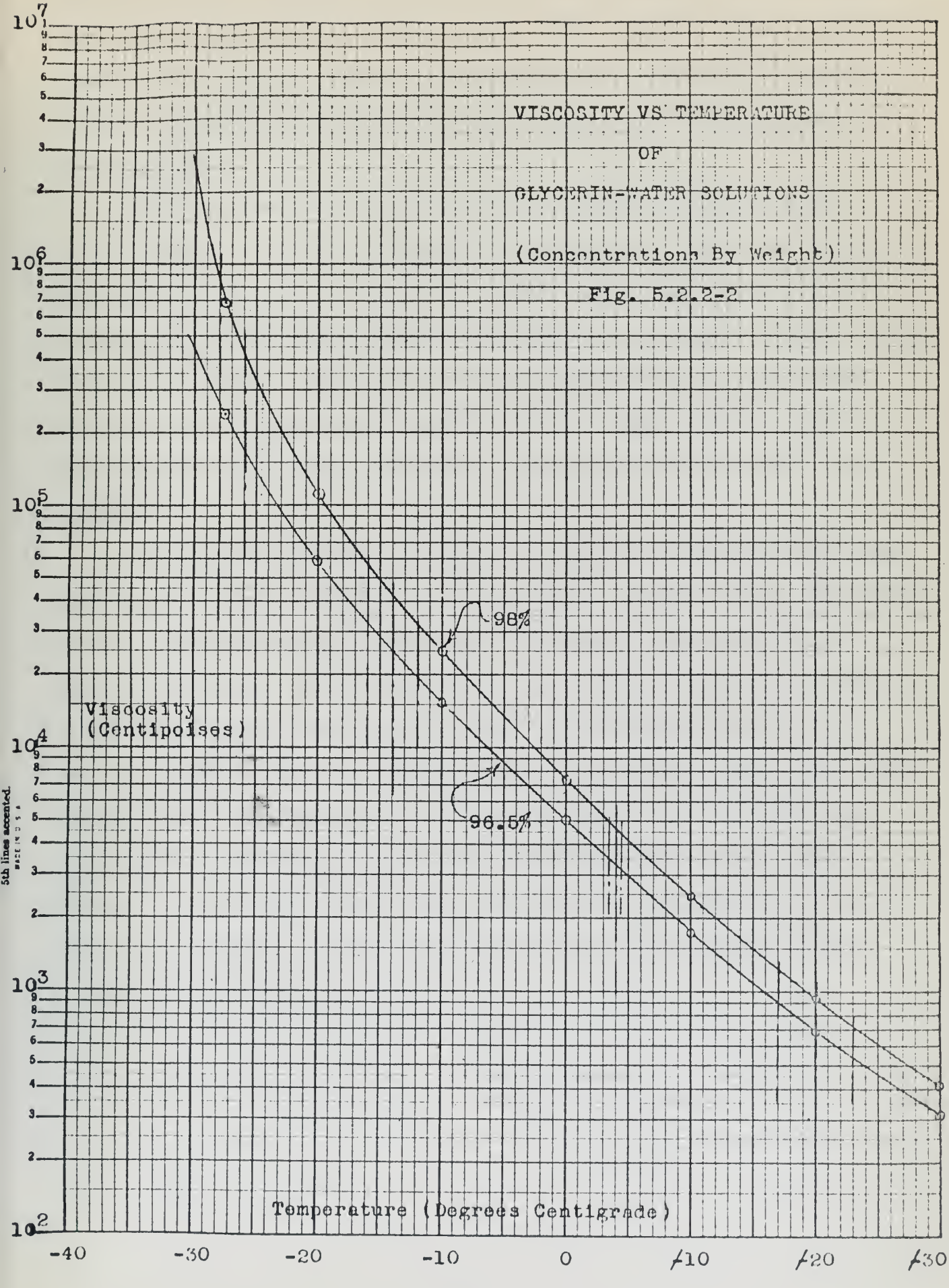
VISCOSITY VS TEMPERATURE
OF
GLYCERIN-WATER SOLUTIONS
(Concentrations By Weight)
Fig. 5.2.2-2
98%
96.5%
Viscosity
(Centipoises)
Temperature (Degrees Centigrade)
10^7
10^6
10^5
10^4
10^3
10^2
-40
-30
-20
-10
0
+10
+20
+30

Points for zero degrees and above were from (1M53); points below zero were experimentally determined. Fig. 5.2.2-3 shows a photograph of the source mounting arrangement for the In^{114} - Glycerin source. The activity of each of the liquid In^{114} sources was about 1.5 mc.

Three separate Na^{22} sources were prepared, each of about 100 uc activity. Two of these were prepared in "extended source" containers, and one in a "point source" container (Fig. 5.2.2-1). Of the two in "extended source" containers, one had a thermo-couple and one did not. This was to check on variations in scattering conditions as discussed in Section 5.2.1. Fig. 5.2.2-4 shows a photograph of the source mounting arrangement for the Na^{22} point source.

It is worthwhile at this time to mention something about the schedule followed relative to the sources. First of all, the complete, undisturbed correlation was measured, using the dilute aqueous solution. Following this, the various disturbed "anisotropy only" measurements were taken, interleaving from day to day in a random manner the source to be measured. Also, the "anisotropy only" measurements for the undisturbed correlation was measured about midway through the disturbed "anisotropy only" runs. In this way it was hoped to minimize the possibility that long term "drifts" in the electronics could be mistaken as an effect of the source.

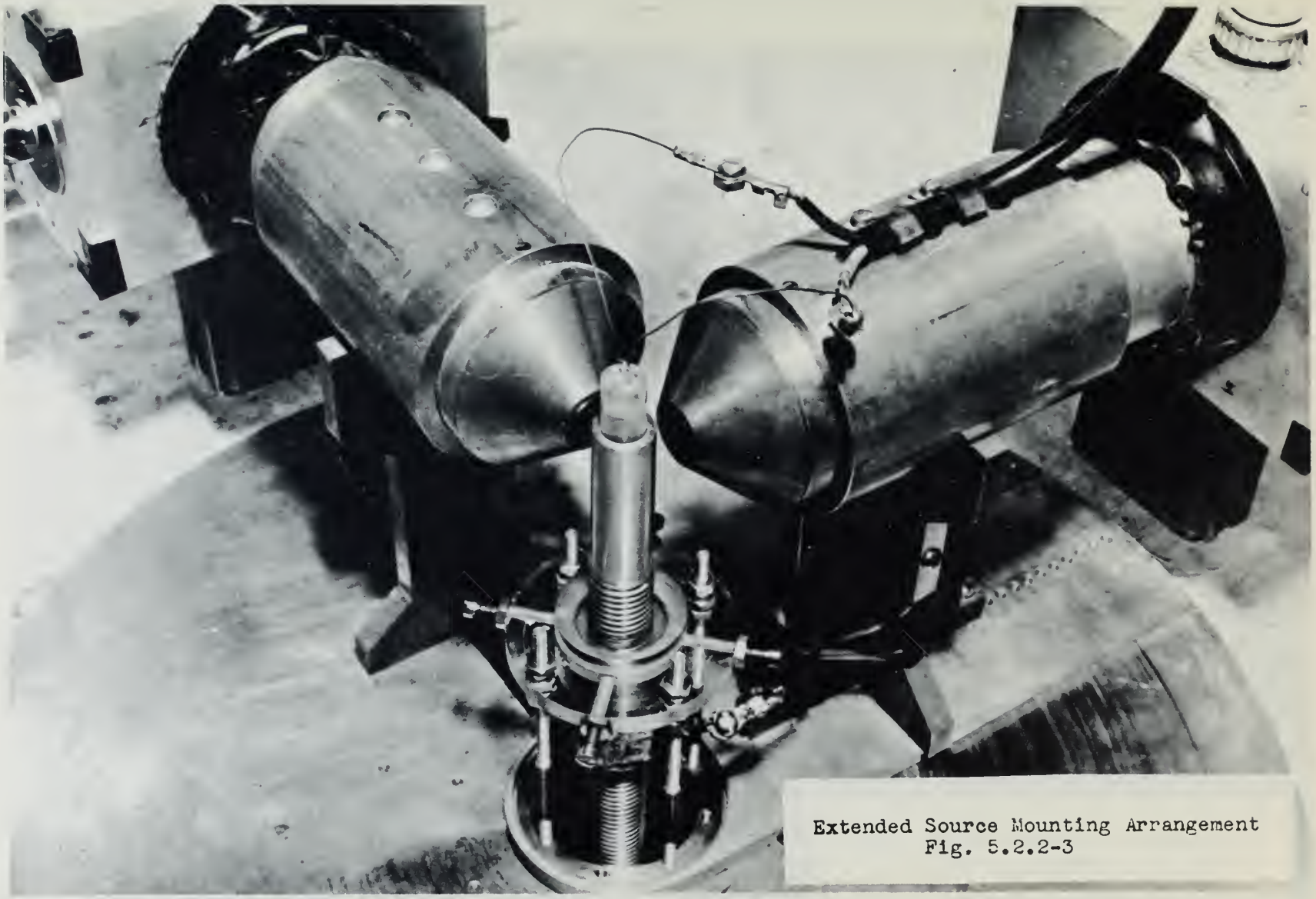

Extended Source Mounting Arrangement
Fig. 5.2.2-3

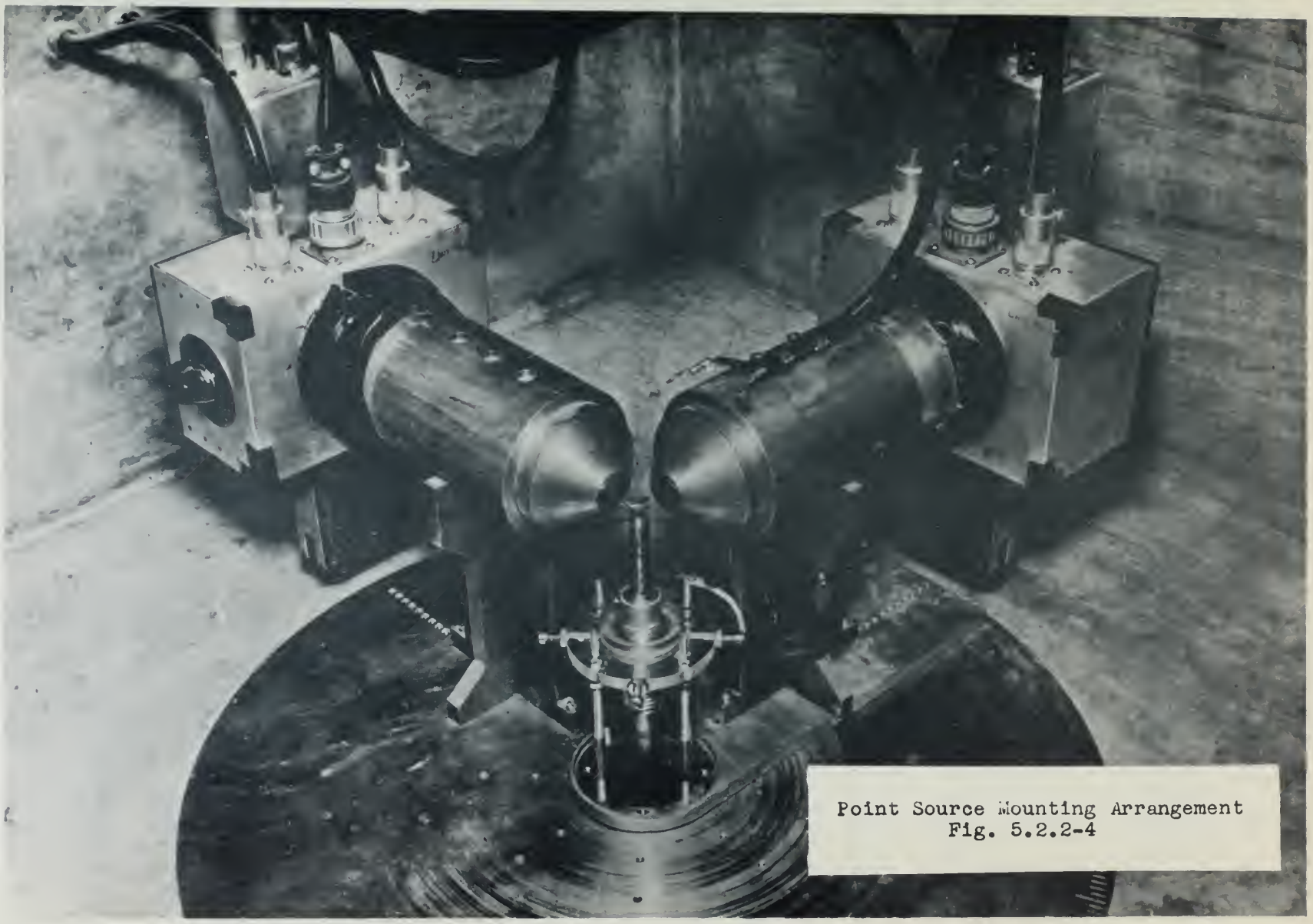

Point Source Mounting Arrangement
Fig. 5.2.2-4

Part 5.3 - Data Reduction

Section 5.3.1 - Errors in General

The raw data as it is measured has in it many errors. We can divide these errors into five groups:

1. Systematic Errors - Errors due to malfunctioning or misalignment of the apparatus, such as electronic drifts or source eccentricities.

2. Inherent Errors - Errors inherent in the design of the apparatus, present even when adjustments are perfect and operation stable, such as errors due to finite detector and source size.

3. Statistical Errors - Errors observed due to the random nature of the events counted.

4. Lifetime Errors - Errors due to the continually changing strength of the source due to its radioactive decay.

5. Decay Scheme Errors - Errors in the observed results due to the nature of the decay scheme, such as the presence of an annihilation coincidence rate at 180° due to the presence of a positron component in the decay.

Corrections must be made for each of the above errors. The sections in which they are discussed are listed below:

Error No.	Section No.	Title
1, 4	5.3.2	Data Normalization
2	5.3.3	Geometrical Corrections
3	5.3.4	Statistics
4	5.3.5	Decay Scheme Corrections

Section 5.3.2 - Data Normalization

Assume that one has a source which decays in a single gamma-gamma cascade. Let the source strength be N_0 decays per second. One observes a coincidence rate as a function of the angle between the detectors. Assuming no coincidences arising from crystal-to-crystal scattering (Section 5.2.1), the observed coincidence rate is the sum of two independent rates:

(1) a true coincidence rate, N_{TR}, due to the two gammas in the same decay, and

(2) a chance coincidence rate, N_{CH}, arising completely by chance from separate but simultaneous decays.

Letting the observed, or total, coincidence rate be $N_{TO}(\theta)$, we have:

(1) $N_{TO}(\theta) = N_{TR}(\theta) + N_{CH}$.

Furthermore, considering also the time dependence,

(2) $N_{TR}(\theta,t) \quad N_0(t)W(\theta)[\lambda_{1a}\lambda_{2b} + \lambda_{2a}\lambda_{1b}]\gamma$

where $W(\theta)$ is some function of the angle between the detectors, λ_{ij} is the probability that an isotropically emitted gamma ray, i, will be detected and recorded in channel j, and γ is a further reduction factor due to the electronics. It includes the efficiencies of the fast double and slow triple coincidence circuits, and the scaler counting efficiency.

The chance rate is expressed by,

(3) $N_{CH}(t) = 2\tau N_0^2(t)[\lambda_{1a}+\lambda_{2a}][\lambda_{1b}+\lambda_{2b}]\gamma$

where τ is the "resolving time" of the apparatus, i.e., the maximum amount of time by which two pulses can be separated and still considered "in coincidence".

If we express the single channel rate by N_i, then,

(4) $N_i(t) = N_0(t)[\lambda_{1i} + \lambda_{2i}] \qquad i = a, b$

Combining (1), (2), (3), and (4) we come down to:

$$(5)\qquad \frac{N_{TO}(\theta,t)}{N_a(t)N_b(t)} = \frac{W(\theta)}{N_0(t)}\left[\frac{\lambda_{1a}\lambda_{2b}+\lambda_{2a}\lambda_{1b}}{(\lambda_{1a}+\lambda_{2a})(\lambda_{1b}+\lambda_{2b})}\right]\gamma + 2\tau\gamma$$

But we are interested in the true coincidence rate. By a slight transformation (5) becomes:

$$(6)\qquad N_{TR}(\theta,t) = N_{TO}(\theta,t) - N_{CH}(t) = W(\theta)\,\frac{N_a(t)N_b(t)}{N_0(t)}\left[\frac{(\lambda_{1a}\lambda_{2b}+\lambda_{2a}\lambda_{1b})\gamma}{(\lambda_{1a}+\lambda_{2a})(\lambda_{1b}+\lambda_{2b})}\right]$$

Now, to a first approximation the factor on the right in brackets is independent of systematic errors consisting of small eccentricities of the source and small electronic drifts. This will be shown later in more detail.

The ratio of $W(\theta)$ at two different angles θ_1 and θ_2, at two different times t_1 and t_2 can be extracted from (6) by dividing the true coincidence rates at these angles, remembering that the factor in brackets is to first order a constant. We then have:

$$(7)\qquad \frac{W(\theta_2)}{W(\theta_1)} = \frac{N_{TR}(\theta_2,t_2)\,N_a(\theta_1,t_1)\,N_b(\theta_1,t_1)\,N_0(t_2)}{N_{TR}(\theta_1,t_1)\,N_a(\theta_2,t_2)\,N_b(\theta_2,t_2)\,N_0(t_1)}$$

which is our desired form, normalized against the small errors already mentioned. It is also the form in which we are interested in the correlation function, $W(\theta)$, i.e., as a ratio rather than as an absolute value.

In order to show that the factor in brackets in (6) is approximately constant we begin by defining,

$$(8)\qquad \mu_{i,jk} \equiv \frac{\lambda_{ji}}{\lambda_{ki}} \qquad \begin{matrix} j,k = 1,2 \\ i = a,b \end{matrix}$$

and examining λ_{ii} a little more closely:

$$(9)\qquad \lambda_{ii} = \omega_{ii}\,\epsilon_{ii}\,\delta_{ii}$$

where ω is the effective relative solid angle presented by the detector to the gamma ray, and

ϵ is the detection efficiency of the detector, or counter

as it is often called, for the gamma ray, and

δ is the channel factor, i.e., the fraction of the detected gamma rays which fall within the window.

Then,

$$\mu_{i,jk} = \frac{\omega_{ji}\,\epsilon_{ji}\,\delta_{ji}}{\omega_{ki}\,\epsilon_{ki}\,\delta_{ki}} \qquad \begin{matrix} j,k = 1,2 \\ i = a,b \end{matrix} \tag{10}$$

Now, the assertion is that (10) is insensitive to small electronic drifts and small eccentricities in the source. For although both δ_{ji} and ω_{ji} will change with the fluctuation in various voltage levels, the ratio $\frac{\omega_{ji}}{\omega_{ki}}$ and $\frac{\delta_{ji}}{\delta_{ki}}$ will not change if the window is properly chosen. Similarly, ω_{ji} is a function of θ for an eccentric source, but $\frac{\omega_{ji}(\theta)}{\omega_{ki}(\theta)}$ is a constant for small eccentricities.

By making use of (8) we can express the factor in brackets in (6) as follows:

$$\left[\frac{(\mu_{a,21} + \mu_{b,21})\gamma}{(1+\mu_{a,21})(1+\mu_{b,21})}\right]$$

From the discussion in the previous two paragraphs, we see that the μ's are approximately time and angle independent. Assuming an approximately constant coincidence circuit efficiency, expressed by γ, we have thus shown that the factor above is approximately time and angle independent; hence (7) is justified.

Section 5.3.3 - Geometrical Corrections

General

The directional correlation function, $W_{(\theta)}$, as derived by Hamilton (1H40), represents a microscopic phenomenon, viz., the relative directional probability for the decay of a single nucleus. The apparatus, however, observes a "macroscopic phenomenon macroscopically", i.e., it observes a finite volume of many millions of nucleii, whose exact location is uncertain to the extent of the linear dimensions of the source volume, and it observes these with extended detectors which introduce an additional angular uncertainty. Hence we are not precisely sure where the gamma ray we count came from nor exactly where it went. What we measure is a weighted average of $W_{(\theta)}$ integrated over the detectors and through the volume of the source. We wish to determine how the coefficients of our measured function, $\overline{W}_{(\Theta)}$, are related to the coefficients of the "microscopic" function, $W_{(\theta)}$, where Θ is the angle between the axes of the detectors and, as usual θ is the angle between the propagation vectors of the two radiations involved in the cascade. These relations we call "geometrical corrections".

The reader is referred to Appendix III for a general treatment of the philosophy of these corrections. There we present the basic arguments for our consideration of the geometrical corrections under the following two headings:

(a) Finite Detector - Point Source, and

(b) Point Detector - Finite Source.

In this section we will discuss (a) in some detail, but merely quote the results pertaining to (b) which is treated more extensively in Appendix III.

Finite Detector - Point Source

In 1F51 Frankel shows that the effect of the finite detector solid angle subtended at a point source is to cause a simple reduction in the magnitude of the correlation coefficients. That is, the observed function,

(1) $$W'_{(\theta)} = \sum_{K} Q_{2K} A_{2K} P_{2K}(\cos\theta)$$

where the A_{2K} are the coefficients of the "microscopic" function,

(2) $$W_{(\theta)} = \sum_{K} A_{2K} P_{2K}(\cos\theta)$$

In 1C52 Church and Kraushaar indicate a convenient method of experimentally determining the Q_{2K} using the "combined" relative angular resolution curve, $H_{(\theta)}$, which is the directional correlation of annihilation radiation. That is,

(3) $$Q_{2K} = \int H_{(\theta)} P_{2K}(\cos\theta) d(\cos\theta)$$

where $H_{(\theta)}$ is the "combined" relative angular resolution curve using annihilation radiation, and θ is the angle between the axes of the detectors.

In 1L53 Lawson and Frauenfelder point out essentially that the $H_{(\theta)}$ of 1C52 does not give a true picture of the overall response under most conditions. This is because the individual detector resolution curves, which Lawson and Frauenfelder call $\epsilon_{(\alpha)}$, α being the angle between the detector axis and an element of detector solid angle, $d\omega$, are strongly dependent on gamma ray energy, E_g, and the window base line energy, E_b, i.e., the minimum gamma ray energy accepted by the pulse height selector. In other words, gamma rays of different energies "see" apparently different solid angles, and in addition any change in "base line" discriminator setting will also cause apparent solid angles to change. All this points up serious limitations to the annihilation radiation methods of 1C52. However, calibrating

each detector with gamma rays of energies identical with, or close to, the ones in question, as required by the method of 1L53, is by no means easy; it is sometimes impossible to obtain a single gamma ray of the required energy and effective collimation is difficult.

The purpose of this discussion is to point out a refinement of the method of Church and Kraushaar which will remove some of the difficulties indicated by Lawson and Frauenfelder, and still retain the experimental simplicity of the former method.

The proposed method is based on the assumption that we can imagine a combined angular resolution curve, H', based on hypothetical gamma rays of the energies in the cascade but which have an agular correlation like the 511 KEV annihilation radiation, i.e., a delta function, and that aside from an arbitrary normalizing factor,

$$(4) \qquad H'(\theta, E_{g1}, E_{g2}, E_{b1}) \approx H(\theta, E_{g3}, E'_{b1}, E'_{b2})$$

where E_{g1} and E_{g2} are the energies of the cascade gamma rays and E_{g3} is the energy of annihilation radiation, 511 KEV. E_{b1} is the window base line energy used in practice and E'_{b1} and E'_{b2} are "calibrating" window base line energies chosen so that the combination:

$E_{g1} \leftrightarrow E_{b1}$ "sees" the same solid angle as $E_{g3} \leftrightarrow E'_{b1}$,

and $E_{g2} \leftrightarrow E_{b1}$ "sees" the same solid angle as $E_{g3} \leftrightarrow E'_{b2}$.

Or, expressed symbollically:

$$(5) \qquad \beta_1(E_{g1}, E_{b1}) \approx \beta_3(E_{g3}, E'_{b1})$$

and

$$\beta_2(E_{g2}, E_{b1}) \approx \beta_3(E_{g3}, E'_{b2})$$

where β_i is the angle of Compton scattering which degrades the gamma ray from E_{gi} to E_{b1} . $i = 1, 2$ These calibrating base line energies, E'_{b1} and E'_{b2} are determined using Fig. 5.2.1-8. For reasons discussed in Section 5.2.1, a value of E_{b1}

of 430 KEV was used throughout the experiment.

In other words (4) and (5) assume that the half width of the resolution curve, but not its essential shape, is different for various E_γ, E_b combinations. This assumption seems justified up to about $E_\gamma = 1$ MEV. There is also the implicit assumption that the differential cross section per unit solid angle for Compton scattering remains approximately the same:

(6) $$\frac{d\sigma}{d\Omega}(\beta_i) \approx \frac{d\sigma}{d\Omega}(\beta_3) \qquad i = 1, 2$$

Thus, the procedure is to determine from Fig. 5.2.1-8 the base line energies E'_{b1} and E'_{b2} which bear to $E_{\gamma 3}$ the same relation (via the Compton scattering mechanism) as does E_{b1} to $E_{\gamma 1}$ and $E_{\gamma 2}$ (5), then measure $H(\theta, E_{\gamma 3}, E'_{b1}, E'_{b2})$ and by (4) use it for $H'(\theta, E_{\gamma 1}, E_{\gamma 2}, E_{b1})$. Obviously the method is only an approximation, but the smaller the difference $E_{\gamma i} - E_{\gamma 3}$, the better the approximation. $i = 1, 2$

Now let us apply (3)' with a slight modification as follows:

Since we measure coincidences in two ways indicated in the following table, both of the following combinations apply:

Combination No.	Gamma Ray No.	Detector
1	1	a
	2	b
2	1	b
	2	a

We must take two "combined" angular resolution curves, $H_i(\theta, E_{\gamma 3}, E'_{b1}, E'_{b2})$, using annihilation radiation where i represents the combination number above, and the respective window base lines are given below:

Combination No.	Channel 1 (Detector a) Base Line	Channel 2 (Detector b) Base Line
1	E'_{b1}	E'_{b2}
2	E'_{b2}	E'_{b1}

Then (3) becomes:

(7) $$Q_{2K} = \frac{1}{2}\left[J_{1,2K} + J_{2,2K} \right]$$

where:

(8) $$J_{i,2K} = \int P_{2K}(\cos\theta)\, H_i(\theta)\, d(\cos\theta) \qquad i = 1,2$$

It turns out that in this apparatus that:

(9) $$H_1(\theta) \approx H_2(\theta)$$

Hence by (7):

(10) $$Q_{2K} = \int P_{2K}(\cos\theta)\, H_1(\theta)\, d(\cos\theta)$$

We thus have a method for calculating the coefficient correction factors of our "Finite Detector - Point Source" correction. The method retains the experimental simplicity of 1C52 while removing to first order at least the major objection raised to 1C52 by 1L53.

Point Detector - Finite Source

As remarked previously, we shall only quote here the results which are considered in more detail in Appendix III.

We observe a function, $\overline{W}(\Theta)$, where Θ is the angle between the detectors, and $\overline{W}(\Theta)$ is given by:

(11) $$\overline{W}(\Theta) = \sum_K C_K P_K(\cos\Theta)$$

(Note that K may possibly include odd integers).

We wish to determine the relationship between the C_K's and the $Q_{2K} A_{2K}$'s of (1) which we will designate by B_{2K}.

Then from Appendix III:

$$
\begin{aligned}
(12)\qquad C_0 &= B_0+\xi_0^2\left(B_0+\tfrac{1}{12}B_2+\tfrac{7}{16}B_4\right)+\gamma_0^2\left(-\tfrac{2}{3}B_0-\tfrac{1}{3}B_2-\tfrac{1}{3}B_4\right)\\
C_1 &= \xi_0^2\left(B_0-\tfrac{13}{20}B_2-\tfrac{3}{4}B_4\right)+\gamma_0^2\left(B_2+B_4\right)\\
C_2 &= B_2+\xi_0^2\left(\tfrac{5}{4}B_4\right)+\gamma_0^2\left(-\tfrac{4}{3}B_2-\tfrac{5}{3}B_4\right)\\
C_3 &= \xi_0^2\left(\tfrac{12}{5}B_2-\tfrac{3}{4}B_4\right)+\gamma_0^2\left(\tfrac{7}{3}B_4\right)\\
C_4 &= B_4+\xi_0^2\left(-3B_4\right)+\gamma_0^2\left(-2B_4\right)\\
C_5 &= \xi_0^2\left(5B_4\right)
\end{aligned}
$$

Where ξ_0 is the ratio of the radius of the source volume consisting of a centered right circular cylinder coaxial with the z axis of the coordinate system to the distance from the origin to the detectors and γ_0 is the ratio of the "half-height" of the cylinder to the origin-to-detector distance. Actually, the B_K's appearing in (12) do not yet correspond exactly to the $Q_{zK}A_{zK}$'s of (1), but when normalized to $B_0=1$ they will. It is almost too obvious to mention that the finite source does cause "mixing" of the coefficients, and it thus behooves one to keep ξ_0 and γ_0 as small as the requirements of the experiment will allow.

Other Geometrical Sources of Error

A pitfall that must be guarded against is the distorting effect of the lips of the lead shields of the detectors, which have the effect of making the crystal response more sensitive to the exact position of the source than would be the case in the absence of the lead. (For this reason there would have been some advantage in the specific case of Cd^{114}, where the gammas being investigated are fairly close in energy, in eliminating the lead shields and in relying upon the available energy discrimination to avoid crystal-to-crystal scattered coincidences (Section 5.2.1), but in general this method fails when the gammas

are far apart in energy).

The distorting effects of the lead shields take place in two ways:

(a) The lips of the shields accentuate the spurious correlations arising from source eccentricities in the plane of the detector axes, as indicated in the figure at right. For an unshielded detector the principal effect of this horizontal eccentricity is that caused by variation in source-detector distance as the angle between the detector axes is varied; with lead shields this effect is accentuated by the undesired shielding of the detector by the lips of the shield at certain angles.

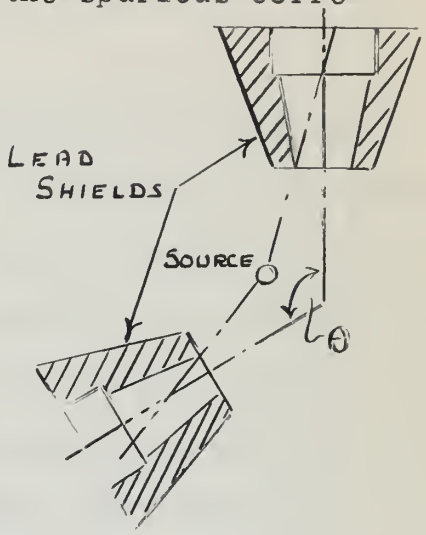

(b) For a point source which is off center in the vertical direction, the lips of the shields, by shielding the detector in an asymmetric manner relative to the source, cause the effective detector angular resolution curve to lose its symmetry with respect to the detector axis. The fact that there is no mixing of coefficients in the "Finite Detector - Point Source" correction (1), is based on the detector axial symmetry of this resolution curve; hence in this case if we apply (1), we will introduce error. In this case not only does the effective resolution curve lose its aforementioned axial symmetry, but its half width changes also as the source position is varied in the region where the optical view of the detector from the source is masked by the lips of the shields. We have spoken so far of a point source, but what we have said applies equally well to each element of a finite source.

Of the two types of error, (b) is the more insidious in that it has no well defined symptom which arises in practice. Type (a), for instance, manifests itself immediately by an anisotropy in the single channel rates, whereas (b) shows up only as an error in the results.

The precautions taken against these errors are careful mechanical and electronic adjustments. In case (a), we center our source in the plane of the detector axes by observing the single channel rates as a function of detector angle and choosing that position which yields the most isotropic single channel response. In the vertical direction, case (b), the Na^{22} point source was aligned at the position of maximum coincidence counting rate, which is very sensitive to vertical eccentricities, at a relative detector angle of 180 degrees. The same procedure was followed for the extended Na^{22} source, and the position thus found was used for the In^{114} sources which used the same geometry as the extended Na^{22} source.

One might think that errors arising from case (b) might best be handled by measuring the resolution curve associated with the Na^{22} extended source and using this in a calculation as per (1) - (10) above, but from (12) we see that the coefficient mixings introduced by the source extent would cause error if we used in (10) the results obtained with an extended source. The procedure followed was first to take a combined angular resolution curve, as defined by (3) and (9) above, using the Na^{22} point source, then determine the "Finite Detector - Point Source" corrections from (10) above. Then the coefficients of the In^{114} correlation, B_{2k} , uncorrected for finite detector size, were extracted from the observed coefficients, C_k , using (12). The

true coefficients, A_{2K}, were then determined from the B_{2K} by the application of (10). In applying (12), there is an ambiguity in $\mathcal{J}_o$ corresponding to the fact that the "half-height" of the source is defined in part by the aperture in the lead shield of the detector; but this correction was small enough not to be sensitive to assumptions on this point. The same calculations also assume that the "Finite Detector - Point Source" corrections, based on the detector angular resolution curves, were the same for source elements at all heights. That this is not exactly true is discussed under case (b) above, but since we have an extended source, for small displacements of the source center, there is always a source region of the same size which has a "view" of the detectors uninterrupted by the lips of the shields. Thus, the resolution curves from source elements in this region, which contribute much more to the coincidence rate than those elements in the "shadow" zone, still retain their symmetry and shape necessary to the application of (10) as previously mentioned. We find then that with careful vertical positioning of an extended source, the corrections are stationary with respect to vertical motion of the source center and thus the errors arising from case (b) are second order in nature.

Section 5.3.4 - Statistics

By the nature of the processes involved the measurements we take are samples from a probability distribution. The correlation function itself, $W_{(\theta)}$, is a probability function, i.e., it represents the relative probability for the emission of two successive quanta at an included angle, θ , between their propagation vectors. If, for example, we take two successive readings of the anisotropy, A, where $A = W(180)/W(90) - 1$, there is but a vanishingly small chance that they would read exactly the same, but this does not mean something is wrong with the equipment. It means that we are sampling from a probability distribution of A, centered we think at some mean value, and if we take enough samples we think we can specify that mean with a given degree of accuracy. In connection with statistical accuracy, there are several questions that may be asked. Among these are:

(1) Is there an optimum source strength?

(2) How long must one take data to obtain a given statistical accuracy?

(3) Is there an optimum division of time to be spent on the measurement of the chance rate?

Notation

Let $N_i \equiv$ Number of counts in time, T_i.

Let $m_i \equiv$ Number of counts in unit time.

Where if:

i = TO We mean TOTAL counts.

i = TR We mean TRUE coincidence counts.

i = CH We mean CHANCE coincidence counts.

i = o We mean SOURCE STRENGTH in Number of Decays.

First of all:

(1) $N_i = m_i T_i$

The apparatus measures the number of TOTAL coincidences. This number is made up of two components, (1) the TRUE coincidences due to cascade radiations proceeding from the same nucleus, and (2) the CHANCE coincidences due to radiations arising in separate but simultaneously decaying nucleii. Then we can write:

(2) $N_{TO} = N_{TR} + N_{CH}$

and

(3) $m_{TO} = m_{TR} + m_{CH}$

If we define $(\Delta N_{TR})^2$ as the variance, or mean square deviation in N_{TR}, then it is desired to see the functional dependence of the fraction $\frac{\Delta N_{TR}}{N_{TR}}$, which we define as d.

Since the variance in the TOTAL and CHANCE coincidences are independent:

(4) $\Delta N_{TR} = \sqrt{(\Delta N_{TO})^2 + (\Delta N_{CH})^2}$

If we assume a normal distribution for our directly measured quantities, then we have from elementary statistical methods:

(5) $\Delta N_i = \sqrt{N_i} \qquad i = TO, CH$

Let us make one more assumption: that we have available a total time, T, which is to be divided between T_{TO} measuring the total rate and T_{CH} measuring the chance rate. That is:

(6) $T = T_{TO} + T_{CH}$

Note that:

(7) $T_{TO} = T_{TR}$

Define:

(8) $\alpha \equiv \frac{T_{CH}}{T}$

That is, α is the fraction of the total time spent on the measurement of the chance rate.

Then:

(9) $T_{TO} = (1-\alpha)T$

And:

(10) $T_{CH} = \alpha T$

Now during that fraction of the total available time, T, to be spent on the measurement of the TOTAL rate, we measure the following number of TOTAL counts, by (1) and (9):

(11) $$N_{TO} = m_{TO}(1-\alpha)T$$

And in accordance with (5), since this is a directly measred quantity it is equal to its variance, or:

(12) $$(\Delta N_{TO})^2 = N_{TO}$$

We recall again from (5) that the mean deviation in the MEASURED chance counts would be just the square root of those measured during time αT, or $\sqrt{m_{CH}\alpha T}$, but we must remember that we do not necessarily spend the same length of time measuring CHANCE as we do measuring TOTAL. Hence this mean deviation must be normalized to $(1-\alpha)T$, the time spent on measuring TOTAL. Then we get:

(13) $$\Delta N_{CH} = \frac{(1-\alpha)}{\alpha}\sqrt{m_{CH}\alpha T}$$

Or:

(14) $$(\Delta N_{CH})^2 = \frac{(1-\alpha)^2}{\alpha} m_{CH} T$$

Combining (2), (4), (12), and (14) we have:

(15) $$\frac{\Delta N_{TR}}{N_{TR}} = d = \sqrt{\frac{\alpha + \pi}{m_{TR} T \alpha (1-\alpha)}}$$

Where:

(16) $$\pi \equiv \frac{m_{CH}}{m_{TR}}$$

We are now in a positon to answer question (3) above. There is indeed an optimum division of time, for d has a minimum with respect to α. It turns out that the optimum α is given by:

(17) $$\alpha = \pi\left[\sqrt{1+\pi^{-1}} - 1\right]$$

Substituting (17) into (15), we finally obtain:

(18) $$d = \sqrt{\frac{\left[\sqrt{1+\pi^{-1}} + 1\right]}{\left[\sqrt{1+\pi^{-1}} - 1\right] m_{TR} T}}$$

(18)' represents the obtainable statistical accuracy if time is used to the best advantage. On the other hand, it has no minimum with respect to $\mathcal{R}$. However the normal way of changing $\mathcal{R}$ would be to change the source strenth, in the process of which $\mathcal{R}$ and m_{TR} are proportional to each other. A more useful form of (18)' in which the dependence of m_{TR} and $\mathcal{R}$ on m_o appears explicitly will now be developed. If we now make the substitutions (See Section 5.3.2):

(19) $$m_{CH} = K_1 \tau m_o^2$$

(20) $$m_{TR} = K_2 W(\theta) m_o$$

Where the K's are constants, then by (16)':

(21) $$\mathcal{R} = \frac{K_1 \tau}{K_2 W(\theta)} m_o$$

Putting (20) and (21) into (18) we obtain:

(22) $$d = \frac{\sqrt{K_1 \tau / T}}{K_2 W(\theta)} \left[\sqrt{1 + \frac{K_2 W(\theta)}{K_1 \tau m_o}} + 1 \right]$$

which has no minimum with respect to m_o except as $m_o \to \infty$. Hence we have answered question (1) above in the negative; there is no optimum source strength. There is however, an effective upper limit on m_o. This is determined either by the counting rates at which the electronics cease to function efficiently or by safety considerations, whichever yields the lower value (See Section 5.2.2).

We answer question (2) by transposing (18):

(23) $$T = \frac{1}{m_{TR} d^2} \left[\frac{\sqrt{1+\mathcal{R}^{-1}} + 1}{\sqrt{1+\mathcal{R}^{-1}} - 1} \right]$$

This function is plotted in Fig. 5.3.4-1 as T vs. m_{TR} for various values of the parameters d and $\mathcal{R}$. Thus, if we have a given source and resolving time, τ, characterized by a given m_{TR} and $\mathcal{R}$, and desire a given accuracy, d, the necessary

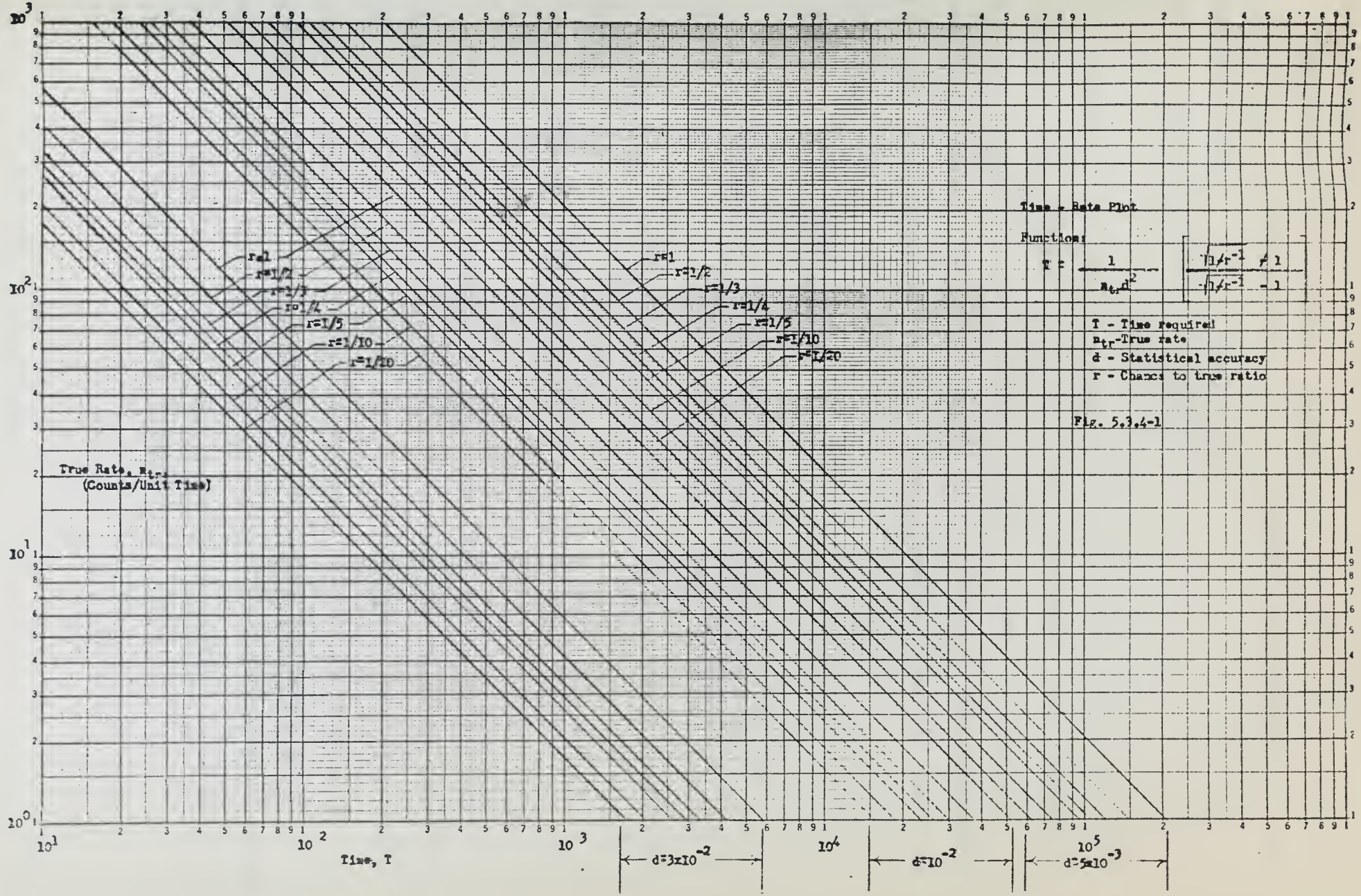
Time - Rate Plot
Function:
$T = \frac{1}{n_{tr} d^2} \left[\frac{\sqrt{1+r^{-1}} + 1}{\sqrt{1+r^{-1}} - 1} \right]$
T - Time required
n_{tr} - True rate
d - Statistical accuracy
r - Chance to true ratio
Fig. 5.3.4-1
True Rate, $n_{t.r.}$ (Counts/Unit Time)
Time, T
r=1
r=1/2
r=1/3
r=1/4
r=1/5
r=1/10
r=1/20
$d=3\times10^{-2}$
$d=10^{-2}$
$d=5\times10^{-3}$

total running time may be read directly from the figure.

We insert here a slight reformulation of (18) which is useful in that it indicates how $d(\mathcal{R})$ changes as we change $\mathcal{R}$ by whatever means:

$$(24) \qquad d(\mathcal{R}) = d(0)\sqrt{\frac{\sqrt{1+\mathcal{R}^{-1}}+1}{\sqrt{1+\mathcal{R}^{-1}}-1}}$$

The statistics we have considered so far have been those of a single large number. However, in this experiment our interest lies finally in the uncertainty of a ratio, close to unity, of two large numbers. What we finally want to know is the anisotropy, A, of the correlation where A is defined, neglecting the small corrections of Section 5.3.2:

$$(25) \qquad A \equiv \frac{N_{TR(180)}}{N_{TR(90)}} - 1$$

It can be shown that the uncertainty in A is given by:

$$(26) \qquad \Delta A = (A+1)\sqrt{\left[\frac{\Delta N_{TR(180)}}{N_{TR(180)}}\right]^2 + \left[\frac{\Delta N_{TR(90)}}{N_{TR(90)}}\right]^2}$$

Since the two terms under the square root are each approximately equal to d^2, we have:

$$(27) \qquad \frac{\Delta A}{A} \approx \frac{(A+1)}{A}\sqrt{2}\, d$$

For example, assume A = .14, what TRUE coincidence statistical accuracy would be necessary to reduce the relative uncertainty in A to 1%? The answer from (27) is $d = .000869$. And using (23) assuming $\mathcal{R} = 1/5$ and a true coincidence rate of 10 counts per minute, to attain this accuracy would require 528 hours of running time! For this reason the uncertainty in A is somewhat large. It was the practice in this experiment to run until $d = 8 \pm 3\times10^{-3}$ which yields $6\times10^{-2} \lesssim \frac{\Delta A}{A} \lesssim 1.3\times10^{-1}$.

We now wish to investigate briefly the interpretation of statistical samples. That is, if we take some readings each of which has a certain plus or minus attached to it, and if we draw in the curve which gives the least squares fit to these readings, then we ask the question: "How well do my observed points 'fit' the curve drawn through them?" Or: "What is the probability that a sample set of readings each chosen completely by chance, having in mind the probability distribution at each point on the curve, would give no better fit?" To answer these questions we use the well known χ^2 test, whose table answers this question directly. If then, it turns out that, say 99 times out of a hundred chance alone would give a better fit, then we have a strong suspicion that our apparatus is not performing its function of "random sampling" properly. However, it must be borne in mind that we are not sure that the apparatus is malfunctioning. Perhaps we have just measured that sample which is the one in a hundred instance when chance would give just the fit we measured, or worse. And if we take several hundred samples we are bound to run across this situation. This is to say that the probability distribution as given in the χ^2 table is spread evenly from zero to one. In such a situation, if a repeated group of readings give the same probability, then in only one case in ten thousand would two such random samples appear in succession with such a χ^2 ; then we would be well justified in looking to our equipment for non-random errors. One characteristic of the χ^2 test, however, is that it is concerned with three or more readings, or samples. We develop below a way of looking at just two readings.

Let us ask ourselves the following question: "Given a normal distribution, what is the probability, $P(x_0)$, that two suc-

cessive samples taken from this distribution will lie X_o or greater standard deviations apart?" The following expression (28) gives the required probability, where the terms used together with a "picture" of the integrating process is shown in the diagram.

$$(28) \quad P_{(X_o)} = \int_{-\infty}^{+\infty} P_{(X_1)} \left[1 - \int_{X_1 - X_o}^{X_1 + X_o} P_{(X_2)}\, dX_2 \right] dX_1$$

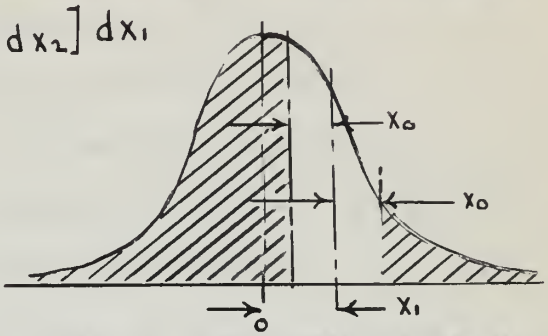

is plotted in Fig. 5.3.4-2, and is tabulated below for some rational values of X_o .

X_o	$P_{(X_o)}$
0	1.000
.25	.870
.50	.733
.75	.595
1.00	.479
1.50	.287
2.00	.157
3.00	.033

In using this data one must remember that one started with the assumption that the two samples were from the same normal distribution; it does not neccessarily follow that the inverse is inferable, that given two samples of a given separation, that Fig. 5.3.4-2 gives the probability that they are from the same distribution. It may happen that there are two separate distributions very close together, and the probability that the points are from the same distribution in this case would be less than indicated in Fig. 5.3.4-2. However, with this limitation in mind it seems that Fig. 5.3.4-2 is useful in that it gives at least an upper limit of the probability that two points are from the same distribution.

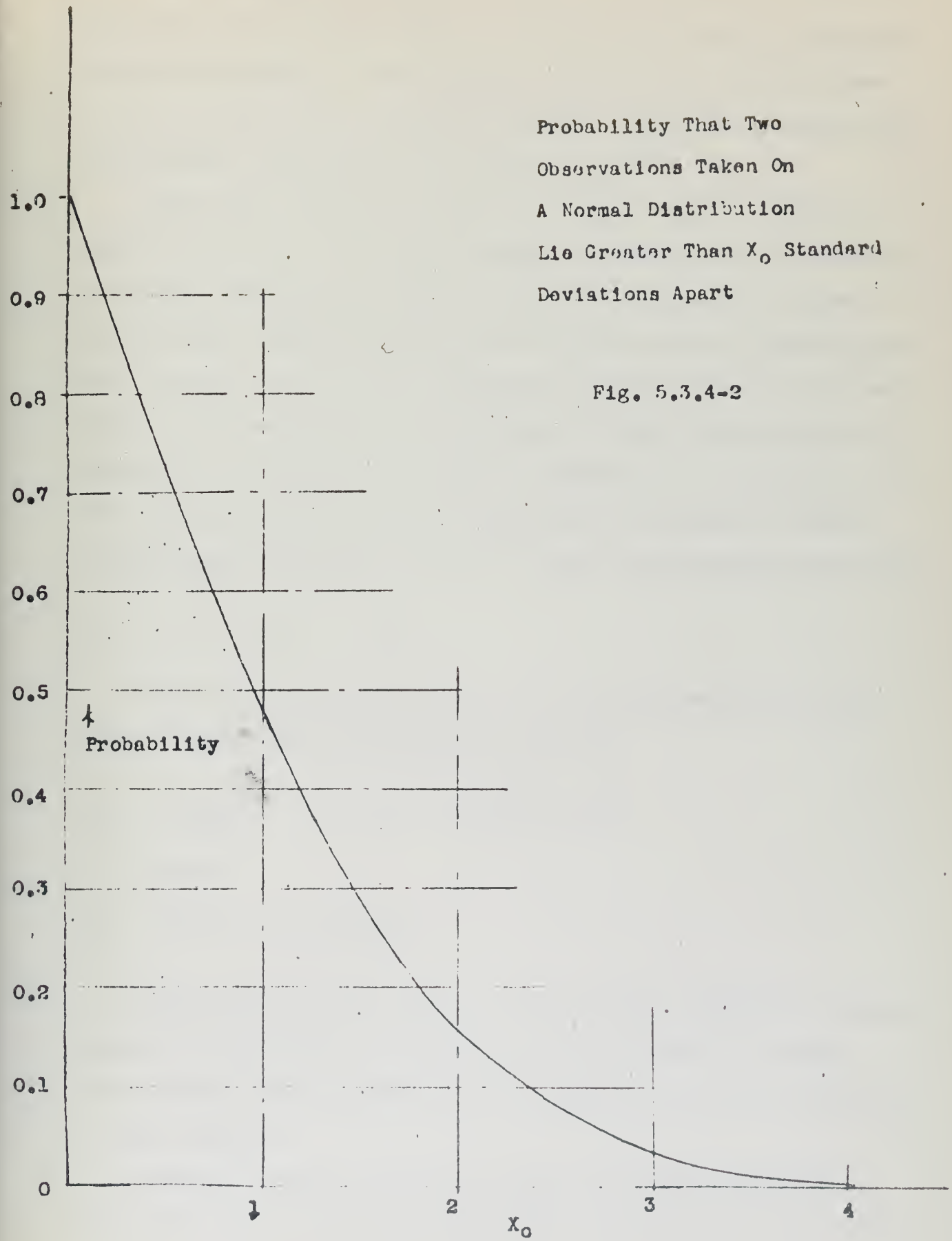

Probability That Two Observations Taken On A Normal Distribution Lie Greater Than X_o Standard Deviations Apart

Fig. 5.3.4-2

Section 5.3.5 - Decay Scheme Corrections

The observed counting rate must be corrected for certain features of the decay scheme. In this experiment the most important correction of this nature, and only one of any consequence, is that due to the annihilation radiation arising from the positron component in the decay of In^{114}.

The decay scheme as verified by Johns et. al. (1J54) is shown in Fig. 4-1. The annihilation radiation of the positron component although exceedingly weak is sufficient to cause a troublesome, unwanted coincidence counting rate at angles near 180 degrees, which if not corrected for will yield an erroneous value of the anisotropy. The method by which this problem is attacked is discussed at length in Appendix I. The result is that the positron corrected anisotropy is obtained by simply subtracting a factor, β, ($\beta \ll 1$) from the observed anisotropy.

$$(1) \qquad A'' = A''' - \beta$$

Each of the observed points are then corrected for positrons by applying the following relation:

$$(2) \qquad C_{o_g}(\theta) = C_o(\theta) - \beta(\theta) C_o(90)$$

where:

$$(3) \qquad \beta(\theta) = H_1(\theta) \beta$$

where $H_1(\theta)$ is the positron annihilation radiation angular correlation function normalized so that $H_1(180) = 1$, using the extended source geometry and a window base line of 430 KEV in each channel.

Another possible source of error which bears mention is the presence of the 576 KEV transition from the 1856 KEV level

in Cd^{114}. However since this transition is very much weaker than the 722-556 KEV cascade (relative intensity $\approx$ .03) (LJ54), it is neglected. All other gamma rays presnt in the decay are effectively excluded by energy selection.

Section 5.3.6 - Curve Fitting

After data reduction the observed function $W'''(\theta)$ was fit to the observed points by a least squares procedure. Where:

$$(1)\quad W'''(\theta) = a_0''' + a_2'''\cos^2\theta + a_4'''\cos^4\theta$$

The parameters, a_0''', a_2''', a_4''', are varied so as to minimize χ^2 where:

$$(2)\quad \chi^2 = \sum_i \left[\frac{N_{TR}(\theta_i) - W'''(\theta_i)}{\Delta N_{TR}(\theta_i)}\right]^2$$

Since approximately equal times were spent on each point:

$$(3)\quad \Delta N_{TR}(\theta_i) \approx \Delta N_{TR}(\theta_j)$$

Then we can write:

$$(4)\quad \chi^2 \sim \sum_i \left[N_{TR}(\theta_i) - W'''(\theta_i)\right]^2$$

A total of 10 points were measured, 5 each in the arcs from 90 to 180 degrees and 270 to 180 degrees. Since there was no phase shift in the correlation the points were numbered as follows:

θ	90,270	120,240	135,225	150,210	180,180
i	0	1	2	3	4

By minimizing (4) with respect to the parameters we arrive at a perscription for the parameters:

$$(5)\quad a_0''' = \frac{1}{35}\left(31y_0 + 9y_1 - 3y_2 - 5y_3 + 3y_4\right)$$

$$a_2''' = \frac{1}{35}\left(-108y_0 + 26y_1 + 80y_2 + 54y_3 - 52y_4\right)$$

$$a_4''' = \frac{1}{7}\left(16y_0 - 8y_1 - 16y_2 - 8y_3 + 16y_4\right)$$

Where:

$$(6)\quad y_i \equiv N_{TR}(\theta_i)$$

Section 5.3.7 - Data Analysis Procedures

In this experiment we observed the following:

(a) Complete Correlation - Enough points were observed to make a specific determination of the correlation coefficients. This was done only in the case of the undisturbed correlation (dilute aqueous solution of $InCl_3$).

(b) Anisotropy Only - Measurements taken only at 90-180 and 270-180 degree points. This was done in the case of all the disturbed correlations (glycerin solutions, salts, and frozen solutions), and also in case of undisturbed correlation.

The procedure in case (a) is as follows:

1. Normalize the data, i.e. correct for systematic errors as discussed in Section 5.3.2.

2. Obtain a least squares fit and calculate tentative coefficients.

3. Using results of "2" make first approximation of positron correction.

4. Using results of "3" correct observed points for positrons and recalculate the coefficients.

5. With these new coefficients recalculate positron correction for the second approximation.

6. Repeat "4" and "5" until two successive approximations of the coefficients do not change the positron correction.

7. Correct for finite source size.

8. Correct for finite detector angular resolution.

9. Find correction factor for anisotropy in undisturbed case and apply this to results of the measurement of "anisotropy only" in the unspoiled case.

10. From "9" and "8" determine final coefficients by finding the center of the areas of overlap in a plot of one correlation coefficient versus the other (See Fig. 5.4.3-1).

Solid, Polycrystalline Sources

In Chapter 3 we discussed a theory due to Abragam and Pound (1A53) related to the correlation spoilage in polycrystalline sources. We will now apply this theory; the justification for the application will be discussed in Chapter 6.

We proceed by obtaining the observed anisotropy, corrected for positrons but not for geometry, of the correlation as a function of $\Omega_0\tau_N$ where Ω_0 is the angular frequency associated with the maximum electric quadrupole or magnetic dipole level splitting, i.e. the energy difference between the highest and lowest levels in the previously degenerate state which has been perturbed by the interaction. From the plots of the above functions (Figs. 5.4.4-2,3) we can obtain a lower limit for $\Omega_0\tau_N$ for each assumed interaction. Then knowing an upper limit on τ_N, the nuclear lifetime of the intermediate state, we can set a lower limit on Ω_0.

Let A''' be the observed anisotropy corrected for systematic errors as defined in Section 5.3.2,

A'' be the observed anisotropy corrected as above but also corrected for positrons, and

A be the observed anisotropy corrected as above but also corrected for geometry.

The anisotropy is defined:

$$(1) \qquad A = \frac{W(180)}{W(90)} - 1$$

If we express the correlation function in a LeGendre polynomial expansion:

$$(2) \qquad W(\theta) = 1 + A_2P_2(\cos\theta) + A_4P_4(\cos\theta)$$

then the anisotropy is given by:

$$(3) \qquad A = \frac{12A_2 + 5A_4}{8 - 4A_2 + 3A_4}$$

From (AI-36):

$$(4) \qquad A'' = A''' - \beta$$

where β is the positron correction term.

In Section 5.3.3 is was shown that for sufficiently small values of ξ_0 and δ_0 the geometrical corrections cause:

(a) no mixing of the coefficients for finite solid angle effect, and

(b) only negligible mixing of the coefficients for finite source effect.

We can then write:

$$(5) \qquad W'' = 1 + F_2A_2P_2(\cos\theta) + F_4A_4P_4(\cos\theta)$$

where the F's are simple reduction factors arising from the above mentioned geometrical corrections.

Then by (5) and (3), the observed unspoiled anisotropy corrected for positrons becomes:

$$(6) \qquad A'' = \frac{12F_2A_2 + 5F_4A_4}{8 - 4F_2A_2 + 3F_4A_4}$$

And from the spoilage theory mentioned above, the spoiled anisotropy as a function of $\Omega_0\tau_N$, defined above, is given by:

$$(7) \qquad A''(\Omega_0\tau_N) = \frac{12F_2G_2(\Omega_0\tau_N)A_2 + 5F_4G_4(\Omega_0\tau_N)A_4}{8 - 4F_2G_2(\Omega_0\tau_N)A_2 + 3F_4G_4(\Omega_0\tau_N)A_4}$$

where the G's are expressed in Chapter 3 as a function of $\omega_0\tau_N$ where ω_0 is the angular frequency associated with the minimum level splitting in each case, and F_iA_i are the undisturbed coefficients corrected for positrons but not geometry.

We restate the expression developed in Chapter 3 for the

G's for the two types of interactions in polycrystalline sources assuming classically describable fields of axial symmetry.

(a) Electric Quadrupole Interaction:

$$(8)\quad G_{2e}(\omega_o\tau_N) = .372 + \frac{.057}{1+\omega_o^2\tau_N^2} + \frac{.343}{1+9\omega_o^2\tau_N^2} + \frac{.228}{1+16\omega_o^2\tau_N^2}$$

$$G_{4e}(\omega_o\tau_N) = .460 + \frac{.191}{1+\omega_o^2\tau_N^2} + \frac{.254}{1+9\omega_o^2\tau_N^2} + \frac{.095}{1+16\omega_o^2\tau_N^2}$$

(b) Magnetic Dipole Interaction:

$$(9)\quad G_{2m}(\omega_o\tau_N) = .2 + .4\left[\frac{1}{1+\omega_o^2\tau_N^2} + \frac{1}{1+4\omega_o^2\tau_N^2}\right]$$

$$G_{4m}(\omega_o\tau_N) = .111 + .222\left[\frac{1}{1+\omega_o^2\tau_N^2} + \frac{1}{1+4\omega_o^2\tau_N^2} + \frac{1}{1+9\omega_o^2\tau_N^2} + \frac{1}{1+16\omega_o^2\tau_N^2}\right]$$

where the subscripts "e" and "m" refer to electric and magnetic interactions respectively.

We now wish to express Ω_o in terms of ω_o, both of which have been defined above:

Electric Quadrupole Case:

It can be shown that the minimum level splitting in an axially symmetric field for integral I is given by:

$$(10)\quad \omega_{oe} = \frac{eQ\left(\frac{\partial^2 V}{\partial z^2}\right)3}{\hbar\, 4I(2I-1)}$$

where eQ is the quadrupole moment as defined in Chapter 3 and $\left(\frac{\partial^2 V}{\partial z^2}\right)$ is the gradient of the electric field along the axis of symmetry.

The maximum splitting is given by:

$$(11)\quad \Omega_{oe} = \frac{eQ\left(\frac{\partial^2 V}{\partial z^2}\right)3I}{\hbar\, 4(2I-1)}$$

So that the ratio:

(12) $\Omega_{oe} = \omega_{oe} I^2$ (For integral I)

Magnetic Dipole Case:

The minimum level splitting here is just the angular velocity associated with Larmour precession:

(13) $\omega_{om} = \frac{\mu H}{\hbar I}$

where μ is the magnetic moment, and the maximum splitting is:

(14) $\Omega_{om} = \frac{2\mu H}{\hbar}$ (For integral or half integral I)

So that the ratio:

(15) $\Omega_{om} = \omega_{om} 2I$ (For integral or half integral I)

We use Ω_{om} as an argument instead of ω_{om} because as the fields take on lower degrees of symmetry than axial the angular frequency associated with the maximum splitting, Ω_{om}, to a first approximation remains constant, while this is not necessarily so for ω_{om}.

For illustrative purposes only we also include in our plots (Figs. 5.4.4-2,3) the previously discussed (Chapter 3) square wave G'_k's.

(16) $G'_k(\omega_o\tau_N) = 1 - e^{-\frac{\delta_K}{\omega_o\tau_N}} + \frac{2\sinh(\frac{\delta_K}{\omega_o\tau_N})}{e^{\frac{2\pi}{\omega_o\tau_N}} - 1}$

where for $I = 2$ we have (again from Chapter 3):

(17) $5\delta_2 + 9\delta_4 = 4$

where the δ's are the half widths in radians of the square waves.

The purpose of including (17) and (18) is to show graphically

how G's of a widely different nature than those based on conditions of axial symmetry will yield curves of approximately the same shape near the origin (where $\Omega_o \tau_N \rightarrow 0$)

Liquid Sources:

The analysis of the spoilage of the anisotropy in liquid sources as a function of the viscosity of the source shows that we cannot apply Abragam and Pound's (1A53) liquid theory (Chapter 3). The reason is as follows. Abragam and Pound develop coefficient attenuation factors for liquid sources in the form:

$$(18) \quad G_K = \frac{1}{1 + \lambda_K \tau_N}$$

where λ_K is directly proportional to the "correlation time", τ_c , of the liquid. Correlation time can be thought of as the average time it take for an ion in a liquid to interchange its neighbors. As τ_c gets much larger than τ_N we approach the condition of the solid state; hence for the liquid theory to apply $\tau_c < \tau_N$. We observed however, no detectible dimunition in the anisotropy of the liquid sources until τ_c was of the order of 3×10^{-7} seconds which is at least three orders of magnitude larger than τ_N ; hence we cannot apply the liquid theory to this spoilage. This point will be discussed further in Chapter 6. We present therefore the liquid data merely in tabular form.

Part 5.4 - Results

Section 5.4.1 - General

In this section we will consider only the results of the experiment and leave their interpretation to Chapter 6.

Lifetime measurements were taken on the intermediate state of Cd^{114} by the method of delayed coincidences using a coincidence circuit similar to that of Bell et al. (1B52).

Result: $\tau_N \leqslant 2.3 \times 10^{-10}$ s.

Section 5.4.2 - Corrections

Decay Scheme Corrections

Calculation of β (AI-31)

Following are entries for equation (AI-31) for the calculation of the positron correction, β . Only significant plus and minuses are shown.

$\mu^a_{2,1} = 1.39$	$\mu^b_{2,1} = 1.23$	$\mu_{2,1} = 1.31$
$\mu^a_{3,4} = 0.65$	$\mu^b_{3,4} = 0.49$	$\mu_{3,4} = 0.57$

$S_{0a} = 2.79(6)$	$S_{0b} = 3.14(6)$	$S_0 = 2.96(6)$
$S_{1a} = 3.50(5)$	$S_{1b} = 4.20(5)$	$S_1 = 3.84(5)$
$S_{2a} = 2.42(6)$	$S_{2b} = 3.19(6)$	$S_2 = 2.78(6)$

$C_{0g}(90) = 1.27(3)$

$C_{1p}(180) = 2.79(3)$

$C_{1gp}(90) = 3.04(2)$

$C_{2p}(180) = 6.19(4)$

$a_2 = 0.039 \pm .046$ *

$a_4 = 0.085 \pm .038$

Note: Numbers in parentheses indicate 10 to the power.

$\alpha_p = 4(-5) \pm (-5)$

$\alpha_k = 3.5(-2)$

$\omega_3 = 2.48(-2)$

* Second approximation did not change β.

Entering these figures in (AI-31) we obtain:

$$\beta = 0.015 \pm .004$$

Geometrical Corrections

Finite Source Correction

For significance see Appendix III.

$$\xi_0^2 = .010 \qquad \gamma_0^2 = .007$$

Then (AIII-7) becomes:

$$C_0 = 0.972B_0 + 0.013B_2 + 0.009B_4$$
$$C_2 = 0.942B_2 + 0.084B_4$$
$$C_4 = 0.893B_4$$

Finite Solid Angle Correction

See Eq. (5.3.3-13) and Fig. 5.4.2-1:

$$Q_2 = 1.19Q_0 \qquad Q_4 = 1.68Q_0$$

Section 5.4.3 - Undisturbed Correlation

General procedure

a. Performed least squares fit on points corrected for systematic and decay errors as defined in Section 5.3.2.

b. Applied positron correction to points and obtained another least squares fit.

c. Corrected the LeGendre coefficients for finite source effect.

d. Corrected the LeGendre coefficients for finite solid angle.

e. Introduced the closely observed and corrected "anisotropy only" measurements in comparison with "d" and obtained final coefficients by using center of "overlap" of the two areas in Fig. 5.4.3-1.

These results are tabulated below.

$$W(\theta) = 1 + a_2\cos^2\theta + a_4\cos^4\theta = 1 + A_2P_2(\cos\theta) + A_4P_4(\cos\theta)$$

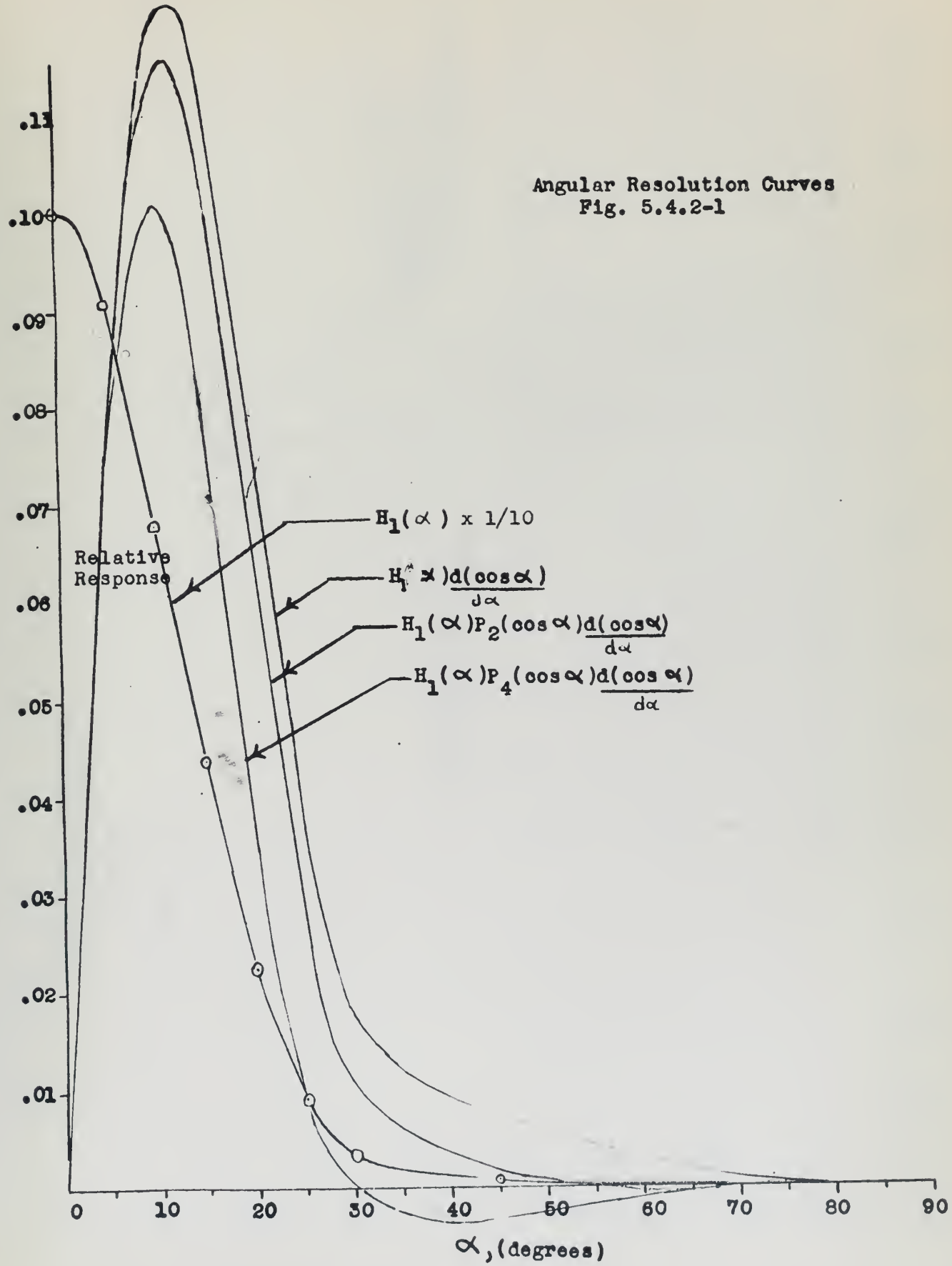

Angular Resolution Curves
Fig. 5.4.2-1

Determination of Observed
Correlation Coefficients
A_2 and A_4

Fig. 5.4.3-1

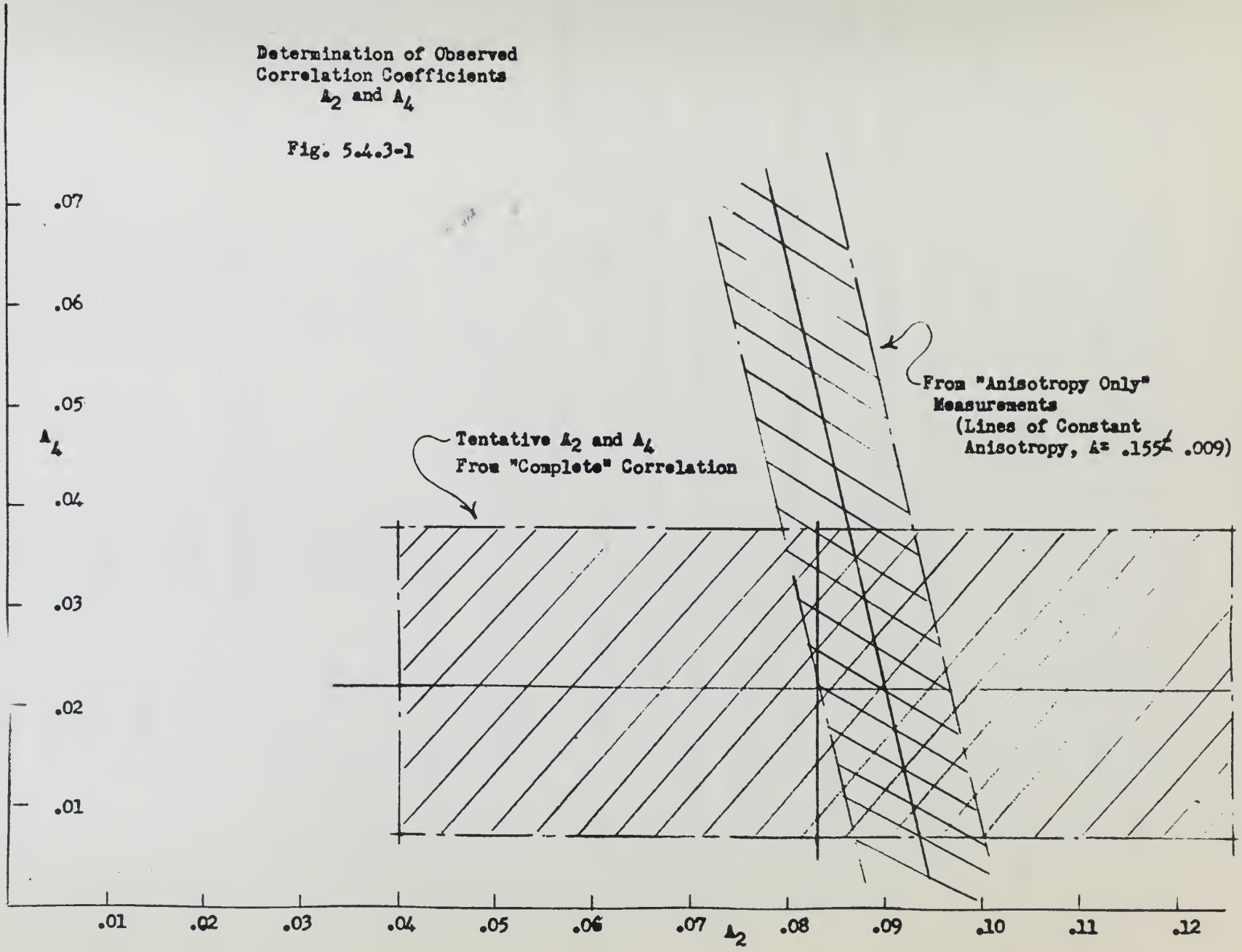

Procedure	a_2	a_4	A_2	A_4
a	.039 ± .040	.087 ± .041		
b	.059 ± .040	.052 ± .039	.067 ± .035	.012 ± .009
c			.070 ± .037	.013 ± .010
d	.044 ± .030	.100 ± .075	.083 ± .043	.022 ± .016
e	.055 ± .062	.099 ± .070	.090 ± .011	.022 ± .016

Experimental points together with curves "b" and "e" are shown in Fig. 5.4.3-2.

We list below the possible correlation coefficients for various spin assignments in the $\cos^{2k}\theta$ scheme from (1H40) for pure multipole transitions of order L. The spin assignments of the three states involved are given without parentheses; the multipole order of the transition is given in parentheses. Since Cd^{114} is an even-even nucleus we assume the ground state has a spin-parity assignment of zero-plus and the first excited state two-plus; hence for the second transition the only possibility is electric quadrupole, E2.

Group a - First Transition Dipole - Second Transition Quadrupole:

	a_2	a_4
1(1)2(2)0	-0.333	0
2(1)2(2)0	0.429	0
3(1)2(2)0	-0.103	0

Group b - Both Transitions Quadrupole:

0(2)2(2)0	3.000	4.000
1(2)2(2)0	5.000	-5.330
2(2)2(2)0	-1.154	1.231
3(2)2(2)0	0	-0.333
4(2)2(2)0	0.125	0.042

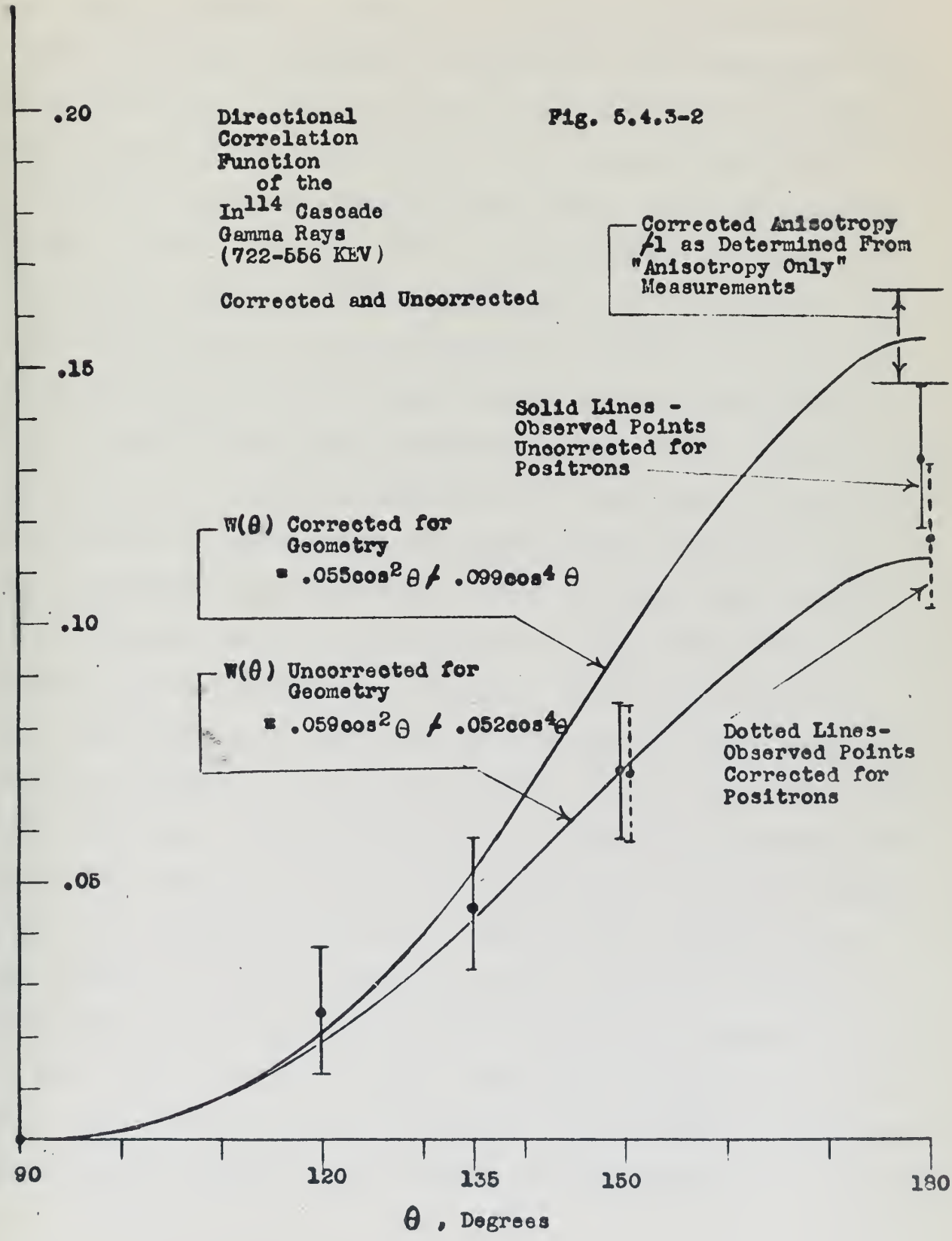
.20
.15
.10
.05
Directional Correlation Function of the In^{114} Cascade Gamma Rays (722-556 KEV)
Corrected and Uncorrected
Fig. 5.4.3-2
Corrected Anisotropy A1 as Determined From "Anisotropy Only" Measurements
Solid Lines - Observed Points Uncorrected for Positrons
W(θ) Corrected for Geometry
= .055cos²θ + .099cos⁴θ
W(θ) Uncorrected for Geometry
= .059cos²θ + .052cos⁴θ
Dotted Lines- Observed Points Corrected for Positrons
90
120
135
150
180
θ , Degrees

As will be shown in the table which follows, none of the observed coefficients supports any possible spin assignment in Group a. In Group b the 4(2)2(2)0 agrees with Steffen (1S51) but none of the others; however it is closer to the others than any other assignment in Group b. However, Steffen and Zobel (1S52) have shown subsequent to Steffen's first measurement of this correlation (1S51), that the second excited level (1278 KEV) in Cd^{114} is fed directly from the ground level (one-plus) of In^{114} by K-capture (See Fig. 4-1) which indicates a spin of two for this level in Cd^{114}. The assignment of one-plus to the ground level in In^{114} is based partly on the election rules for the beta decay to the ground state of Sn^{114}. This proceeds by an allowed transition (log ft=4.5), and since the ground state of Sn^{114} has a spin assignment of zero-plus (being an even-even nucleus), the ground state of In^{114} must have a spin-parity of one-plus or zero-plus on the basis of the selection rules. The K-capture transition to the second excited state of Cd^{114}, being allowed, implies that the spin of this state (in Cd^{114}) is zero-plus or one-plus or two-plus. If it were zero-plus, the first transition would have to be E2 and the Cd^{114} cascade would be 0(2)2(2)0, with no possibility of modification by multipole mixtures. And as will be seen, this fits no observed correlation; hence, we can eliminate zero-plus. Of the two remaining possibilities, one-plus or two-plus, the former is ruled out because it is not possible to find a multipole mixing ratio which will fit any of the observed correlations, whereas as will be seen, this is possible with a spin-parity assignment of two-plus, yielding the following cascade: 2(1,2)2(2)0. In addition, in assigning two-plus to the second excited state of Cd^{114}, we

are supported by the knowledge that most other even-even nucleii have either two-plus or four-plus for this level.

We find that we can obtain a good theoretical fit to the observed curve by considering the first transition to be a mixture of M1 and E2. From the tables of Ling and Falkoff (1L49) we construct Fig. 5.4.3-3 which gives the LeGendre coefficients of the correlation as functions of the quadrupole mixing ratio. In Fig. 5.4.3.-3 the curve A_2 is part of a tilted eccentric ellipse and A_4 is a straight line; only that part of A_2 corresponding to a relative phase of zero between the quadrupole and dipole matrix elements is given, for the best fit is in this region. Using Fig. 5.4.3-3 we obtain the mixing ratio and resulting theoretical coefficients. These are given below in comparison with those of Steffen and Zobel (1S52) and Johns et al. (1J54):

	E2 (%)	M1 (%)
Steffen and Zobel	4.4	95.6
Johns et al.	4.0	96.0
Daubin	4.2 $\pm$ .006	95.8 $\pm$ .006

Following is tabulated the coefficients as observed by various workers:

	Name	Ref.	a_2	a_4	A_2	A_4
a.	Klema & McGowan	1K52	.084	.106	.111	.023
b.	Johns et al.	1J54	-.0028	.190	.087	.059
c.	Steffen	1S51	.125	.042	.103	.009
d.	Steffen & Zobel	1S52	.090	.070	.096	.015
e.	Daubin		.055 $\pm$ .062	.099 $\pm$ .070	.090 $\pm$ .011	.022 $\pm$ .016
f.	Theoretical 2(M1,E2)2(2)0 E2 - 4.2 % M1 - 95.8 %		.086	.064	.090	.014

With the exception of "c" these curves are shown in Fig. 5.4.3-4.

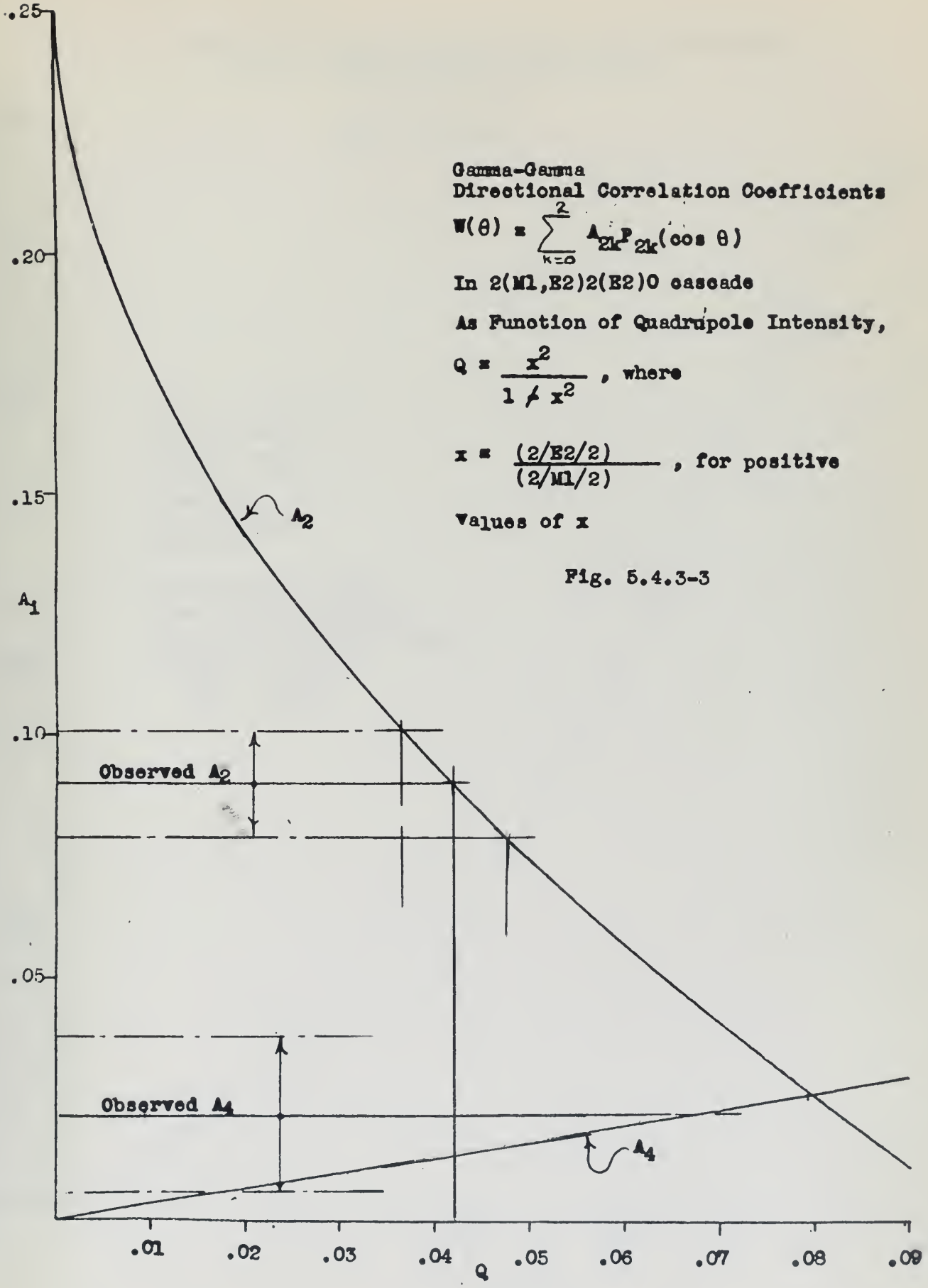

Gamma-Gamma
Directional Correlation Coefficients

$$W(\theta) = \sum_{k=0}^{2} A_{2k} P_{2k}(\cos\theta)$$

In 2(M1,E2)2(E2)0 cascade

As Function of Quadrupole Intensity,

$$Q = \frac{x^2}{1 + x^2}$$, where

$$x = \frac{(2/E2/2)}{(2/M1/2)}$$, for positive

Values of x

Fig. 5.4.3-3

Comparative Directional Correlation Functions
of the In^{114} Cascade Gamma Rays
(722-556 KEV)

Fig. 5.4.3-4

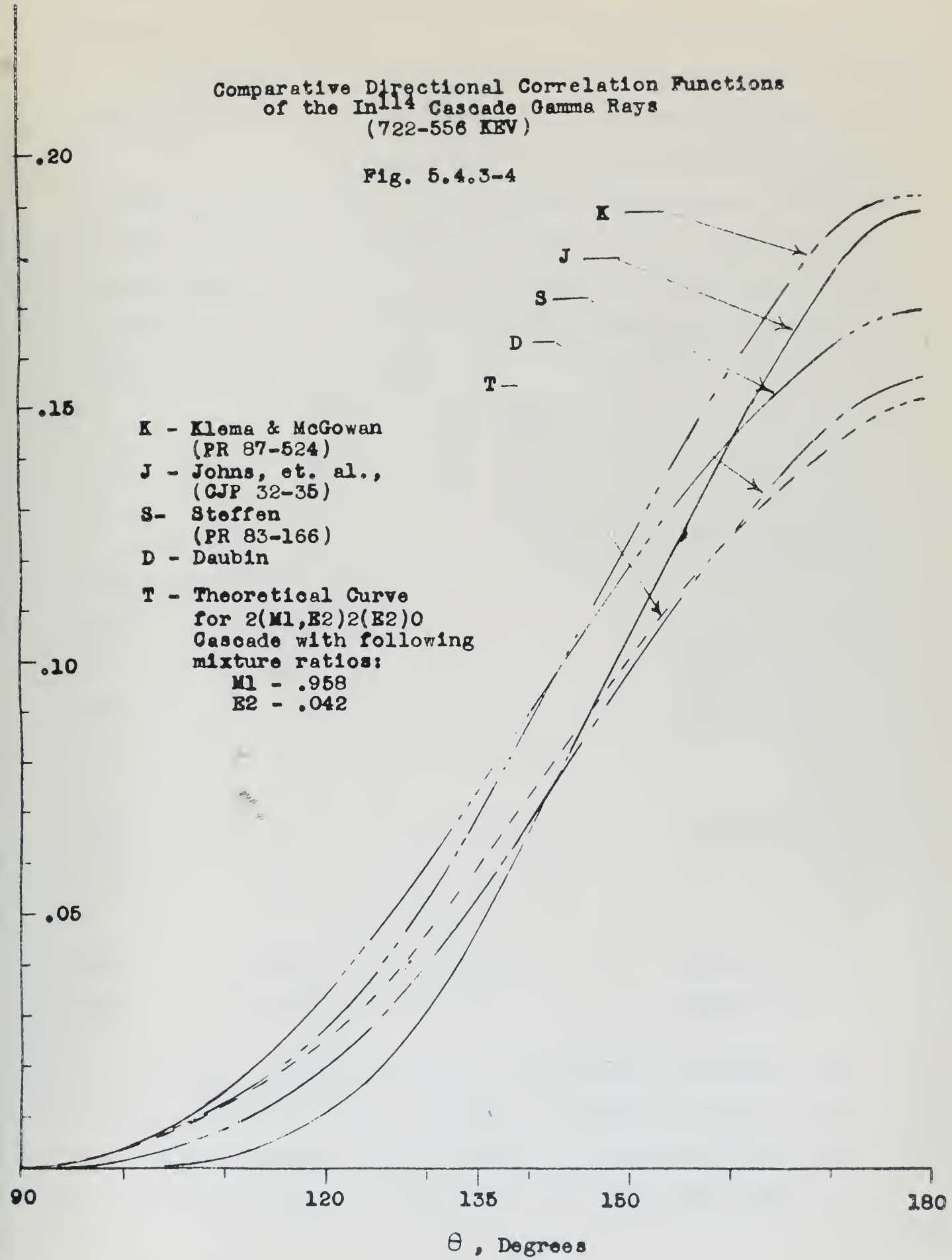

Section 5.4.4 - Disturbed Correlations

Polycrystalline Sources

See Section 5.3.7 for a discussion of how the following curves are constructed and the meansing of the different paramters used.

The source of $InCl_3$ dissolved in a dilute aqueous solution of HCl yielded the true, or undisturbed, correlation. This will be discussed further in Chapter 6. Since we use the anisotropy so measured as a starting point for the curves in Figs. 5.4.4-2,3, we list below the apparently undisturbed anisotropy together with the correlation coefficients:

$$A''(0) = .124 \pm .009$$

$$A_2''(0) = .074 \pm .037$$

$$A_4''(0) = .015 \pm .012$$

The observed anisotropies for the various polycrystalline sources are given below:

Source	Description	A''
(1)	$InCl_3$ Salt	$.097 \pm .013$
(2)	Frozen ($\sim -104^\circ C$) dilute aqueous solution of $InCl_3$ in HCl (.4N)	$.102 \pm .011$
(3)	Frozen ($\sim -104^\circ C$) dilute solution of $InCl_3$ and HCl in $> 99\%$ glycerin.	$.087 \pm .010$
(4)	Average of (1), (2), (3)	$.095 \pm .007$
(5)	Average of (2), (3)	$.095 \pm .007$

In Fig. 5.4.4-1 we show the theoretically predicted perturbed anisotropy based on Abragam and Pound's theory of classically describable, axially symmetric perturbing fields and an electric quadrupole interaction (1A53) (See also Section

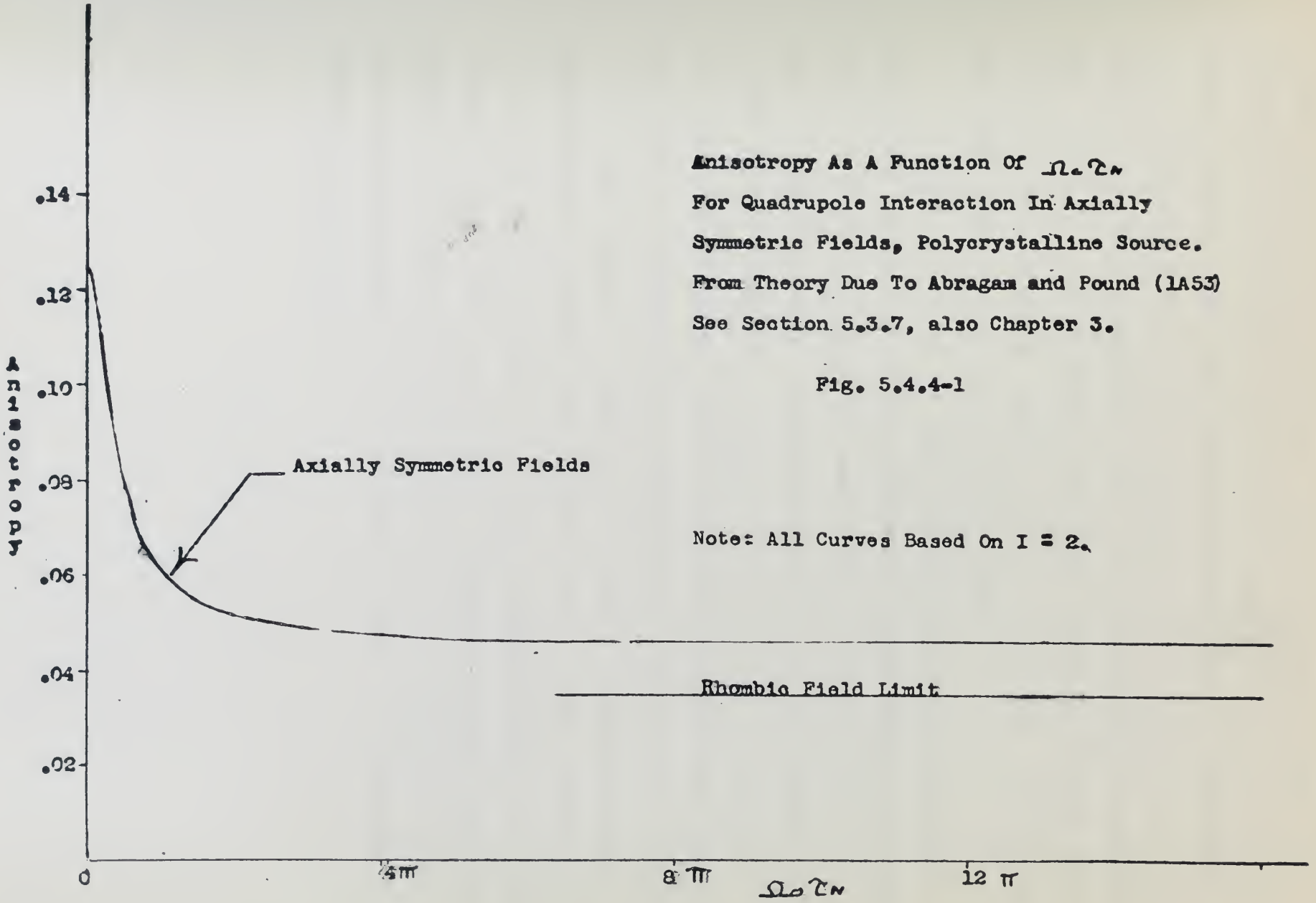

Anisotropy As A Function Of $\Omega \cdot \tau_N$
For Quadrupole Interaction In Axially
Symmetric Fields, Polycrystalline Source.
From Theory Due To Abragam and Pound (1A53)
See Section 5.3.7, also Chapter 3.

Fig. 5.4.4-1

Note: All Curves Based On I = 2.

5.3.7 and Chapter 3). The purpose of this plot is to show the overall shape of the function. The predicted anisotropy A'', corrected for positrons but not geometry, and normalized to the value actually obtained in the undisturbed case, is plotted against the magnitude of the interaction, $\Omega_0\tau_N$, where Ω_0 is the angular frequency associated with the total quadrupole splitting (Eq. 5.3.7-11). Also shown is the "hard core" anisotropy to be expected from fields of rhombic symmetry for I=2. In this case the "hard core" G's are $G_2 = G_4 = 2/7$ (1A53)

In Figs. 5.4.4-2,3 we again plot theoretically predicted anisotropy normalized to the undisturbed value versus magnitude of the interaction using the same total splitting angular frequency discussed above. In both Figs. 5.4.4-2 and 5.4.4-3 we assume axially symmetric, classically describable fields; in the former we assume an electric quadrupole interaction and in the latter a magnetic dipole interaction. The elliptic looking curves drawn within the statistical limits of the various observed points represent approximate lines of equal probability for one standard deviation, i.e. 68% of samples should lie within closed curves. The lower vertical tangents to these curves represent the lower statistical limits of the interaction, $\Omega_0\tau_N$. The observed anisotropies of sources (1) and (5) as defined above are considered.

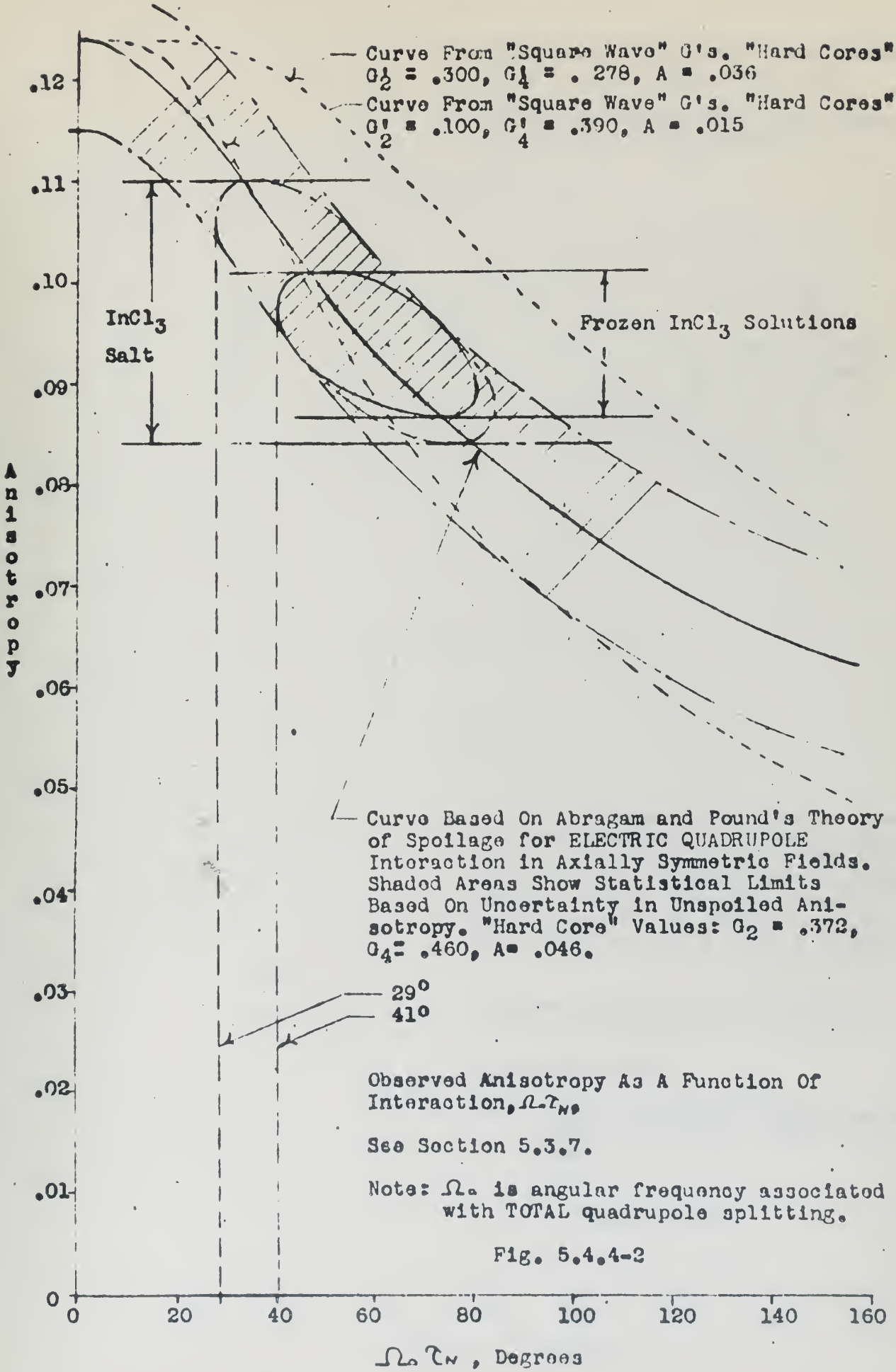
— Curve From "Square Wave" G's. "Hard Cores": $G_2' = .300$, $G_4' = .278$, $A = .036$
— Curve From "Square Wave" G's. "Hard Cores": $G_2' = .100$, $G_4' = .390$, $A = .015$
$InCl_3$ Salt
Frozen $InCl_3$ Solutions
Anisotropy
.12
.11
.10
.09
.08
.07
.06
.05
.04
.03
.02
.01
0
0
20
40
60
80
100
120
140
160
$\Omega_a \tau_N$, Degrees
— Curve Based On Abragam and Pound's Theory of Spoilage for ELECTRIC QUADRUPOLE Interaction in Axially Symmetric Fields. Shaded Areas Show Statistical Limits Based On Uncertainty in Unspoiled Anisotropy. "Hard Core" Values: $G_2 = .372$, $G_4 = .460$, $A = .046$.
— 29°
— 41°
Observed Anisotropy As A Function Of Interaction, $\Omega_a \tau_N$.
See Section 5.3.7.
Note: Ω_a is angular frequency associated with TOTAL quadrupole splitting.

Fig. 5.4.4-2

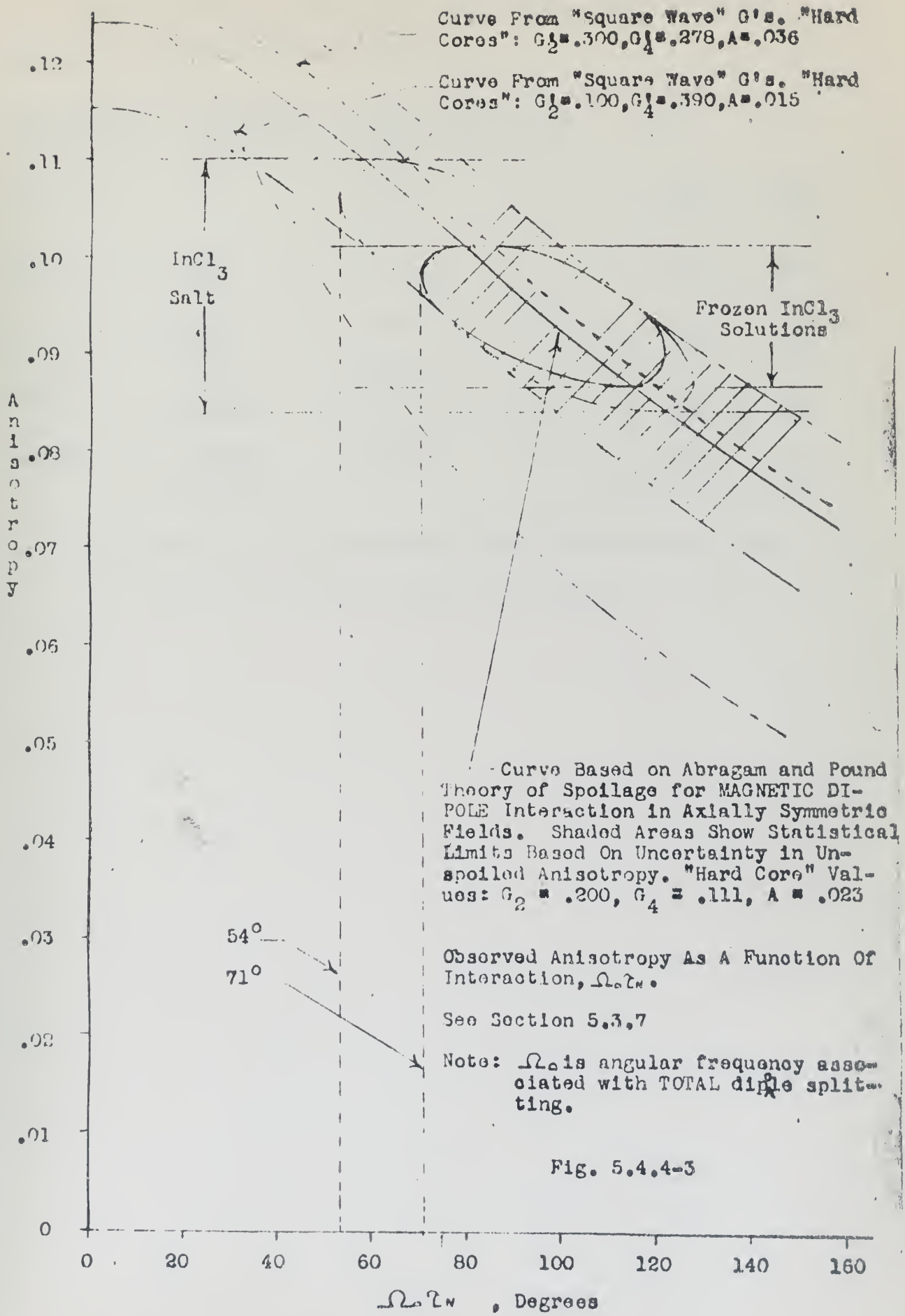

Curve Based on Abragam and Pound Theory of Spoilage for MAGNETIC DIPOLE Interaction in Axially Symmetric Fields. Shaded Areas Show Statistical Limits Based On Uncertainty in Unspoiled Anisotropy. "Hard Core" Values: G_2 = .200, G_4 = .111, A = .023

Observed Anisotropy As A Function Of Interaction, $\Omega_o\tau_N$.

See Section 5.3.7

Note: Ω_o is angular frequency associated with TOTAL dipole splitting.

Fig. 5.4.4-3

Liquid Sources

We tabulate the results of the observations on liquid sources. See also Fig. 5.2.2-2.

Temperature (Deg. Cent.)	Viscosity (Centipoise)	Mean Correlation Time (Seconds)	A'''	A''
20 ± 3	1	(-11)	± .139 ± .008	± .124 ± .009
20 ± 3	± 800 ± 260	8(-9)	± .133 ± .010	± .118 ± .011
4 ± ½	± 4000 ± 800	4(-8)	± .133 ± .010	± .118 ± .011
-14 ± 2	± 33000 ± 10000	3.3(-7)	± .107 ± .008	± .092 ± .009
-28 ± 2	± 600000 ± 200000	6(-6)	± .121 ± .010	± .106 ± .011

Note: Numbers in parentheses under "Correlation Time" represent 10 to the power indicated.

Chapter 6 - Interpretation and Discussion

Part 6.1 - Undisturbed Correlations

One of the questions frequently asked when a value of anisotropy is alleged to be from the "undisturbed correlation" is, "How do you know the correlation to be undisturbed?" We shall attempt to answer this question using two lines of argument. The first involves a comparison with the results obtained from Cd^{111}, and the second involves a method of successive approximations among the results pertaining to Cd^{114}. In both arguments we shall assume that in the dilute aqueous solution Abragam and Pound's theory of spoilage in liquids applies; this is to say that we will assume that $\tau_c < \tau_N$ although we do not know this to be true with certainty in the case of Cd^{114}. Both arguments make use of (3-26) which give the spoilage G_k factors in liquids as a function of the electric quadrupole moment, lifetime, and correlation time.

In the comparison of Cd^{111} with Cd^{114} in the aqueous solution, we begin by quoting from (2H53) a value of 500 mcs for $\frac{eQ^{111}\left(\frac{\partial^2 V}{\partial z^2}\right)}{h}$ where eQ^{111} is the quadrupole moment of the first excited state of Cd^{111}. We make the further assumption that $\left(\frac{\partial^2 V}{\partial z^2}\right)$ is the same in the Cd^{111} aqueous solution as it is in the Cd^{114} aqueous solution. We find that when these values are put into (3-26) with the additional value of $\tau_N \lesssim 2.3 \times 10^{-10}$ seconds for the Cd^{114} lifetime and an estimation of 10^{-11} seconds for the value of τ_c, that we have but negligible attenuation, i.e. $G_2 \approx G_4 \approx 1$. Further, attenuation in the aqueous solution does not become appreciable in Cd^{114} unless we make the unrealistic assumption that we have a quadrupole moment in Cd^{114} about thirty times as large as that found in Cd^{111}. We sum-

marize by saying that on the basis of this test, our aqueous solution gives the true undisturbed correlation if we assume that the ratio of the quadrupole moments of Cd^{114} to Cd^{111} is no larger than thirty to one.

To begin our second argument let us assume that out results from the dilute aqueous solution at room temperature represent the true unperturbed correlation. Then we use the anisotropy so determined as a starting point for calculating the values of the interaction in the polycrystalline sources (Figs. 5.4.4-2,3). Then, let us take the magnitude of $\frac{eQ^{114}\left(\frac{\partial^2 V}{\partial z^2}\right)}{h}$ so determined and place it in (3-26), just as we did in the first argument with the results of the Cd^{111} interaction. If this in turn causes a reduction in the G_k's from unity then we will apply this correction to the original anisotropy and re-calculate the interaction. If, however, such a substitution leaves the G_k's essentially equal to unity, then we can say that our aqueous solution does indeed represent the undisturbed correlation. We have also made the implicit assumption, which seems justified at least in order of magnitude, that the average electric field gradient experienced by the nucleus in liquid sources is no larger than that experienced in polycrystalline sources. If we make these substitutions we find again that the G_k's again remain essentially equal to unity, and from this we conclude that we may consider for our purposes that the aqueous solution yields the truly unperturbed correlation.

In regard to the complete correlation, it is interesting to not that our value for the mixing ratio in the first transition:

$$M1 \rightarrow .958 \pm .006$$

$$E2 \rightarrow .042 \pm .006$$

agrees within the limits of error to those ratios found both by

Johns et al. (1J54) and Steffen and Zobel (1952) (Section 5.4.3) and thus lends added confirmation to the accuracy of these values.

On the other hand our fit to the theoretical curve based on the above mixing ratios (Fig. 5.4.3-4) seems better than that of the others. This adds credence to our values for the LeGendre coefficients of the correlation:

$$A_2 = .090 \pm .011$$
$$A_4 = .022 \pm .016$$

Part 6.2 - Disturbed Correlations

Section 6.2.1 - Polycrystalline Sources

Our results for the magnitudes of the interactions and moments are based on various general and particular assumptions. We shall first state the assumptions, then our conclusions based on these assumptions; then we shall discuss both the validity of the assumptions and the firmness of the conclusions.

General Assumptions:

1. The perturbing fields are classically describable.
2. The perturbing fields are static.
3. The perturbing fields are axially symmetric.

Particular Assumptions:

a-1. The interaction is electric quadrupole in nature.

a-2. The interaction is magnetic dipole in nature.

b-1. The primary perturbing field is due to the crystalline structure and the average electric field gradient at the nucleus is about 1.6×10^{16} statvolts/cm^2.

b-2 The primary perturbing field is due to the electronic cloud of the atom of which the nucleus is a part and the average electric field gradient at the nucleus is about 4.5×10^{16} statvolts/cm^2.

b-3 The primary perturbing field is due to the crystalline structure and the average magnetic field at the nucleus is about 10^4 Oersteds.

b-4 The primary perturbing field is due to the electronic cloud of the atom of which the nucleus is a part and the average magnetic field at the nucleus is about 10^6 Oersteds.

Conclusions:

$$\text{Let } \Delta\nu_e \equiv \left[\left(\frac{eQ\left\langle\frac{\partial^2 V}{\partial z^2}\right\rangle}{h}\right)^2\right]^{\frac{1}{2}} = \frac{\Omega_{oe}}{\pi}$$

$$\text{Let } \Delta\nu_m \equiv \left[\left(\frac{g\,\mu_K\langle H\rangle}{h}\right)^2\right]^{\frac{1}{2}} = \frac{\Omega_{om}}{8\pi}$$

where eQ is the nuclear quadrupole moment,

μ_K is the nuclear magneton, and

g is the nuclear gyromagnetic ratio.

Then we list below for the various sources, a lower limit for the $\Delta\nu$ and the moments based on our known upper limit for the nuclear lifetime ($\leqslant 2.3\times10^{-10}$ seconds), and the statistical limits from Figs. 5.4.4-2,3:

Source:		Partic. Assump.	
(a) Magnitude of the Interactions:			
(1)	$InCl_3$ Salt	a-1	$\Delta\nu_{oe} \geqslant$ 700 mcs
(2)	Frozen Solutions of $InCl_3$	a-1	$\Delta\nu_{oe} \geqslant$ 990 mcs
(3)	$InCl_3$ Salt	a-2	$\Delta\nu_{om} \geqslant$ 163 mcs
(4)	Frozen Solutions of $InCl_3$	a-2	$\Delta\nu_{om} \geqslant$ 214 mcs

(b) Magnitude of the Moments

(5)	$InCl_3$ Salt	a-1,b-1	$\|Q\| >$ .60 *
(6)	$InCl_3$ Salt	a-1,b-2	$\|Q\| >$ .21
(7)	Frozen Solution of $InCl_3$	a-1,b-1	$\|Q\| >$ .85
(8)	Frozen Solution of $InCl_3$	a-1,b-2	$\|Q\| >$ .30
(9)	$InCl_3$ Salt	a-2,b-3	$\|\mu\| >$ 42
(10)	$InCl_3$ Salt	a-2,b-4	$\|\mu\| >$ .42
(11)	Frozen Solution of $InCl_3$	a-2,b-3	$\|\mu\| >$ 56
(12)	Frozen Solution of $InCl_3$	a-2,b-4	$\|\mu\| >$ .56

* Note: The units for the quadrupole moment: $x10^{-24}$ cm^2.
The units for the magnetic dipole moment: Nuclear Magnetons.

Discussion

That the fields at the nucleus are classically describable would hold in both the magnetic and electric cases if we could neglect the excited condition of the cadmium atomic configuration following K capture; for the ground atomic state of cadmium is an S state. But from the discussion in Chapter 3 we see that we cannot neglect the "excited configuration effect" whose general theoretical interpretation requires the introduction of the quantum mechanical coupling between the nucleus and electronic configuration. This in turn would be complicated by the uncertainty of the total electronic angular momentum, J, following K capture. However, as pointed out by Abragam and Pound, in the case of the electric quadrupole interaction (particular assumption a-1) we can still use the classically described fields because in polycrystalline sources orbital electronic degeneracies have been removed. This is not possible in the

case of the magnetic interaction because of the remaining spin degeneracy. This effect can be seen on semi-classical grounds as follows. When a nucleus is acted upon by an external field it also reacts upon the field; i.e. just as it is possible for an external field to induce nuclear transitions, it is also possible for the field produced by the nucleus in a transition to induce transitions in the configurations giving rise to the initial field. If the energy levels of the states giving rise to the initial are well separated (no degeneracies) then the nuclear transition reaction can cause no transitions among these states; this corresponds to the classically describable field. However, on this basis it is easy to see that the reaction due to a nuclear transition could induce transitions among degenerate states which are the sources of the initial field. These "reaction induced" transitions among degenerate states could, in turn, alter the initial field. In such a situation the only valid treatment is a quantum mechanical one. With this limitation clearly in mind, we have made certain calculations (assumption b-4) in which we neglected this quantum mechanical coupling in the case of magnetic interactions with the electron cloud, realizing that there still remains a possible spin degeneracy even in polycrystalline sources. However, in an order of magnitude estimate, as this calculation is, this procedure seems justified. In the light of the above, conclusions (9)-(12) should be viewed with a certain amount of reservation.

That the perturbing fields are static seems to be well taken. (1H52) indicates a shell relaxation time of greater than 10^{-8} seconds for ionic crystal impurity centers which is

some two hundred times as large as our nuclear lifetime. Hence the Cd^{114} nucleus experiences essentially a constant perturbing field due to the "quasi-static configuration" effect (Chapter 3).

That the perturbing fields are axially symmetric is not at all clear. As discussed in Chapter 3 even if an individual crystal did provide axially symmetric fields (where two of the field gradients are equal) at the nucleus these fields would probably be distorted by inter-crystalline pressures in a polycrystalline source and by nuclear recoils out of axially symmetric sites following K capture. However, a redeeming feature is that the hard core values for rhombic fields (where all three field gradients differ) are not much different from the hard cores for axially symmetric fields; as we saw in Chapter 3 for I=2:

	Axially Symmetric	Rhombic
$G_2(\text{lim})$	13/35	10/35
$G_4(\text{lim})$	29/63	16/63

And from Fig. 5.4.4-1 we see that the hard core anisotropies in the two cases are:

	A(lim)
Axially Symmetric	.046
Rhombic	.035

The $G_k(\Omega_o\tau_N)$ for axially symmetric fields fall off quadratically with $\Omega_o\tau_N$ as $\Omega_o\tau_N \to 0$, with a second derivative nearly equal to the square of the angular frequency associated with the total splitting (Ω_o) times the nuclear lifetime (τ_N) (3-21). Simple arguments indicate that this same general quadratic behavior with the same relation to total splitting should apply for fields of lower symmetry. Since the total splitting is

approximately independent of the exact degree of field asymmetry for a given value of maximum field gradient, we would expect that the G_k for axially symmetric and the G_k for rhombic fields would lie very close together for small values of the argument, $\Omega\tau$.

In regard to particular assumptions a-1 and a-2 we will make no effort to favor one type of interaction. Abragam and Pound (1A53) show that even if a magnetic decoupling experiment shows negative results, i.e. no detectable increase in anisotropy, as reported by Albers-Schonberg et al. (2A53), this is not conclusive to the absence of a magnetic interaction. We will thus keep a-1 and a-2 on an equal footing and not try to argue for either. However, if the interaction is electric quadrupole (a-1) our quantitative results are in general more credible than otherwise because of the discussion above relating to classically describable fields.

As for particular assumptions b-1 to b-4 relative to the sizes of the fields; these are only order of magnitude approximations and are not to be taken too literally. This indeed is one of the greatest obstacles to the more fruitful use of disturbed angular correlations for the determination of moments, i.e. our ignorance concerning the magnitude of fields experienced by the nucleus. The value relating to the electric field gradients in crystals (b-1) came from the appendices of (1G53) by averaging a number of cases which ranged from 8.3×10^{15} to 3.5×10^{16} statvolts/cm^2. These values of the gradients were calculated from instances where both Q and the splitting in megacycles were known. The value relating to the electric field gradient due to the electron cloud (b-2) is from (1T49) and

is based on the gradient due to the p-electron of iodine; this would correspond roughly to one of the first excited states in cadmium. The values for the magnetic fields (b-3,4) are from (1H52) and (1F52).

The only conclusions backed by direct experimental evidence relative to spoilages are (1) - (4) relating to the magnitudes of the splitting frequencies; these are to be taken as firm within the limits of statistical validity and of the indicated assumptions.

Conclusions (5) - (12) concerning the moments themselves are uncertain due to the obscurity as to the sizes of the perturbing fields as mentioned above. However, it seems we can eliminate conclusions (9) and (11) as being far too large based on typical nuclear magnetic moments; then we can say that if the interaction is magnetic it arises from the "quasi-static configuration" effect, i.e. an interaction between the nucleus and the magnetic moment due to its own electron cloud. For comparison purposes the quadrupole moment of the first excited state of Pd^{106}, an even-even nucleus, as estimated by Abragam and Pound (1A53) is at least $.2 \times 10^{-24}$ cm^2.

The complexities of the processes going on in the source introduce a great deal of uncertainty in the results, and it must be borne in mind that an exact theoretical calculation of the "quasi-static configuration" effect may well lower our values of the interaction. However, if the highly excited state of the electronic configuration following K capture is primarily responsible for the perturbing interaction, as it seems to be in the case of Steffen (1S53), then these large fields could provide an excellent means for the determination of the moments

of very short lived ($< 10^{-10}$ seconds) excited states. There seem to be three great experimental hurdles at present in the way of specification of these moments more precisely:

(a) Measurements of nuclear lifetimes less than 10^{-10} secs.

(b) Measurements of the magnitudes of the fields experienced by nucleii under various conditions.

(c) Specification of the nature of the interaction, i.e. whether electric or magnetic in nature.

Furthermore, supposing we could perform (a) and (c), but not necessarily (b), then comparative measurements of the spoilage due to the "quasi-static effect" would give us the ratio of moments for different isotopes of the same element. Or, using known moments, the spoilage ratio in two isotopes could give us information as to the atomic physics of the "quasi-static" field.

Section 6.2.2 - Liquid Sources

The data from the variable viscosity glycerin solutions yields no information as to the magnitudes of the interactions. This is because (as can be seen from the table in Section 5.4.4) at the viscosity at which spoilage may perhaps be taking place (about 3×10^5 centipoises) the theory of spoilage in liquids (Chapter 3) developed by Abragam and Pound (1A53) no longer applies. At this viscosity the liquid correlation time is about 10^{-7} seconds which is some 700 times as large as the nuclear lifetime, and a basic postulate of the liquid theory is that the correlation time be shorter than the nuclear lifetime. At such a large correlation time, our nucleus with a lifetime of less than or equal to 2.3×10^{-10} seconds, ex-

periences practically static fields very similar to those associated with the solid state.

Another phenomenon in the liquid sources that bears investigation is that there is no observable spoilage in the range where $10\tau_N \leq \tau_c \leq 7000\tau_N$; here the nucleus is in a region of transition where it is begining to experience fields which are practically constant, and hence related to polycrystalline phenomena. A possible answer may be that in liquids even of this high a viscosity there is some mechanism which shortens the atomic shell relaxation time appreciably, and thus reduces the average field at the nucleus.

Part 6.3 - Statistical Validity

In arriving at the statistical validity of the results we will make the following tests:

1. A Chi-Square test on the average anisotropy of the four sources, viz., aqueous solution at room temperature, $InCl_3$ salt, frozen aqueous solution, and frozen glycerin solution, all considered simultaneously.

2. A Chi-Square test on the average anisotropy of the last three of the above mentioned sources considered together.

3. The two-point statistical test developed in Section 5.3.4 wherein, if one assumes two points come from the same normal distribution, the probability of finding them separated by more than so many standard deviations is given. When worked in reverse, i.e. given two points not closer than so many standard deviations, it gives an upper limit on the probability that they are from the same normal distribution. This gives only an upper limit due to the possibility of their being from different distributions. We will perform this

test, comparing the aqueous solution with each of the three other sources.

Results of the Tests:

Test No.	Probability that a random sample gives no better fit:	
1	.041	
2	.59	
	Upper limit on probability that two given values are from same distribution	
3	Aqueous Sol. - $InCl_3$ Salt -	.032
	Aqueous Sol. - Frozen Aq. Sol. -	.089
	Aqueous Sol. - Frozen Glyc. Sol. -	.001

None of the above tests is in itself conclusive. The fact that Test 1 gives a probability of .041 is certainly not conclusive evidence that the aqueous solution and the other three sources do not give results which really lie on the same distribution. However, from Test 2 one can state with a high degree of certainty that the three polycrystalline sources give results which lie on the same distribution or on distributions which are very close together. When, on the other hand, one considers Test 1 in the light of Test 2 and the fact that a spoilage correlation actually seemed to exist, i.e. any deviation in the anisotropy from the aqueous solution was in the downward direction and this under conditions that predict "spoilage", then one has strong reason to believe the existence of a true effect.

Appendix I - Positron Annihilation Component of Coincidence Rate

At 180 degrees the In^{114} cascade gamma coincidence rate is "polluted" with a rate due to the positron annihilation component of the decay. We wish to determine what fraction of the observed true coincidence rate at 180 degrees is due to this annihilation component.

We will consider three different sources, which we will designate as follows:

N_0 - In^{114} extended source

N_1 - Na^{22} extended source

N_2 - Na^{22} point source

Notation:

ω - effective counter solid angle

ϵ - counter efficiency

δ - channel factor, i.e., fraction of detected pulses falling within "window".

The probability that a single gamma ray of energy E, emitted isotropically, will register a single channel count in the i th channel is given by:

$$\lambda_{Ei} = \omega_{Ei}\, \epsilon_{Ei}\, \delta_{Ei}$$

Note that all three factors are energy dependent.

A more precise definition of ω and hence of ϵ will be presented later (App. II); for present purposes, however, we may speak as though the counter had a uniform efficiency ϵ for all gamma gays within solid angle ω, and zero efficiency outside .

We designate the In^{114} branching ratios as follows:

α_p - positron emission

α_K - electron capture for the process which leads to the 722-556 KEV cascade in Cd^{114}.

The intensities of the various gamma rays are as follows:

$\alpha_K N_o$ - Each of the two In^{114} cascade gammas

$2\alpha_P N_o$ - Both of the In^{114} annihilation gammas

N_i - The Na^{22} cascade gamma (β^+-γ cascade) $i = 1,2$

$2N_i$ - Both of the Na^{22} annihilation gammas $i = 1,2$

In this discussion we will consider gamma rays of four different energies. For simplicity in notation each energy will be represented by an integer as follows:

1 - 722 KEV

2 - 556 KEV

3 - 511 KEV

4 - 1277 KEV

Single Channel Rates

Let the i th ($i = a,b$) channel rate for In^{114} be S_{oi}

Let the i th ($i = a,b$) channel rate for Na^{22} be S_{ji} $j = 1,2$

Then:

(1) $$S_{oi} = N_o\left[\alpha_K(\lambda_{1i} + \lambda_{2i}) + 2\alpha_P\lambda_{3i}\right]$$

but since $\alpha_P \ll \alpha_K$, (1) becomes:

(2) $$S_{oi} \approx \alpha_K N_o(\lambda_{1i} + \lambda_{2i})$$

and similarly for Na^{22}:

(3) $$S_{ji} = N_j(2\lambda_{3i} + \lambda_{4i}) \qquad j = 1,2$$

In order to simplify the following derivations, we will use a term we call "the" single channel rate, S_o. In order to present the relationship of S_o to S_{oa} and S_{ob}, consider the case where there is present only a gamma ray of energy j. Then by (2):

(4) $$S_{oi} = \alpha_K N_o \lambda_{ji} \qquad j = 1,2$$

If we define S_o:

(5) $$S_o \equiv \sqrt{S_{oa} S_{ob}}$$

and λ_1:

(6) $S_o \equiv \alpha_K N_o \lambda_1$

Then, by (5) and (6):

(7) $\lambda_1 = \sqrt{\lambda_{1a}\lambda_{1b}}$

Extending the above to the case where there are two gamma rays, we have a more general definition for the λ's :

(8) $S_o \equiv \alpha_K N_o (\lambda_1 + \lambda_2)$

Coincidence Rates

Let the In^{114} cascade gamma coincidence rate be $C_{og}(\theta)$

Let the In^{114} annihilation gamma coincidence rate be $C_{op}(180)$

Let the Na^{22} annihilation gamma coincidence rate be $C_{jp}(180)$ $j=1,2$

Let the Na^{22} cacade-annihilation gamma coincidence rate be $C_{jgp}(180)$

The In^{114} cascade gamma coincidence rate may be expressed as follows:

(9) $C_{og}(\theta) = \alpha_K N_o W(\theta)\left[\lambda_{1a}\lambda_{2b} + \lambda_{2a}\lambda_{1b}\right]$

Combining (2), (5) and (8), we see that:

(10) $(\lambda_1 + \lambda_2)^2 = (\lambda_{1a} + \lambda_{2a})(\lambda_{1b} + \lambda_{2b})$

If we introduce (7):

(11) $2\lambda_1\lambda_2 = \lambda_{1a}\lambda_{2b} + \lambda_{2a}\lambda_{1b}$

Then we have:

(12) $C_{og}(\theta) = 2\alpha_K N_o W(\theta)\lambda_1\lambda_2$

The annihilation gamma coincidence rate at 180 degrees, however, is expressed:

(13) $C_{op}(180) = \dfrac{2\alpha_p N_o \Omega \lambda_{3a}\lambda_{3b}}{\omega_3}$

where Ω is a reduction factor due to the finite size of the source, i.e., $\Omega=1$ if the mate of every annihilation gamma entering one counter, enters the other counter. One obtains this with a centered point source, but not with an extended one.

By (7) we have directly:

$$(14)\quad C_{op(180)} = \frac{2\alpha_p N_o \Omega \lambda_3^2}{\omega_3}$$

Since out knowledge of N_o is limited at best, we can be rid of this factor by considering the ratio of (14) and (12) at 180 degrees:

$$(15)\quad \frac{C_{op(180)}}{C_{og(180)}} = \frac{\alpha_p \Omega \lambda_3^2}{\alpha_k W(180) \omega_3 \lambda_1 \lambda_2}$$

We are rid of N_o again, and have another relation, if we consider the ratio of the single channel to coincidence rates at 90 degrees where we know there is no positron component. Then by (12) and (8):

$$(16)\quad \frac{S_o}{C_{og(90)}} = \frac{\lambda_1 + \lambda_2}{2 W(90) \lambda_1 \lambda_2}$$

We now define the term:

$$(17)\quad \mu_{21} \equiv \frac{\lambda_2}{\lambda_1}$$

And for the sake of completeness:

$$(18)\quad \mu_{i,21} \equiv \frac{\lambda_{2i}}{\lambda_{1i}} \qquad i = a, b$$

Since one can actually measure $\mu_{i,21}$ by comparing relative areas under lines in the single channel spectrum, it is worthwhile to show the explicit relation between (18) and (17).

From (11) we have:

$$(19)\quad \frac{\lambda_2}{\lambda_1} = \tfrac{1}{2}\left[\frac{\lambda_{1a}\lambda_{2b}}{\lambda_1^2} + \frac{\lambda_{2a}\lambda_{1b}}{\lambda_1^2}\right]$$

And introducing (7) and the definitions (17) and (18):

$$(20)\quad \mu_{21} = \tfrac{1}{2}\left[\mu_{a,21} + \mu_{b,21}\right]$$

or, the arithmetic mean of the single channel μ's.

Then, by (17) and (16):

$$(21)\quad \frac{S_o}{C_{og(90)}} = \frac{1 + \mu_{21}}{2 W(90) \lambda_2}$$

By substituting (21) into (15), again using (17), we come to:

$$(22)\quad \frac{C_{op(180)}}{C_{og(180)}} = \frac{4 \alpha_p W^2(90) \Omega S_o^2 \mu_{21} \lambda_3^2}{\alpha_k W(180) \omega_3 C_{og}^2(90) (1 + \mu_{21})^2}$$

If we compare the single channel to coincidence rates for the Na^{22} sources, both point and extended, we find an expression for Ω:

(23) $$\Omega = \frac{C_{1P}(180)\, S_2}{C_{2P}(180)\, S_1}$$

We get a grip on λ_3 by considering the coincidence rate in Na^{22} between the annihilation and cascade gammas, which fortunately is isotropic. By a procedure similar to the above we obtain:

(24) $$\lambda_3 = \tfrac{1}{4}\, \frac{C_{1gP}(90)}{S_1}\,(1+2\mu_{34})$$

By substituting (24) and (23) into (22) we have:

(25) $$\frac{C_{0P}(180)}{C_{0g}(180)} = \frac{\alpha_P W^2(90)\, C_{1P}(180)\, C^2_{1gP}(90)\, S_0^2\, S_2\,(1+2\mu_{34})^2\,\mu_{21}}{4\alpha_K W(180)\,\omega_3\, C_{2P}(180)\, C^2_{0g}(90)\, S_1^3\,(1+\mu_{21})^2}$$

All terms have been expressly defined except ω_3 which is defined more precisely in App. II, where also a method for measuring it is derived.

The presence of the second power of $W^2(90)$ in (25) is unfortunate, but not seriously so. It would be much neater to have the ratio $W(90)/W(180)$ appear. To this end, we will proceed to calculate $W(90)$:

(26) $$W(\theta) = K(1 + a_2\cos^2\theta + a_4\cos^4\theta)$$

where K is a normalizing factor whose magnitude is determined by the following constraint:

(27) $$\int_{\text{UNIT SPHERE}} W(\theta)\, d\omega = 4\pi$$

If we carry out the integration in (27), it turns out that:

(28) $$K = \left[1 + \tfrac{1}{3}a_2 + \tfrac{1}{5}a_4\right]^{-1}$$

"a_2" and "a_4" are to be determined by a least squares fit to the observed data.

By (28):

(29) $$W(90) = K = \left[1 + \tfrac{1}{3}a_2 + \tfrac{1}{5}a_4\right]^{-1}$$

And substituting (29) into (25) we have:

(30) $$\frac{C_{0P}(180)}{C_{0g}(180)} = \frac{\alpha_P W(90) K\, C_{1P}(180)\, C^2_{1gP}(90)\, S_0^2\, S_2\,(1+2\mu_{34})^2\,\mu_{21}}{4\alpha_K W(180)\,\omega_3\, C_{2P}(180)\, C^2_{0g}(90)\, S_1^3\,(1+\mu_{21})^2}$$

Let us define β and σ as follows:

$$(31)\quad \beta \equiv \frac{\alpha_p K C_{1P}(180) C^2_{1g P}(90) S_0^2 S_2 \mu_{21} (1+2\mu_{34})^2}{4\alpha_K \omega_3 C_{2P}(180) C^2_{0g}(90) S_1^3 (1+\mu_{21})^2}$$

$$(32)\quad \sigma \equiv \frac{C_{0p}(180)}{C_{0g}(180)}$$

Then (30) becomes:

$$(33)\quad \sigma = \frac{W(90)}{W(180)} \beta$$

And since:

$$(34)\quad C_0(\theta) = C_{0g}(\theta) + C_{0p}(\theta)$$

where $C_0(\theta)$ is the total, true rate, it is easily shown that:

$$(35)\quad \frac{W(180)}{W(90)} = \frac{C_0(180)}{C_0(90)} \left(\frac{1}{1+\sigma}\right)$$

And by (32):

$$(36)\quad \frac{W(180)}{W(90)} = \frac{C_0(180)}{C_0(90)} - \beta$$

We thus arrive at the pleasant result that the correction for positrons to the observed anisotropy consists merely of subtracting some number which we can calculate explicitly by (31). The procedure must be carried out by successive approximations, however, because of the uncertainty in K in (31).

Appendix II - Effective Solid Angle

In equation (AI-25) we find the quantity ω_3, which has been referred to roughly as the "effective relative solid angle". It is the purpose of this discussion to obtain for this term a precise functional form.

As a precise definition we use an equation similar to AI-14.

$$(1) \quad C_{2p(180)} \equiv \frac{2 N_2 \lambda_3^2}{\omega_3}$$

$$(2) \quad \omega_3 = \frac{2 N_2}{C_{2P(180)}} \lambda_3^2$$

But we can represent λ as the integral of some relative response function, $F(\alpha)$, over the counter, so normalized that:

$$(3) \quad \lambda = \frac{1}{4\pi} \int_{\omega} F(\alpha)\, d\omega$$

where α is the angle subtended at the source between the detector axis and the element of solid angle, $d\omega$.

We can write the coincidence rate at 180 degrees for the N_2 (Na^{22}, point) source as follows:

$$(4) \quad C_{2P(180)} = \frac{2 N_2}{4\pi} \int_{\omega} F^2(\alpha)\, d\omega$$

Substituting (4) into (2) we have; remembering (3):

$$(5) \quad \omega_3 = \frac{1}{4\pi} \frac{\left[\int F(\alpha)\, d\omega\right]^2}{\left[\int F^2(\alpha)\, d\omega\right]}$$

We observe an angular resolution curve, $G(\theta)$, from the directional correlation of the annihilation radiation. Making use of the counter axial symmetry of the function $F(\alpha)$ and referring to the diagram on the top of the next page, we can express

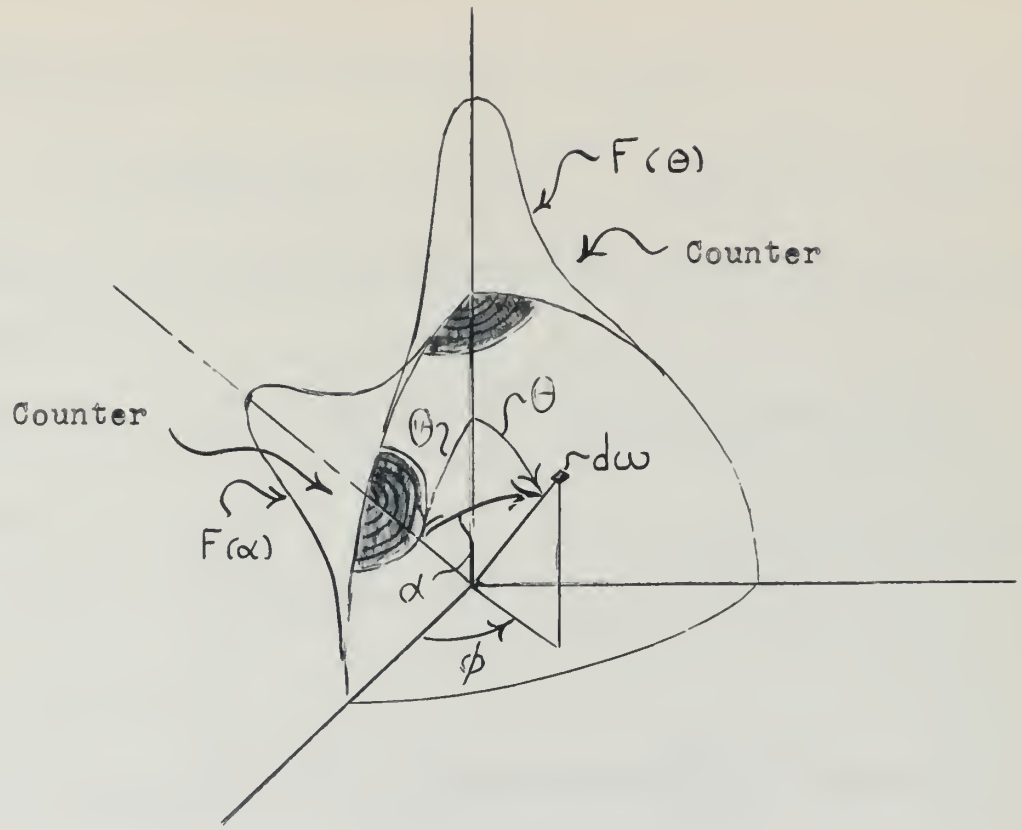

$G(\Theta)$ as follows:

(6) $$G(\Theta) = K \int_{4\pi} F(\theta)\, F(\alpha)\, d\omega$$

where $\alpha = \alpha(\Theta, \theta, \phi)$ and K is an undetermined constant.

We obtain the resolution curve as a relative function, $H(\Theta)$, where:

(7) $$H(\Theta) = \frac{G(\Theta)}{G(0)} = \frac{\int F(\theta)\, F(\alpha)\, d\omega}{\int F^2(\theta)\, d\omega}$$

We can expand $F(\theta)$ in LeGendre Polynomials:

(8) $$F(\theta) = \sum_m C_m P_m(\cos\theta)$$

and using the addition theorem:

(9) $$F(\alpha) = \sum C_m \left[P_m(\cos\theta)\, P_m(\cos\Theta) + 2 \sum_{\ell=0}^{m} \frac{(m-\ell)!}{(m+\ell)!} P_m^{\ell}(\cos\theta)\, P_m^{\ell}(\cos\Theta) \cos \ell\phi \right]$$

The terms in $\cos l\phi$ vanishes on integration over ϕ . Hence:

$$(10)\quad \left[\int F^2(\theta)\,d\omega\right] H(\Theta) = 2\pi \int_{-1}^{+1} \sum_{m,j} C_m C_j P_m(x) P_j(x)\,dx\, P_j(\cos\Theta)$$

Making use of the orthogonality of Pn(x):

$$(11)\quad \left[\int F^2(\theta)\,d\omega\right] H(\Theta) = 2\pi \sum_m C_m^2 \left(\frac{2}{2m+1}\right) P_m(\cos\Theta)$$

Multiplying through by Pn(cosΘ) and integrating again we come down to:

$$(12)\quad C_m^2 = \frac{1}{2\pi}\left[\frac{2m+1}{2}\right]^2 \left[\int_{-1}^{+1} H(\theta) P_m(\cos\theta)\,d(\cos\theta)\right] \times \left[\int F^2(\theta)\,d\omega\right]$$

From (8) we have:

$$(13)\quad 4\pi C_0 = \int_{-1}^{+1} F(\theta)\,d\omega$$

Or, using (12):

$$(14)\quad \left[\int_{-1}^{+1} F(\theta)\,d\omega\right]^2 = 2\pi \left[\int_{-1}^{+1} H(\theta)\,d(\cos\theta)\right]\left[\int F^2(\theta)\,d\omega\right]$$

Then by (5):

$$(15)\quad \omega_3 = \frac{1}{2}\int_{-1}^{+1} H(\theta)\,d(\cos\theta)$$

Note: A factor increasing the apparent source size for annihilation radiation is the range of the positrons. Although this is taken into consideration by (15) it may be of interest to know the positron "halo" around the source. In the decay of In^{114} the positrons have a maximum kinetic energy of about 1 mev. This means that their range in the lucite source holder is about .13 inches, as compared to length 1.10 inches and diameter .37 inches which geometrically define the extended source.

Appendix III - Geometrical Corrections For A Finite Source

When one observes a directional correlation function, one is observing a phenomenon in the macroscopic domain. The observed function consists of a weighted sum of micro-scopic functions, each related to an element of source and an element of solid angle on each counter. The function, $W(\theta)$, which theory predicts is related to the microscopic domain, i.e. it is concerned with well defined directions in the decay of a single nucleus. However, the observed function, which for the purposes of this discussion we will designate $\overline{W}(\Theta)$, results from radiations proceeding in directions uncertain to the extent of the counter solid angle and which result from the decays of millions of nucleii whose position is uncertain to the extent of the source.

Let our observed function be:

(1) $$\overline{W}(\Theta) = \sum_i C_i P_i(\cos\Theta)$$

where Θ is the angle between the axes of the two counters. Note that we do not restrict the i's to even integers.

And let our well known micro-scopic function be:

(2) $$W(\theta) = 1 + A_2P_2(\cos\theta) + A_4P_4(\cos\theta)$$

where θ, as usual, is the angle between the propagation vectors of the two radiations involved in the cascade.

We now ask, "What is the functional dependence of the C's on the A's?"

To answer this we must first specify the model of our detection system very carefully. For our first model refer to the diagram on the next page.

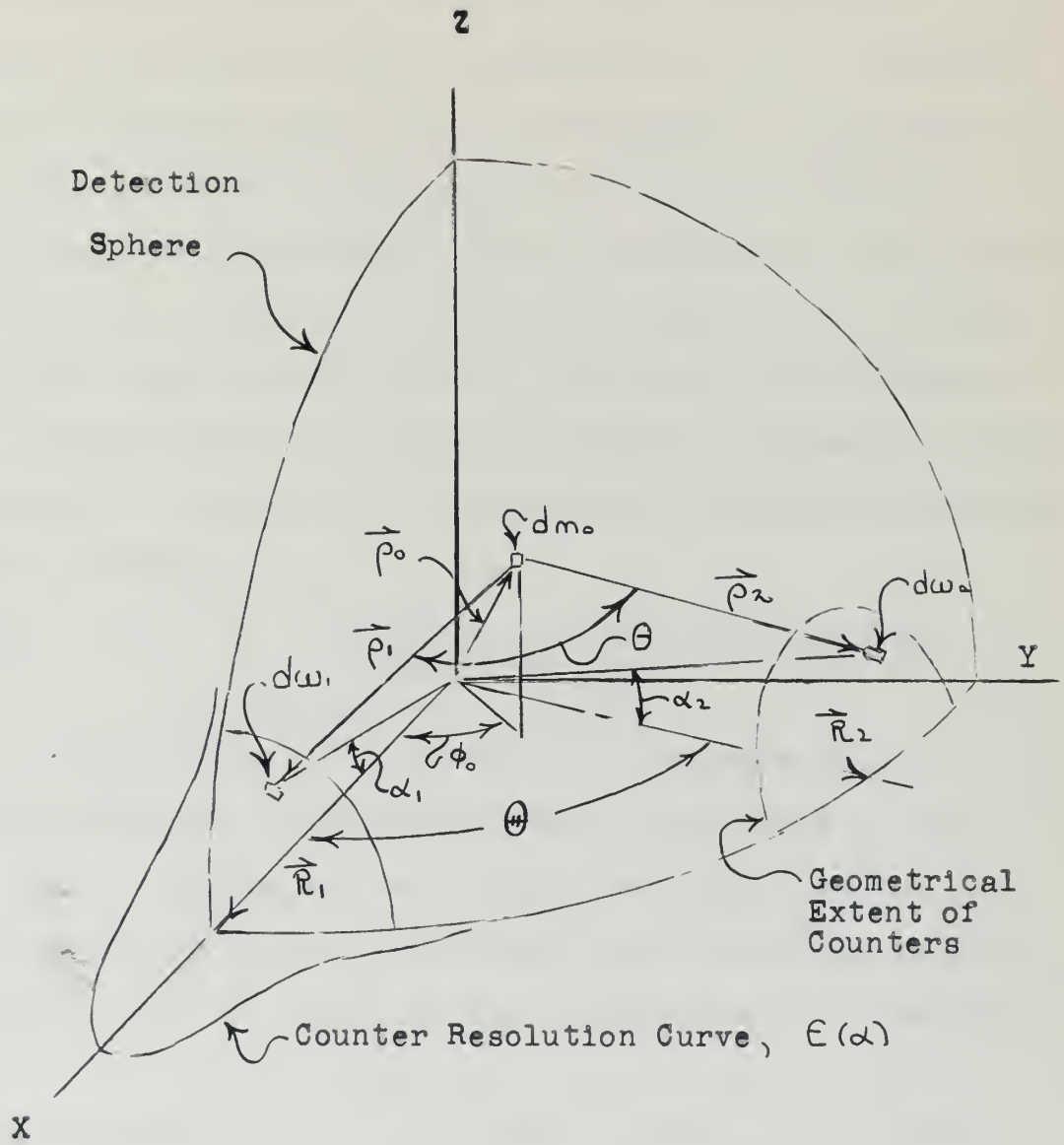

In the diagram dn_0 represents an element of source, $d\omega_1$ and $d\omega_2$ are elements of solid angle on the counters. The counter angular resolution curve for one counter is shown, the radial direction being the coordinate of relative response.

We make now a few comments about this model. Certain

artificialities have already been introduced in that we are representing our counters by spherical caps concentric with the origin. Obviously, this is only an approximation, since a real counter has a radial extent and all detection does not take place at exactly the same distance from the origin. We assume in this model that the relative counter sensitivity, $\epsilon(\alpha)$, is symmetric about the counter axis and is independent of the slight deviations from normality to the counter surface of radiations from different parts of the source. This, it seems, is a good approximation for small sources, i.e. where the direction of the propagation vector from various parts of the source to an element of counter surface, does not change appreciably in direction. With these comments in mind we can then write our observed correlation function as follows:

$$(3)\quad \overline{W}(\oplus) = \int_{4\pi}\int_{4\pi}\int_{\text{SOURCE}} \frac{W(\theta)\epsilon_1(\alpha_1)\epsilon_2(\alpha_2)\,dm_0\,d\omega_1\,d\omega_2}{\rho_1^2\,\rho_2^2}$$

Now, in principle it is possible to integrate (3) and thus obtain the functional dependence of the C's on the A's (1,2). We would then be making our solid angle and finite source corrections simultaneously and accurately to the limit of validity of this model. But in practice this integration is exceedingly tedious.

We now proceed to alter our model slightly to facilitate the integration (3). We do this by separating the corrections for finite counter solid angle and finite extent of source. As was pointed out in Section 5.3.3 the corrections for finite solid angle with a centered point source cause no "mixing" of the coefficients. In this case, assume that our observed function is $W'(\theta)$, where:

(4) $W'(\theta) = 1 + B_2P_2(\cos\theta) + B_4P_4(\cos\theta)$

Then it can be shown that:

(5) $B_{2k} = Q_{2k}A_{2k}$

where A_{2k} is the undisturbed coefficient and Q_{2k} is a simple reduction factor, i.e. no mixing of coefficients occur.

If we now alter our model and assume that each element of source can be first corrected in turn for solid angle without introducing mixings we can separate the two corrections, i.e. for finite solid angle and for finite source. This is equivalent to saying that in our model the spherical caps can be tilted slightly to bring each element of source in turn to the cap's spherical center, without deviating too far from the true state of affairs.

Then from this model we can construct another diagram:

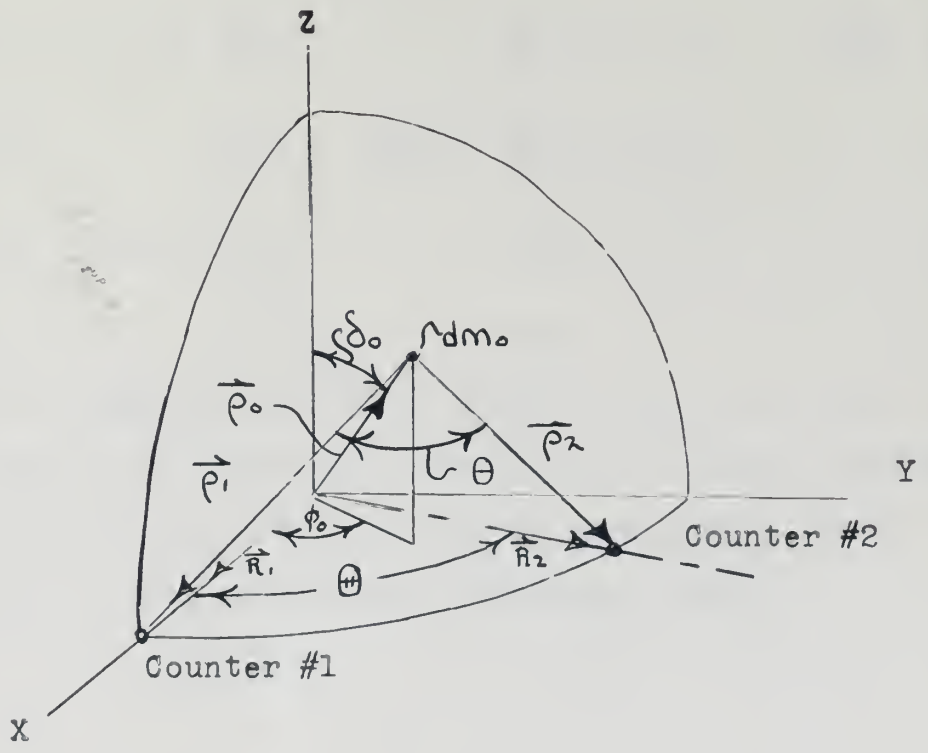

Here we have already carried out the solid angle integration so each counter can be replaced by a spherical point at its center:

$$(6)\qquad \overline{W}(\theta) = \int \frac{W'(\theta)\,dm_o}{\rho_1^2\,\rho_2^2}$$

expresses the observed correlation. If now we assume $R_1 = R_2$ and that the source is in the form of an upright right circular cylinder centered at the origin, of "half-height" z_o and radius r_o then we obtain an explicit expression for the C's (1) in terms of the B's (4). Letting $z_o/R = \zeta_o$, and $r_o/R = \xi_o$, we have after carrying out the integration in (6) to second order in ξ_o and ζ_o :

$$(7)\qquad \begin{aligned}
C_0 &= B_0 + \xi_o^2\left(B_0 + \tfrac{1}{12}B_2 + \tfrac{7}{16}B_4\right) + \zeta_o^2\left(-\tfrac{2}{3}B_0 - \tfrac{1}{3}B_2 - \tfrac{1}{3}B_4\right)\\
C_1 &= \qquad \xi_o^2\left(B_0 - \tfrac{13}{20}B_2 - \tfrac{3}{4}B_4\right) + \zeta_o^2\left(\qquad B_2 + B_4\right)\\
C_2 &= B_2 + \xi_o^2\left(\qquad\quad \tfrac{5}{4}B_4\right) + \zeta_o^2\left(\quad -\tfrac{4}{3}B_2 - \tfrac{5}{3}B_4\right)\\
C_3 &= \qquad \xi_o^2\left(\quad \tfrac{12}{5}B_2 - \tfrac{3}{4}B_4\right) + \zeta_o^2\left(\qquad\quad \tfrac{7}{3}B_4\right)\\
C_4 &= B_4 + \xi_o^2\left(\qquad\quad -3B_4\right) + \zeta_o^2\left(\qquad\quad -2B_4\right)\\
C_5 &= \qquad \xi_o^2\left(\qquad\quad 5B_4\right)
\end{aligned}$$

We can express the B's in terms of the A's by (5). We thus have answered the original question, i.e. we have expressed the C's in terms of the A's. Our answer is accurate to the limit of validity of the second model discussed above.

ACKNOWLEDGEMENT

I find it difficult to express my gratitude to Professor Donald R. Hamilton for his great assistance and for the many hours of consultation over the course of this research. His advice was often sought, and his counsel always wise. His never failing, kindly good humor is an inspiration to those who seek his guidance.

I would also like to extend my thanks to Dr. W. F. Hornyak for the measurements of nuclear lifetime, to the personnel of the radioactive chemistry laboratory, Dr. R. A. Naumann and Miss B. Bamman, for their cooperation in the preparation of sources, and finally to Messrs. J. W. McClain and W. D. Slawson who assisted in the data taking.

S.C.D.

Bibliography

1A51 H. Aeppli, A. S. Bishop, H. Frauenfelder, M. Walter, and W. Zunti - PR 82-550

1A52 K. Alder - HPA 25-235

1A53 A. Abragam and R. V. Pound - PR 92-943

2A53 H. Albers-Schonberg, F. Hanni, E. Heer, T. B. Novey, and P. Scherrer - PR 90-322

1B47 E. L. Brady and M. Deutsch - PR 72-870

1B49 F. Boehm and M. Walter - HPA 22-378

1B52 R. E. Bell, R. L. Graham, and H. E. Petch - CJP 30-35

2B52 L. C. Biedenharn, "Tables of the Racah Coefficients", Oak Ridge National Laboratory, ORNL-1098

3B52 J. M. Blatt and V. F. Weisskopf, "Theoretical Nuclear Physics", Wiley 1952

1C35 E. U. Condon and G. H. Shortley, "The Theory of Atomic Spectra", Cambridge University Press, 1935

1C52 E. L. Church and J. J. Kraushaar - PR 88-419

1F50 D. L. Falkoff and G. E. Uhlenbeck - PR 79-323

1F51 S. Frankel - PR 83-673

2F51 H. Frauenfelder - P R 82-549

1F53 H. Frauenfelder - Ann. Rev. of Nuclear Sc., Vol 2(1953)

1G46 G. Goertzel - PR 70-897

1G49 J. W. Gardner - Proc. Phys. Soc. A(London) 62-763

1G51 M. Goldhaber and A. W. Sunyar - PR 83-906

1G53 W. Gordy, W. V. Smith, and R. F. Trambarulo, "Microwave Spectroscopy", Wiley, 1953

1H40 D. R. Hamilton - PR 58-122

1H50 R. Hofstadter and J. A. McIntyre - PR 80-631

1H52 E. Heer - Physica 18-1214

1H53 J. M. Hollander, I. Perlman, and G. T. Seaborg - RMP 25-469

2H53 P. B. Hemming and R. M. Steffen - PR 92-832

1J54 M. W. Johns, C. C. McMullen, R. J. Donnely, and S. V. Nablo - CJP 32-35

1K52 E. D. Klema and F. K. McGowan - P R 87-524

1K53 J. J. Kraushaar and R. V. Pound - BNL-1559 (Brookhaven National Laboratory Report)

1L49 D. S. Ling and D. L. Falkoff - PR 76-1639

1L51 S. P. Lloyd - PR 83-716

2L51 S. P. Lloyd - PR 81-161

1L52 B. A. Lippmann PR 81-162

1L53 J. S. Lawson and H. Frauenfelder - PR 91-649

1M47 F. Marshall and J. W. Coltman - PR 72-528

1M53 Miner and Dalton, "Glycerol" , ACS Monograph Series, Reinhold Publishing Corp., 1953

1R42 G. Racah - PR 62-438

1R51 D. M. Roberts and R. M. Steffen - PR 82-332

1S51 R. M. Steffen - PR 83-166

1S52 R. M. Steffen and W. Zobel - P R 88-170

1S53 R. M. Steffen - PR 89-903

2S53 R. M. Steffen - PR 90-1119

3S53 G. Scharff-Goldhaber - PR 90-587

1T49 C. H. Townes and B. P. Dailey - Jour. Chem. Phys. 17-782

1Y48 C. N. Yang - PR 74-764

Legend: PR - Physical Review, RMP - Reviews of Modern Physics, HPA - Helvetica Physica Acta, CJP - Canadian Journal of Physics

SEP 29 DISPLAY

Thesis D163 c.1 Daubin 25143
The perturbed gamma-gamma directional correlation of Cd 114.
SEP 29 DISPLAY

25143
Thesis D163 c.1 Daubin
The perturbed gamma-gamma directional correlation of Cd 114.

thesD163
The perturbed gamma-gamma directional co
3 2768 002 09556 4
DUDLEY KNOX LIBRARY